Temperature-induced swelling/shrinking behavior of adsorbed PNIPAM microgels

vorgelegt von
Diplom-Physikerin
Anna Burmistrova
Moskau

von der Fakultät II - Mathematik und Naturwissenschaften
der Technischen Universität Berlin
zur Erlangung des akademischen Grades

Doktor der Naturwissenschaften
Dr. rer. nat.

genehmigte Dissertation

Promotionsausschuss:
Vorsitzender: Prof. Dr. Reinhard Schomäcker
Berichter/Gutachter: Prof. Dr. Regine von Klitzing
Berichter/Gutachter: Prof. Dr. Thomas Hellweg

Tag der wissenschaftlichen Aussprache: 17.02.2011

Berlin 2011
D 83

.

Acknowledgment

This thesis is dedicated to my mother, Lydia Burmistrova.

The present PhD thesis was elaborated under the supervision of Prof. Dr. Regine v. Klitzing from the Technical University of Berlin in the time from February 2007 to December 2010.

I want to thank Regine v. Klitzing for her constant and friendly support, many informative and efficient discussions and for giving me opportunity to research in very interesting field.

I thank Prof. T. Hellweg for some useful tips and consultations and Dr. M. Karg for the introduction to the microgel synthesis and Scanning Force Microscopy.

I would like to thank Prof. Dr. Z. Adamczyk, Dr. hab. M. Zembala, Dr. A. Michna and Dr. B. Jachimska from Institute of Catalysis and Surface Chemistry of Polish Academy of Science in Cracow, Poland for the helping in the mobility measurements and their interpretation.

I am grateful to Michael Eisele for carrying out of QCM, mobility, contact angle measurements and titration of microgel dispersions and Jörg Barner from JPK for kindly support in the SFM measurements in the liquid cell.

Dörthe Eisele is acknowledged for the friendly support and inspiration for a scientific activity.

I thank Ksenia Sryvkova for friendly support and motivation and important advice how to optimize my work.

I am grateful to Marcel Richter, who was so kind as to read the whole manuscript and correct the English spelling and contributed also to the scientific discussion.

I want to thank my office mates and colleagues for support in the writing process, many helpful advices and for a nice atmosphere in our office.

I am grateful to Alexey Shaytan, Nikolay Oskolkov and Irina Ostapenko for technical,

scientific and friendly support.
I am forever indebted to my family and Gunnar Lachmann for their understanding, endless patience and encouragement when it was most required.
Finally, I would like to thank the Deutsche Forschungsgemeinschaft within the framework of the priority program SPP 1259, the COST Action D43 and Zentrale Frauenbeauftragte of Technical University of Berlin for financial support.

Contents

1 Introduction **9**

2 Theoretical backgrounds **13**

2.1 Polymers 13

2.2 Gels 15

2.3 Microgels 16

2.4 PNIPAM-based Microgels 17

2.5 Adsorption of microgels particles or microgel films 18

2.6 Investigation Techniques 19

2.6.1 Characterization in Bulk 19

2.6.2 Characterization at Interfaces 22

3 Experimental part **31**

3.1 Materials 31

3.2 Microgel synthesis 32

3.3 Microgel deposition on solid substrates 33

3.3.1 Substrate preparations 33

3.3.2 Microgel deposition by dip coating 34

3.4 Methods and Apparatuses 35

3.4.1 Scanning Force Microscopy (SFM) 35

3.4.2 Ellipsometry 36

3.4.3 Dynamic Light Scattering (DLS) 37

3.4.4 Quartz Crystal Microbalance (QCM) . . . 37
3.4.5 Contact Angle Measurements . . . 37
3.4.6 Mobility Measurements . . . 38
3.4.7 Titration . . . 38

4 Control of microgel number density at solid surfaces 39
4.1 Effect of the rotation speed . . . 40
4.2 Effect of microgel particle concentration . . . 41
4.3 Effect of pH . . . 42
4.4 Effect of number of deposition . . . 43
4.5 Summary . . . 44

5 Influence of internal microgel parameters 45
5.1 Effect of Co-monomer Content . . . 45
5.1.1 Microgel characterizations in volume phase . . . 46
5.1.2 Swelling behavior of adsorbed microgel particles . . . 48
5.1.3 Influence on number density of adsorbed microgel . . . 52
5.1.4 Summary . . . 55
5.2 Effect of Cross-linker Content . . . 55
5.2.1 Microgel characteristics in volume phase . . . 56
5.2.2 Individual adsorbed microgels . . . 57
5.2.3 Summary . . . 62

6 Influence of outer stimulis 65
6.1 Effect of pH and Ionic Strength . . . 65
6.1.1 Aqueous dispersions of P(NIPAM-co-AAc) microgels . . . 66
6.1.2 Behavior of adsorbed microgels . . . 69
6.1.3 Summary . . . 74
6.2 Effect of Cononsolvency . . . 74
6.2.1 Microgel characteristics in bulk . . . 75

6.2.2 Effect of EtOH content on the substrate coverage 78
6.2.3 Swelling/deswelling behavior of adsorbed microgels 79
6.2.4 Summary 86

7 Influence of deposition methods and substrates 89
7.1 Effect of deposition method 89
7.1.1 Summary 97
7.2 Effect of substrate 98
7.2.1 Substrate characterization 99
7.2.2 Thermo-induced swelling/deswelling behavior of adsorbed microgels 100
7.2.3 Summary 107

8 Conclusions 109

9 Outlooks 113

Chapter 1

Introduction

During the last few decades polymer materials became more popular and take place in all areas of human life. One of the most researched polymer materials are gels [1]. Gels are a cross-linked three-dimensional polymer matrix, which can react on changes of the environmental conditions such as pH, temperature, light *etc.* [1–4]. A special class of gels are microgels [5–7]. They have similar properties like macrogels, but due to their small sizes in micrometer range, they can react significantly faster upon environmental changes [7, 8].

There are many publications, which describe the properties of such microgels [5, 7, 9–13]. One of the most popular and mostly investigated microgels are PNIPAM-based microgels [6, 14, 15]. PNIPAM has a lower critical solution temperature (LCST) at about 32°C. That means below this temperature the polymer network exists in a swollen state. Above the LCST the whole gel collapses due to the increasing hydrophobic interactions. In order to obtain microgels with different properties, for example, pH-sensitive microgel particles, organic co-monomers can be used during the synthesis [9, 11, 16–19].

The properties of such multifunctional microgels in bulk are very well investigated. It was shown that the LCST can be shifted by adding different co-monomers, by changing the concentration of cross-linker, as well as by the ionic strength and pH of particle dispersions [9, 17–26].

Such materials can be used in many fields of industry like drug delivery, paints, mi-

crolenses, for emulsion stabilization *etc.* [27, 27–34]. Thermoresponsive microgels offer high potential to be used in coating industry, is resulting in intensive investigation of properties of microgels deposited on solid substrates.

Few groups investigate the microgel abilities to form well packed structures on different solid surfaces affected by the deposition methods, temperature of adsorption, particle charges or ionic strength [35–40].

Thin films made of PNIPAM-based materials were investigated by confocal microscopy [41], video microscopy [14], ellipsometry [36, 42–45], differential scanning calorimetry [46], QCM [47–50]. S. Hoefl *et.al.* [51] showed that adsorbed PNIPAM-based microgels have also thermoresponsive behavior. V. Nerapusri *et.al.* [42] used ellipsometry to determine the dependence of microgel film thickness as function of pH, temperature and ionic strength. Unfortunately, most of these techniques provide average values of film thickness and do not deliver any information about stimuli-induced behavior of individual adsorbed microgel particles.

A suitable method for the investigation of swelling properties of individual adsorbed microgel particles is Scanning Force Microscopy (SFM) [16, 51–53]. O. Tagit *et.al.* [52] observed thermo-induced swelling/deswelling behavior of PNIPAM microgels. They showed that microgels shrink laterally and stretch vertically above the LCST. J. Wiedemair *et.al.* [53] observed the same effect for SFM measurements done by cantilevers covered with aluminum for increasing reflected laser beam. But this phenomenon disappeared by usage of magnetically coated cantilevers. For this reason uncoated silicon cantilevers were chosen.

The aim of this work is to control the number density of microgels deposited on a solid substrate and to investigate thermo-induced swelling/deswelling behavior of individual adsorbed microgel particles. Effect of microgel dispersion concentration, dispersion pH-value, rotation speed and repeated microgel deposition on the number density of adsorbed microgels were investigated. The thermo-induced swelling/shrinking behavior of individual adsorbed microgel were investigated. Effect of outer stimuli (pH, ionic strength and solvent quality), internal parameters (cross-linker and co-monomer content), deposition techniques, and substrates were studied. The main measurement technique used in this

work is Scanning Force Microscopy.

Chapter 2

Theoretical backgrounds

2.1 Polymers

A polymer is a chain molecule consisting of at least few hundred covalently linked repeat units or monomers. Polymers made of one type of monomer are called homopolymers and in case of different monomers they are called co-polymers. Polymers are produced by polymerization process characterized by four steps:

1. Initiation
2. Propagation
3. Termination
4. Transfer step.

In the first step an active center or initiator (I) will be generated (2.1) and reacts with the first monomer molecules (M). This active center is transfered on the monomer (2.2):

$$\mathrm{I} \longrightarrow \mathrm{I}^{*} \tag{2.1}$$

$$\mathrm{I}^{*} + \mathrm{M} \longrightarrow \mathrm{IM}^{*} \tag{2.2}$$

From this point the second step (propagation) takes place. In this step the chain growth starts as a cascade reaction. In this reaction the active center is transfered on the last

monomer in the chain (2.3):

$$\begin{aligned} \mathrm{IM}^* + \mathrm{M} &\longrightarrow \mathrm{IM}_2^* \\ \mathrm{IM}_2^* + \mathrm{M} &\longrightarrow \mathrm{IM}_3^* \\ &\dots \end{aligned} \tag{2.3}$$

In the third step the chain growth is stopped by adding chain-terminating agent S (stopper) (2.4). In the last step the active center is transfered to another molecule T: for example, solvent, monomer, initiator, polymer, etc. (2.5).

$$\mathrm{IM}_\mathrm{n}^* + \mathrm{S} \longrightarrow \mathrm{IM}_\mathrm{n} + \mathrm{S}' \tag{2.4}$$

$$\mathrm{IM}_\mathrm{n}^* + \mathrm{T} \longrightarrow \mathrm{IM}_\mathrm{n} + \mathrm{T}^* \tag{2.5}$$

In dependence of the type of initiator the polymerization is divided in radical and ionic (anionic and cationic) polymerization.

For radical polymerization the initiation is carried out by radicals. The most usable initiators are hydrogen peroxide, potassium peroxydisulfate, dibenzoyl peroxide, *etc.* [54].

For ionic polymerization process monomers with particular charge on one of the atoms of weak bonds are used. For cationic and anionic polymerization cations and anions start the chain growth, respectively and chains carriers are macroions. In contrast to radical polymerization there is no termination by combination because of the electrostatic repulsion between growing chains. Protonic acids and Lewis acids are usually used in cationic polymerization processes. Alkaline metals (Li, Na, K, etc.) and their derivatives are classical initiators of anionic polymerization. Anionic polymerization is also called "living" polymerization due to the absence of termination step [54].

Polymers could also be synthesized via polycondensation. Polycondensation is a stepwise process of a polymer formation. In this process the multifunctional components react with each other with elimination of low weight molecules such as water, alcohol or hydrogen and formation of macromolecules.

2.2 Gels

Gels are cross-linked polymers building a three-dimensional polymer network. According to the cross-linker species one distinguishes between physical and covalently connected gels. Covalently cross-linked polymers loose their solubility and meltability. Physical cross-linkers are hydrogen bonds, electrostatic forces and Van-der-Waals interactions.

Chemical cross-linked polymers can be obtained by two ways: "from monomers" and "from polymers". In the first case, the polymerization process takes place in a monomer-cross-linker mixture. In the second case, pre-synthesized polymers are chemically connected with each other.

The main property of gels is their response to external stimuli. Therefore, gels can be divided into thermo-, pH-, light-sensitive *etc.* [1–3, 55–61].

Within bounds of this work, PNIPAM-based microgels are in sight. PNIPAM gels are thermosensitive and have a so called lower critical solution temperature (LCST). It means that below this temperature water is a good solvent and gels exist in a swollen state. Above this temperature water turns into a bad solvent. Increasing hydrophobic interactions lead to the polymer network collapse. Qualitatively, such behavior is explained by Flory-Rehner theory [62, 63]. The gel free energy F_{gel} is a sum of three components: the free energy of the network elasticity F_{el}, the free energy of the extensional interaction chain units F_{int}, and F_{ch} is connected with Coulomb interactions between charged network units and counterions:

$$F_{gel} = F_{int} + F_{el} + F_{ch} \tag{2.6}$$

Volume changes occurs because of changing osmotic presure

$$\pi_{gel} = -\left(\frac{\partial F}{\partial V}\right)_T = \pi_{mix} + \pi_{el} + \pi_{ch} \tag{2.7}$$

where

$$\pi_{mix} = -\frac{N_A kT}{v}\left(\varphi + \ln(1-\varphi) + \chi\varphi^2\right) \tag{2.8}$$

$$\pi_{el} = \nu kT\left(\left(\frac{\varphi}{2\varphi_0}\right) + \left(\frac{\varphi}{\varphi_0}\right)^{\frac{1}{3}}\right) \tag{2.9}$$

$$\pi_{ch} = f\nu kT\left(\frac{\varphi}{\varphi_0}\right) \tag{2.10}$$

where π_{mix} is the osmotic pressure contributed by solvent/polymer mixing, π_{el} is the osmotic pressure contributed by network elasticity, π_{ch} is the osmotic pressure contributed network charges, N_A is the Avogadro's number, k is the Boltzmann constant, T is a temperature, χ is Flory-Huggins interaction parameter, φ_0 is a volume fraction of a gel in the initial state, φ is a volume fraction of gel in the final state, ν is a chain density, f is a number of counterions per chain, v is a molar solvent volume.

$$\chi = \frac{\Delta F}{kT} \tag{2.11}$$

where, ΔF is the free energy decrease associated with the formation of a contact between chain segments.

In figure 2.1 phase diagrams of gel lower miscibility gap (a) and with upper miscibility gap (b) are shown. There is a two-phase region below the curve and an one-phase region above it for gels exhibiting a lower miscibility gap. Oppositely, the gels demonstrating the upper miscibility gap have a two-phase region above the curve, and an one-phase region below it. The filled points designate the critical temperatures. The lower critical solution temperature (LCST) corresponds to an upper miscibility gap and an upper critical solution temperature (UCST) corresponds to a lower miscibility gap.

2.3 Microgels

According to the gel size, gels can be divided into two classes: macrogels and microgels. Microgels are cross-linked polymer particles with sizes about one micrometer and smaller. Those kinds of particles exhibit a similar property as macrogels made of the same material. They also have an stimuli-responsive behavior [6, 22, 30, 64, 65]. For example, PNIPAM-based microgels demonstrate thermoresponsive swelling/deswelling behavior [9, 16, 22]. T. Tanaka [8] showed that the characteristic time (τ) of gel volume changes is determined by its size (R) and collective diffusion coefficient (D):

$$\tau = R^2/\pi^2 D \tag{2.12}$$

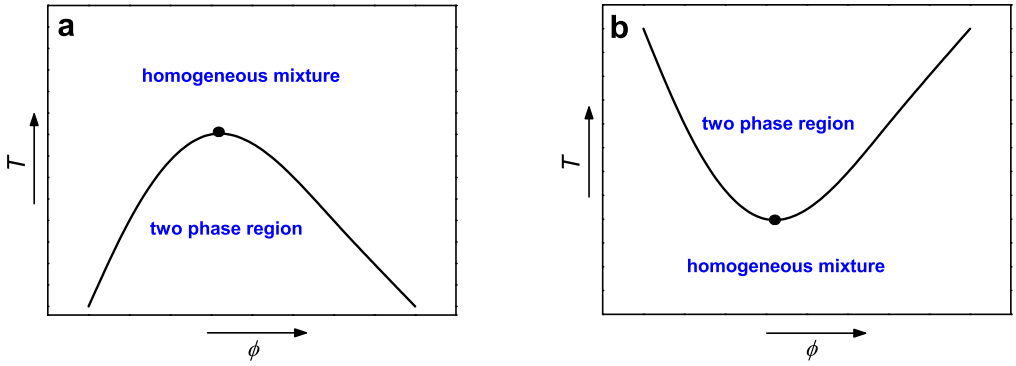

Figure 2.1: *Phase diagrams of a polymer gel with (a) a lower miscibility gap or upper critical solution temperature (UCST) and with (b) upper miscibility gap or lower critical solution temperature (LCST). The filled point is a critical point.*

Resulting from the equation (2.12) the responsibility of external parameters depends extremely on the gel size. Therefore, the microgels exhibit a faster swelling/deswelling behavior. Due to the small sizes and fast response on the changing environment conditions, microgels raise a huge interest for different applications: for drug delivery, emulsion stabilizations, microlenses, coatings, water storage and etc. [28, 54, 66–71].

.

2.4 PNIPAM-based Microgels

In the present work PNIPAM-based microgels are synthesized via surfactant free emulsion polymerization [5]. NIPAM monomers are non-soluble in water at higher temperatures, building droplets and the emulsion formation takes place. Via permanent stirring monomer droplets show a low dispersity. After adding a radical starter the polymerization reaction starts in droplets and colloidal particles are formed.

Thermo-induced swelling/deswelling behavior of PNIPAM microgels in bulk is very well studied by different techniques: Dynamic Light Scattering (DLS), Neutron Scattering, Electrophoresis, etc. [22, 71–75]. It was shown that pure PNIPAM microgel particles have

the LCST at a temperature of about 32°C [6, 73, 76, 77].

In the same manner like macrogels, microgel characteristics such as the size, swelling ratio or the LCST can be tuned by adding charged co-monomers or varying the cross-linker density. With increasing cross-linker content the microgel size and swelling ability decreases due to decreasing chain length between two chemical linkages [21, 24, 75]. Usage of co-monomers allows to change particle sizes and the LCST leading to multiresponsive microgels. For example, in order to obtain thermo- and pH-responsive PNIPAM microgels, weak acids as co-monomers are used [9, 11, 17, 51, 71, 73]. In this work acrylic acid (AAc) was used as a co-monomer. The size of PNIPAM microgels containing AAc as a co-monomer (P(NIPAM-co-AAc)) increases with increasing pH because of the deprotonation of AAc units [16, 17]. It was also shown that acid co-monomers affect the particle sizes and the LCST: the particle sizes increases and the LCST shifts to higher temperatures with increasing co-monomer concentration due to the increasing interchain electrostatic repulsion [4, 9, 17].

The solvent quality also plays an important role in the PNIPAM thermo-induced behavior. It was observed that PNIPAM is cononsoluble in water/alcohol mixtures. Cononsolvency means that pure water or pure alcohol serves as a good solvents for PNIPAM, but their mixture becomes a bad solvent [68, 78–81]. The alcohol/water mixture turns into a bad solvent for PNIPAM due to the formation of different complexes between these two solvents. With increasing alcohol content the PNIPAM starts to reswell again. Wang *et. al.* [68] demonstrated that PNIPAM preferably interacts with the alcohol molecules over water molecules.

2.5 Adsorption of microgels particles or microgel films

Due to the fast swelling/shrinking kinetics, outer stimuli responsive behavior of PNIPAM-based microgels has a high impact for coating industry. There are many theoretical and experimental works investigating the adsorption process and surface ordering of polymer particles [16, 35–38, 40, 42, 82, 83].

Here, a few main tendencies in investigation of adsorbed microgel particles were followed: (1) creation of well ordered structures at solid surfaces [14, 16, 35, 41], (2) investigation of adsorption abilities of microgels [38, 39, 82], and (3) the study of swelling and deswelling behavior of adsorbed microgels [36, 42, 51, 84].

C. D. Sorrell and L. A. Lyon [82] compared the adsorption ability of microgels with different stiffnesses. They showed that the interaction between particles and surface. Particle softness plays the most important role in particle adsorption process. Adsorbed particles did not overlap and did not adhere on the surfaces with the significantly smaller areas than the particle footprints. It leads to a decrease in surface coverage with increasing particle size. However, if the particle-surface interaction was strong enough, soft particles were able to squeeze into the hole between previously adsorbed particles.

A. B. South et. al. [39] compared two deposition methods: active (centrifugation) and passive deposition (deposition of substrate in the particle dispersion). They found out that large particles reached full surface coverage in active deposition faster than the small particles because of their higher sedimentation velocity. Oppositely, small particles reached the full coverage faster in passive deposition due to their larger diffusion coefficient. After active deposition adsorbed particle had smaller footprints and were more closely packed than particles deposited passively because of the high energy of centrifugation procedure.

It was shown that thin films of PNIPAM-based microgel particles are also thermosensitive (are swollen at lower temperatures and shrunk in higher temperatures), pH- and ionic strength-sensitive [16, 36, 42, 51–53, 85].

2.6 Investigation Techniques

2.6.1 Characterization in Bulk

Dynamic Light Scattering (DLS)

Dynamic Light Scattering (DLS) was applied for characterization of microgel particles in bulk [86]. The schematic image of a scattering experiment is introduced in figure 2.2. The

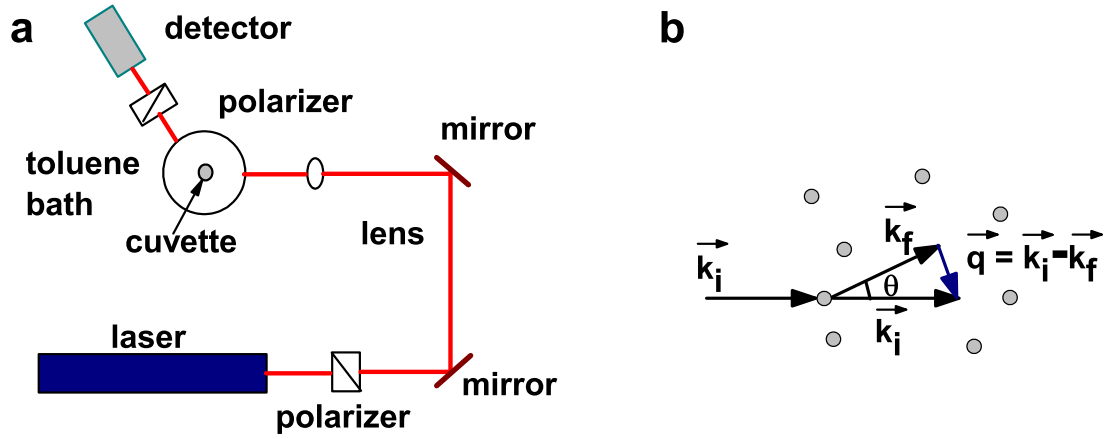

Figure 2.2: *(a) Schematic image of DLS apparatus. (b) Definition of a scattering vector* $\vec{q}$*.* $\vec{k_i}$ *is a wave vector of the incident light,* $\vec{k_f}$ *is a wave vector of the scattered light.* $\left|\vec{k_i}\right| \approx \left|\vec{k_f}\right|$.

coherent laser beam passes through a polarizer, reflects from two mirrors and is focused by a lens. Afterwards, the focused beam incidents on the glass cuvette with a microgel solution. Due to the Brownian movements of microgel the light is scattered in different directions and is collected by a detector at a certain scattering angle. In order to control the sample temperature the cuvette was placed in a toluene bath. Toluene was chosen because of the similar refractive indices of both glass and toluene and glass.

In the DLS measurements, the time autocorrelation function of the scattered light intensity $g_2(\tau)$ is measured:

$$g_2(\tau) = \frac{\langle I(\vec{q},t) I(\vec{q},t+\tau)\rangle}{\langle I(q,t)\rangle^2} \tag{2.13}$$

where $I(\vec{q},t)$ is the intensity of the scattered light, $\vec{q}$ is a scattering vector resulting from figure 2.2b and eq. (2.14).

$$|\vec{q}| = q = \frac{4\pi n}{\lambda} \sin\left(\frac{\theta}{2}\right), \tag{2.14}$$

where n is a refractive index, λ is a wavelength, and θ is a scattering angle.

The $g_2(\tau)$ is also called autocorrelation function of the second order. For further calculation an autocorrelation function of the first order $g_1(\tau)$ determined by Siegert's equation is required:

$$g_2(\tau) = 1 + \beta \left| g_1(\tau) \right|^2, \tag{2.15}$$

where β is coherence factor determined by the detection geometry.

For monodisperse particles $g_1(\tau)$ is a simple exponential function with the relaxation rate Γ:

$$g_1(\tau) = e^{-\Gamma\tau} \tag{2.16}$$

For mixtures of particles with different sizes $g_1(\tau)$ can not be described by one exponential function and should be described as a sum:

$$g_1(\tau) = a_0 + a_1 e^{-\Gamma'\tau} + a_2 e^{-\Gamma''\tau} + a_3 e^{-\Gamma'''\tau} + \ldots, \tag{2.17}$$

where a_0, a_1, a_2, ... are expansion coefficients known as amplitudes, and Γ', Γ'', Γ''', ... are relaxation rates. In order to analyze the autocorrelation function $g_1(\tau)$ the method of cumulants is usually used. Analysis of an autocorrelation function by cumulant expansion is usually performed by fitting a polynom up to the third order to the function $\ln g_2((\tau) - 1)$:

$$\ln g_1(\tau) = \ln A - \Gamma_1\tau + \frac{1}{2!}\Gamma_2\tau^2 - \frac{1}{3!}\Gamma_3\tau^3 + \ldots \tag{2.18}$$

Using Γ_1 the diffusion coefficient D can be calculated:

$$\Gamma_1 = Dq^2 \tag{2.19}$$

According to the Stokes-Einstein equation the hydrodynamic radius of particles R_h can be determined:

$$R_h = \frac{kT}{6\pi\eta D} \tag{2.20}$$

where k is a Boltzmann constant, T is the sample temperature, η is the solution viscosity.

In the course of cumulant expansion other characteristics such as the width of the radius distribution

$$Width = \frac{\sqrt{\Gamma_2}}{\Gamma_1} R_h \tag{2.21}$$

or the polydispersity index (PDI)

$$PDI = \frac{\Gamma_2}{\Gamma_1^2} q^2 \tag{2.22}$$

can be defined.

Mobility measurements

Charged colloidal particles are able to move in solutions under the influence of an electric field [87]. This phenomena is called electrophoresis. The electrophoretic velocity $\vec{v}$ is the velocity during electrophoresis. The electrophoretic mobility μ is the velocity per unit field strength $\vec{E}$:

$$\vec{v} = \mu \vec{E}. \tag{2.23}$$

The mobility is counted positive if colloids move toward lower potential and negative in the opposite case. For hard colloidal particles the mobility could be recalculated to the zeta potential ζ. One distinguishes between two laws: the Helmholtz-Smoluchowski law and the Hueckel-Onsager law. The first law (eq. (2.24)) can be used for large particles ($ka >> 1$, where k is the Debye-length and a is the colloidal particle radius). The second law (eq. (2.25)) is valid for small particles.

$$\mu = \frac{\epsilon_0 \epsilon \zeta}{\eta} \quad (ka >> 1) \tag{2.24}$$

and

$$\mu = \frac{2\epsilon_0 \epsilon \zeta}{3\eta} \quad (ka << 1), \tag{2.25}$$

where ϵ is a relative dielectric permittivity or dielectric constant, ϵ_0 is the electric field constant. Due to the microgel porosity and softness there was no attempts to convert mobility values into zeta potential values.

2.6.2 Characterization at Interfaces

Scanning Force Microscopy (SFM)

In order to get information about the adsorbed microgels Scanning Force Microscopy (SFM) was used. A schematic image of SFM is presented in figure 2.3. In SFM-

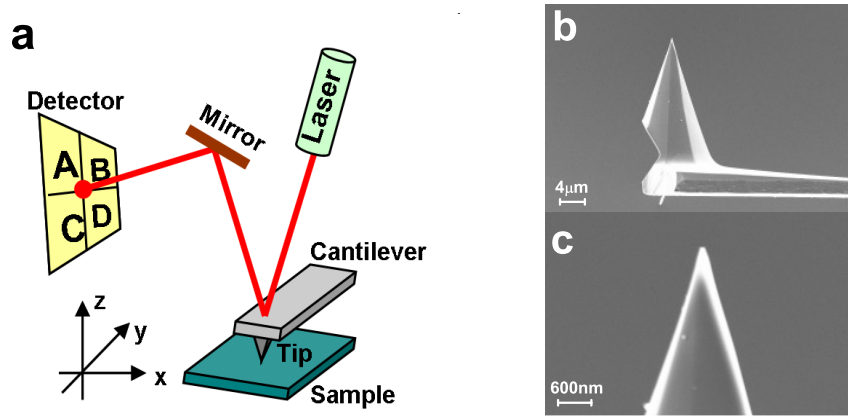

Figure 2.3: *Schematic images of SFM (a) and scanning electron microscopy (SEM) images of CSC37 tips (b,c). SEM images were taken in the group of Prof. Bimberg from Technische Universitaet Berlin.*

measurements a laser is used as a light source. The laser beam falls the back of the cantilever and is reflected to a mirror. The beam, coming from the mirror is collected by the detector.

The SFM-measurements can be done in three modes: contact mode, non-contact mode and intermittent or tapping mode. In contact mode the tip is in direct contact with the sample. The tip repeats exactly the height profile of the sample. Unfortunately, this mode is not appropriate for imaging of "soft" samples. In tapping mode and in non-contact mode the cantilever is excited with appropriate frequency. In tapping mode it is excited with the resonance frequency and tip contacts the sample surface shortly. In non-contact mode the cantilever is excited as well but the cantilever frequency is distinguished from the resonance frequency and the tip does not contact the sample during the scanning process.

All measurements in this work were carried out in tapping (Nanoscope III) or intermittent mode (JPK). How it was discussed above, the cantilever is excited by an external oscillating force $F_{driving} = F_0 \cos(\omega t)$, where F_0 is the force amplitude, ω is the force frequency and t is time. The coordinate of the cantilever is described by an oscillation

equation [88–90]:

$$m\frac{d^2z}{dt^2} + b\frac{dz}{dt} + kz = F_{ts} + F_0\cos(\omega t), \tag{2.26}$$

where m is the cantilever mass, z is the cantilever deflection, k is the cantilever spring constant, b is the friction coefficient, and F_{ts} is the tip-surface interaction. The resonance frequency ω_r is determined by equation (2.27):

$$\omega_r = \frac{\sqrt{\omega_0^2 - 2b^2}}{2\beta} \quad \text{with} \quad \omega_0 = \frac{\mathrm{k}}{\mathrm{m}} \quad \text{and} \quad \beta = \frac{\mathrm{b}}{2\mathrm{m}} \tag{2.27}$$

A steady-state solution of the equation (2.26) has the shape of sinusoidal oscillation:

$$z(z_c, t) = z_0(z_c) + A(z_c)\cos[\omega t - \phi(z_c)], \tag{2.28}$$

where z_0, A, and ϕ are the mean deflection, amplitude, and phase shift of the oscillation, respectively; z_c is the rest tip-surface separation. The phase shift is determined as:

$$\begin{aligned} \sin\phi &= \frac{A\omega}{A_0\omega_0}\left(1 + \frac{P_{ts}}{P_{med}}\right) \\ \cos\phi &= \frac{2Q}{kAA_0}\left[\frac{\langle F_{ts}\rangle^2}{k} - \langle F_{ts}\cdot z\rangle + \frac{1}{2}kA^2\left(1 - \frac{\omega^2}{\omega_0^2}\right)\right] \end{aligned} \tag{2.29}$$

where $Q = \frac{m\omega_0}{b}$ is a quality factor, $A_0 = \frac{QF_0}{k}$ is the free-oscillation amplitude. $P_{ts} = \langle F_{ts}\cdot\dot{z}\rangle$ is the power dissipated by the tip-surface forces, and $P_{med} = \frac{kA^2\omega^2}{2Q\omega_0}$. $\langle F_{ts}\rangle = \frac{1}{T}\oint F_{ts}dt$, and $\langle F_{ts}\cdot z\rangle = \frac{1}{T}\oint F_{ts}zdt$.

In intermittent/tapping mode the phase shift and amplitude changes are detected. The phase shift can supply with information about surface softness, tip-surface interactions, or adhesion between tip and sample. The amplitude changes are recalculated and the height profile of the sample is obtained.

In order to characterize the surface properties the surface roughness can be calculated from SFM height profiles. Usually the root mean squared roughness R_q is calculated:

$$R_q = \sqrt{\frac{1}{n}\sum_{i=1}^{n} h_i^2}, \tag{2.30}$$

where n is an amount of measured points, h_i is the height in point with number i. For roughness determination usually a scan area 1x1 μm^2 is used.

For characterization o the swelling/deswelling behavior of microgel particles, their volume was calculated by using a formula for the volume of a figure of revolution:

$$V_{SFM} = \pi \int_0^H f^2(h)dh, \tag{2.31}$$

where V_{SFM} is a microgel volume, $f(h)$ is a microgel cross section, H is a maximum of particles height, and π is a constant.

Ellipsometry

Ellipsometry is a method allowing to measure a thickness and a refractive index of thin films [91]. It is well known that light is an electromagnetic wave consisting of an electric field $\vec{E}$, a magnetic field $\vec{B}$, and wave vector $\vec{k}$. Vectors $\vec{E}$, $\vec{B}$ and $\vec{k}$ build a right-hand triple. An electromagnetic wave is also characterized by a polarization. All states of polarization are classified according to the trace of the electrical field vector during one period. There are three types of polarized light: linearly, circularly and elliptically. A given state of polarization is based on a superposition of two linearly polarized light waves within an arbitrarily chosen orthogonal coordinate system.

$$\vec{E}(\vec{r},t) = \begin{pmatrix} |E_p|\cos(2\pi\nu t - \vec{k}\cdot\vec{r} + \delta_p) \\ |E_s|\cos(2\pi\nu t - \vec{k}\cdot\vec{r} + \delta_s) \end{pmatrix}, \tag{2.32}$$

where $|E_p|$ and $|E_s|$ are the amplitudes, δ_p and δ_s are the phases, $\left|\vec{k}\right| = \frac{2\pi}{\lambda}$ is the magnitude of the wave vector, λ is a wave length, and ν is the frequency. In order to represent the light polarization only wave amplitudes and phases are required. The time dependence can be neglected. The so called Jones vector is defined as:

$$\vec{E} = \begin{pmatrix} |E_p|\, e^{i\delta_p} \\ |E_s|\, e^{i\delta_s} \end{pmatrix} = \begin{pmatrix} E_p \\ E_s \end{pmatrix}. \tag{2.33}$$

The state of polarization is

- linear, if $\delta_p - \delta_s = 0$ or $\delta_p - \delta_S = \pi$,
- elliptical, if $\delta_p \neq \delta_s$ and $|E_p| \neq |E_s|$,

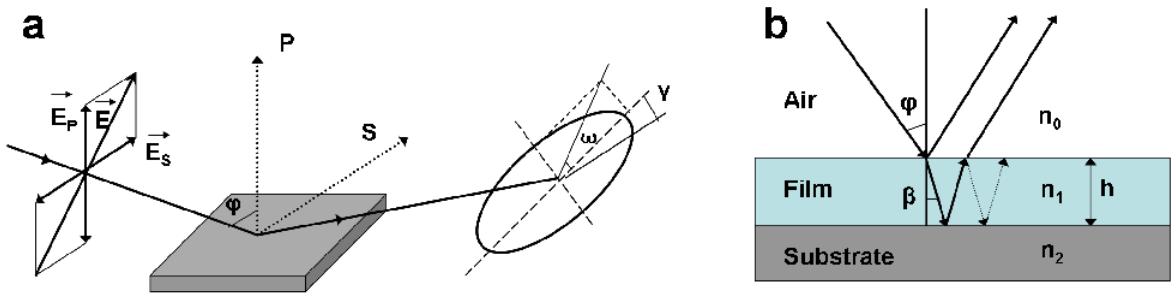

Figure 2.4: *(a) Schematic image of an s- and p-components of an electric field ($\vec{E}$) in an ellipsometric experiment. (b) Illustration of Fresnel's law. n_0, n_1, n_2 are the refractive indeces of air, film, and substrate, respectively. h is a film thickness, ϕ is an angle of incident, β is an angle of refraction.*

- circular, if $\delta_p - \delta_s = \pi/2$ and $|E_p| = |E_s|$

In ellipsometric experiment the light with the defined polarization is incident on a sample ($\vec{E}^i = \begin{pmatrix} |E_p^i|\, e^{i\delta_p^i} \\ |E_s^i|\, e^{i\delta_s^i} \end{pmatrix}$). The polarization of reflected light ($\vec{E}^r = \begin{pmatrix} |E_p^r|\, e^{i\delta_p^r} \\ |E_s^r|\, e^{i\delta_s^r} \end{pmatrix}$) differs from the incident light. In ellipsometry experiments these changes are measured. The wave vector and the normal of the reflecting surface define a plane of incidence. Light with an electric field vector oscillating within the plane of incidence (p-light) remains linearly polarized upon reflection and the same holds for s-light with $\vec{E}$ perpendicular to the plane of incidence (Fig. 2.4a). To describe the changes in the light polarization, two quantities Ψ and Δ are defined:

$$\begin{aligned} \Delta &= \left(\delta_p^r - \delta_s^r\right) - \left(\delta_p^i - \delta_s^i\right), \\ \tan\Psi &= \frac{\left|E_p^r\right| / \left|E_p^i\right|}{\left|E_s^r\right| / \left|E_s^i\right|}. \end{aligned} \tag{2.34}$$

Changes in phase and in amplitude are described by reflection coefficients r_p and r_s:

$$\begin{aligned} r_p &= \frac{\left|E_p^r\right|}{\left|E_p^i\right|} e^{i\left(\delta_p^r - \delta_p^i\right)} \\ r_s &= \frac{\left|E_s^r\right|}{\left|E_s^i\right|} e^{i\left(\delta_s^r - \delta_s^i\right)} \end{aligned} \tag{2.35}$$

With these definitions the basic equation of ellipsometry is obtained:

$$\tan\Psi e^{i\Delta} = \frac{r_p}{r_s} \tag{2.36}$$

The exact formula relating the reflectivity coefficients of a single homogeneous layer with refractive index $n_1 = \sqrt{\epsilon_1}$ in between two infinite media ($n_0 = \sqrt{\epsilon_0}$ and $n_2 = \sqrt{\epsilon_2}$) at an angle of incident ϕ (Fig. 2.4b) is given by:

$$\Delta = \arctan\frac{Im\left(\frac{r_p}{r_s}\right)}{Re\left(\frac{r_p}{r_s}\right)} \quad \text{with} \quad \begin{aligned} r_p &= |r_p| \cdot e^{-i\delta_{r,p}} = \tfrac{r_{01,p}+r_{12,p}e^{-i2B}}{1+r_{01,p}r_{12,p}e^{-i2B}} \\ r_s &= |r_s| \cdot e^{-i\delta_{r,s}} = \tfrac{r_{01,s}+r_{12,s}e^{-i2B}}{1+r_{01,s}r_{12,s}e^{-i2B}} \end{aligned} \tag{2.37}$$

where the reflectivity coefficients $r_{01,p}, r_{12,p}, r_{01,s}$ and $r_{12,s}$ describing the reflection at refractive index jumps $n_0 \to n_1$ and $n_1 \to n_2$ for p- and s-light are given by Fresnel's laws (Fig. 2.4b). $B = 2\pi\frac{h}{\lambda}\sqrt{n_1^2 - n_0^2\sin^2\phi}$ accounts for the phase shift.

If the layer thickness $h << \lambda$ it is allowed to expand the complex reflectivity coefficients in a power series in terms of $\frac{h}{\lambda}$. The first term describes the reflection at a monolayer:

$$\Delta \approx \frac{4\sqrt{\epsilon_0}\epsilon_2\pi\cos\phi\sin^2\phi}{(\epsilon_0-\epsilon_2)((\epsilon_0+\epsilon_2)\cos^2\phi-\epsilon_0)} \cdot \frac{(\epsilon_1-\epsilon_0)(\epsilon_2-\epsilon_0)}{\epsilon_1} \cdot \frac{h}{\lambda} \tag{2.38}$$

Usually, the film thickness and refractive index are determined by computer simulations on basis of measured values of Δ and Ψ.

Quartz Crystal Microbalance (QCM)

Quartz crystal microbalance (QCM) is a simple method for the determination of the adsorbed amount of materials. The material is adsorbed on a disk of crystalline quartz electrodes covered by gold on both sides. Due to the piezoelectric properties of quartz, the quartz plate changes its sizes in an outer alternating electric field, resulting in a plate vibration (Fig. 2.5a). Eigenfrequency of the bare quartz crystal is f_0 (Fig. 2.5b). After the adsorption process the eigenfrequency change takes place, which leads to a frequency shift Δf given by:

$$\Delta f = f - f_0 \tag{2.39}$$

where f is a frequency of a quartz crystal after adsorption. Besides f, a half width of a frequency band at a height equal to half of the band maximum Γ is also important the determination of the dissipation D:

$$D = \frac{2\Gamma}{f} \tag{2.40}$$

$$\Delta D = D - D_0 = \frac{E_{dis}}{2\pi E_{stored}} \tag{2.41}$$

where D_0 and D are the dissipation factors before and after adsorption, respectively. ΔD is the change of a dissipation factor in an adsorption process, E_{dis} is the energy dissipated during one oscillation and E_{stored} is energy stored in the oscillating system.

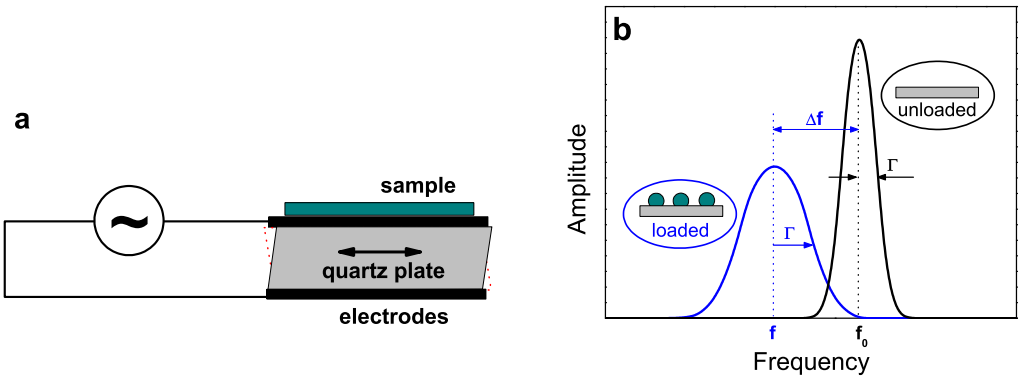

Figure 2.5: Schematic images of quartz plate in outer electric field (a) and resonance curve of the quartz plate (b). Unloaded quartz crystal plate has resonance frequency f_0 and loaded f. Γ is a half-band-half-width, Δf is shift of frequency

In QCM measurements the changes in frequency (Δf) and dissipation (ΔD) in adsorption process are measured (figure 2.6). In measurements three steps take place. In the first step the eigenfrequency of the bare quartz crystal is determined. In the second step the flow of the solution takes place and changes in dissipation and frequency are determined. In the third step the crystal is rinsed with solvent to remove unadsorbed material.

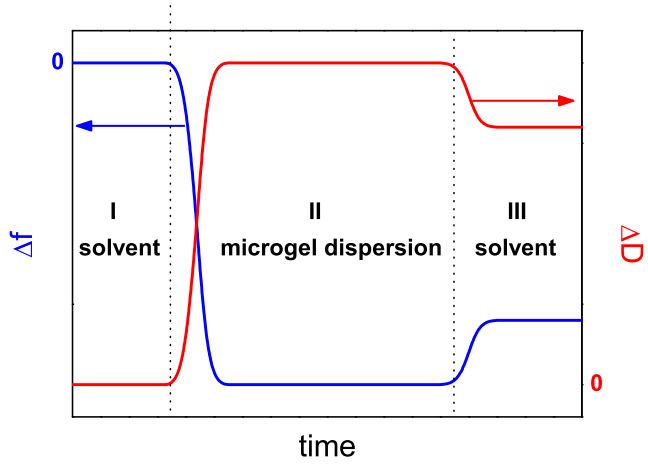

Figure 2.6: Schematic images of Δf and ΔD in QCM measurements. The classical measurement has tree steps: (I) flow of the solvent to determine the eigenfrequency of the bare quartz crystal, (II) the flow of the solution, (III) flow of the solvent to rinse not adsorbed material.

Changes of the frequency are proportional to the mass changes of the substance adsorbed on the surface of quartz crystal (Δm):

$$\Delta f = -\frac{2nf_0^2}{\sqrt{\rho_q \mu_q}} \Delta m \tag{2.42}$$

where $\rho_q = 2.648 g/cm^3$ and $\mu_q = 2.947 x 10^{11} g/(s^2 cm)$ are quartz density and shift coefficient of elasticity, respectively, n is the overtone number, Δm is measured in ng/cm^2. According to (2.42) the mass of adsorbed substance is:

$$\Delta m = -\frac{C\Delta f}{n} \tag{2.43}$$

where $C = \frac{\sqrt{\rho_q \mu_q}}{2f_0^2} = 17.7 \frac{ng}{cm^2 Hz}$. Equation 2.42 or 2.43 is also called Sauerbrey equation.

Contact Angle

One of the important characteristics of different substrates is the contact angle θ. It is a qualitative measure of the wetting of solids by a liquid. The contact angle is defined

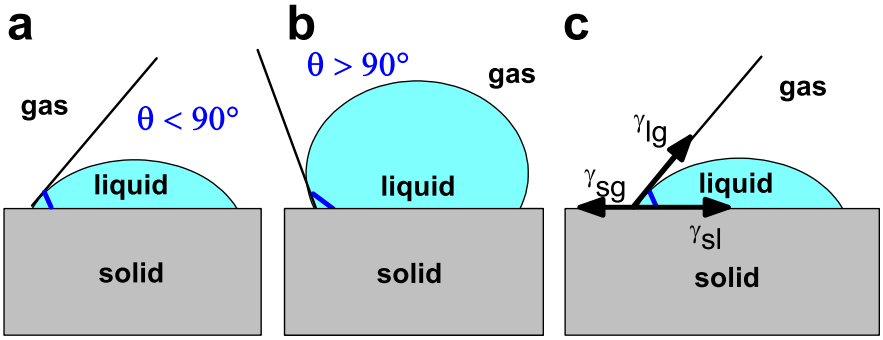

Figure 2.7: Schematic images of contact angle θ measurements. The smaller contact angle ($\theta < 90°$) means wettable surface (a), the higher contact angle ($\theta > 90°$) means non-wettable surface (b). The contact angle in terms of surface tension (c).

geometrically as an angle between a liquid drop at a solid interface in the gas phase (figure 2.7). If the liquid is water and the contact angle is smaller than 90° the surface is wettable and so called hydrophilic (Fig. 2.7a). In case of an angle, which is larger than 90° the surface is non-wettable and so called hydrophobic (Fig. 2.7b). The contact angle is also a result of interface interactions. The contact angle can be also determined according to Young's equation in terms of surface tension as (Fig. 2.7c):

$$\cos\theta = \frac{\gamma_{sg} - \gamma_{sl}}{\gamma_{lg}} \tag{2.44}$$

where γ_{sg} is the surface tension between solid and gas or surface tension of the solid, γ_{sl} is the surface tension between solid and liquid, γ_{lg} is the surface tension between solid and gas or liquid tension of liquid. The determination of the contact angle, which was used in this work, was done via the direct observation by camera of the drop shape.

Chapter 3

Experimental part

3.1 Materials

The monomer N-isopropylacrylamide (NIPAM, Aldrich), cross-linker N,N'-methylenebis-acrylamide (BIS, Aldrich), the co-monomer acrylic acid (AAc, Aldrich) and radical starter potassium persulfate (KPS, Fluka) were used for a microgel synthesis. Sodium chloride (NaCl, Merck), sodium hydroxide (NaOH, Roth), hydrogen chloride (HCl, Roth) were used to regulate the pH value and ionic strength of the microgel dispersions. Poly(ethelen-imine) (PEI, Aldrich), poly(allylamine hydrochloride) (PAH, Aldrich), poly(styrene sul-fonate) (PSS, Aldrich) and poly(diallyl-dimethyl-ammonium chloride) (PDADMAC, syn-thesised by A. Laschewsky), 3-Aminopropyltrimethoxysilane (APMS, Aldrich) were used to modify silicon wafers. The silicon wafers (Si) were obtained from Wacker Syntronic AG. Silicon wafers pre-coated with gold (Si/Au) were received from Georg Albert PVG-Beschichtungen. Ethanol (EtOH, Aldrich) and isopropanol (2-Pr, Aldrich) were used to tune the solvent quality. Water was purified by using a MilliQ-system (Millipore). The final resistance was 18 MΩ.

3.2 Microgel synthesis

Microgels were synthesized via surfactant free emulsion polymerization [92]. NIPAM, AAc, BIS were dissolved in 200 ml Milli-Q water. The mixture was heated to 70°C under a nitrogen atmosphere. To form the emulsion, the mixture was stirred with a rotation speed of 600 rpm. After one hour 1.5 mg KPS was dissolved in 1 ml Milli-Q water and rapidly added to the reaction flask. The transparent emulsion became turbid within 10 minutes after adding KPS. After 4 hours the reaction was switched off via cooling down to room temperature. The cool solution was stirred over the night under nitrogen atmosphere. To remove oligomers and unreacted monomers, microgels were cleaned by 14-days dialysis in Milli-Q water. Water was exchanged every 24 hours. After cleaning, the microgels were freeze-dried.

microgel type	NIPAM, g	BIS, g	AAc, g	BIS, %	AAc, %	$I.r._{AAc}^{titr}$, %
p1	2.26	0.154	0	5	0	0
a1	2.26	0.062	0.072	5	5	65
a3	2.27	0.154	0.144	5	10	58
a7	2.27	0.062	0.072	2	5	53
a16	2.26	0.154	0.289	5	20	75
a20	2.27	0.309	0.072	10	5	45

Table 3.1: *Characteristics of synthesized microgels. In the first column the names of samples are presented. In the second, third and fourth columns the amount of NIPAN, BIS, AAc in gram is given. The molar percentage of BIS and AAc is in the fifth and the sixth columns, respectively. The amount of incorporated AAc units is shown in the last column.* $I.r._{AAc}^{titr}$ *is an incorporation ratio of AAc derived from titration data.*

All synthesized microgels are listed in table 3.1. The first column represents the names of the microgel samples. In the second, third and fourth columns are the amount of NIPAM, BIS and AAc in reaction mixtures, respectively. The fifth and the sixth columns contain the calculated molar percentages of BIS and AAc in the reaction mixtures, re-

spectively. After the synthesis the amount of incorporated co-monomers was determined by titration and the molar percentage of incorporated AAc is given in the last column. A typical titration curve of a P(NIPAM-co-AAc) microgel dispersion is shown in figure 3.1.

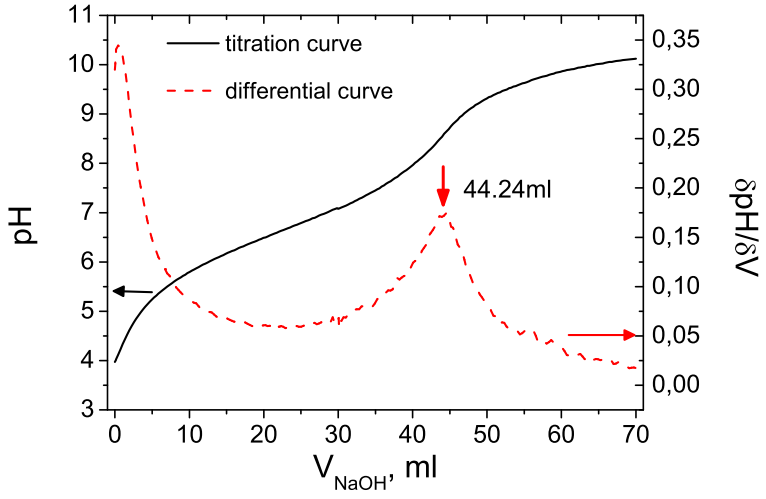

Figure 3.1: *Titration curve (compact line) of an a16 microgel dispersion with a concentration of 0.5 wt% (0.1 g a16 in 20 ml H_2O).* V_{NaOH} *is a volume of added 2.5 mM NaOH solution. The point of inflection was determined by curve numerical differentiation (dotted line).*

3.3 Microgel deposition on solid substrates

3.3.1 Substrate preparations

Two types of solid substrates were used: silicon (Si) wafers and silicon wafers pre-covered with a gold layer (Si/Au), which has a thickness of 100 nm . The silicon wafers were cleaned in piranha solution ($H_2O_2 : H_2SO_4$) for 30 minutes. Si/Au wafers were cleaned by deposition for 5 minutes in a 1:1:5 mixture of $NH_3 : H_2O_2 : H_2O$ at 75°C. Afterwards, wafers were rinsed with Milli-Q water.

For microgel deposition Si wafers were modified by adsorption of surfactants (Si/APMS) and polyelectrolyte layers/multilayers (Si/PEI, Si/PAH, Si/APMS, Si/PEI/$(PSS/PAH)_n$, where n = 1,2,3 represents the number of double layers (PSS/PAH)). Polyelectrolyte layers/multilayers were deposited by the layer-by-layer technique. For polyelectrolyte deposition layer-by-layer technique was used. To deposit PEI, wafers were deposited in a 0.1 M PEI solution for 30 minutes. Afterwards, the wafers were rinsed with MilliQ water for one minute. For deposition of PAH, PSS and PDADMAC layers, the polymers were dissolved in 0.1 M NaCl. The polyelectrolyte concentration was 0.1M. Wafers were deposited in polyelectrolyte solutions for 20 minutes. After every layer deposition wafers were rinsed three times with MilliQ-water for one minute. After rinsing of last layer wafers were dried in nitrogen stream.

For the preparation of the Si/APMS wafers the clean silicon wafers were deposited in APMS solution for ten minutes. Afterwards, the wafers were rinsed with ethanol for one minute. In order to dry the wafers, they were put in a oven at 110°C for another ten minutes.

For all experiments only fresh prepared wafers were used.

3.3.2 Microgel deposition by dip coating

Microgels were deposited by three techniques: dip coating, spin coating and direct adsorption.

Dip coating

In case of deposition at 20°C, the substrate was deposited in microgel dispersion with a concentration of 0.05 wt% for one hour. In case of deposition at 50°C, the wafers were deposited in the dispersion with a concentration of 0.015 wt% for 5 minutes, because for longer deposition and higher concentration the surface was completely covered by microgel particles and it was impossible to get at least three individual particles. After dip coating the samples were placed in the SFM liquid cell filled with water and left for one hour

for reswelling. Wafers were driven out from the microgel solution with the speed of 0.02 mm/s.

Spin coating

For spin coating SCS spin coater was used. The rotation speed varied from 500 rpm to 5000 rpm. The deposition duration was 300 seconds for all samples. In the case of thermo-induced swelling/deswelling microgel experiments, the samples were placed into the SFM liquid cell filled with water and left for one hour. In order to get individual adsorbed microgel particles in swelling/deswelling experiments, the rotation speed was 2000 rpm.

Direct adsorption

Direct adsorption taked place directly in the SFM liquid cell. By deposition at 20°C the liquid cell was filled with the microgel dispersion. After one hour the microgel dispersion in the liquid cell was exchanged twice by water in the SFM liquid cell. By deposition at 50°C few drops of microgel solution was put in the liquid cell. In 5 minutes the microgel dispersion was exchanged by water to avoid aggregate formation and to get individual adsorbed microgel particles. Samples were left for one hour. Samples prepared by direct adsorption were not dried during the preparation process. Due to the very swollen state it was not possible to take images of the particles deposited at 20°C direct after adsorption. The first measurements were carried out at 50°C.

3.4 Methods and Apparatuses

3.4.1 Scanning Force Microscopy (SFM)

SFM measurements against air were carried out with a Nanoscope IIIa from Veeco in tapping mode and with a JPK Nanowizard in intermittent mode. For studying of dry samples in air, silicon cantilevers of the type OMCL-AC160TS from Olympus were used.

SFM measurements in liquids were done in an ECCell (electrochemical cell) from JPK using a JPK NanowizardII instrument in the intermittent contact mode. For these measurements, uncoated silicon cantilevers CSC17 from Micromash were used (Fig. 2.3).

In order to investigate the thermo-induced swelling/deswelling behavior of adsorbed microgels three types of experiments in the liquid cell were carried out:

1. In short cycles (s.c.) the temperature was changed between 20°C, 50°C and 20°C with 15°C steps.

2. In long cycles (l.c.) samples were heated or cooled with 5°C steps.

3. Reswelling cycles (r.c.) were carried out after main measurements (long or short cycles). In reswelling cycles samples were completely dried. In 12 hours the samples were immerse in liquid again and one short cycle was carried out.

The heating/cooling rate was 15°C/30 minutes in short and reswelling cycles and 5°C/15 minutes in long cycles.

For particle characterization, their volume was calculated (equation (2.31)). In order to minimize the effect of scanning rates and setpoint on the particles shape, particle cross sections were evaluated in vertical direction (parallel to the slow scan axis). In every SFM measurement, the particle volume was determined at least for three adsorbed microgel particles.

3.4.2 Ellipsometry

For ellipsometry measurements and their evaluation an Optrel multiscope ellipsometer and software Elli from Optrel GBR were used. Ellipsometry measurements were carried out in a Nullellipsometry mode. Here, the polarization of the incident light is selected in such way that the ellipticity is canceled after reflection. That means incident elliptically polarized light is converted into linear polarized light which is then canceled by analyzer (Fig. 3.2).

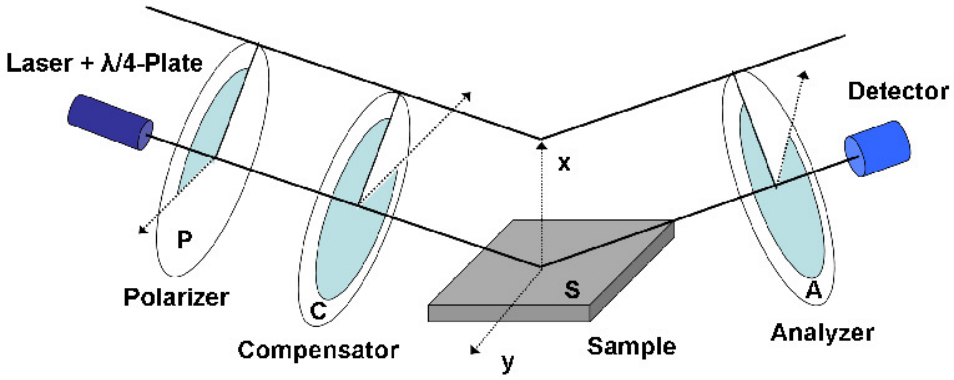

Figure 3.2: *Schematic image of an ellipsometer in a PCSA-configuration.*

3.4.3 Dynamic Light Scattering (DLS)

Dynamic Light Scattering (DLS) measurements were carried at the constant scattering angle of 75° using an ALV goniometer setup. Only one angle was chosen due to the microgel monodispersity. A Nd:YAG laser with a wave-length of 532 nm and an ALV-5000 correlator were used. In DLS measurements auto-correlation functions were recorded and analyzed by inverse Laplace transformation.The calculation was done by using the program CONTIN [86].

The heating/cooling rate was 2°C/30 minutes.

3.4.4 Quartz Crystal Microbalance (QCM)

QCM measurements were carried out with Q-Sense E1 from Q-Sense.

3.4.5 Contact Angle Measurements

Contact angle measurements were carried using the Contact Angle System OCA. For the contact angle estimation, the Sessile Drop-Method was used. All contact angle measurements were done by Michael Eisele from the Technical University of Berlin.

3.4.6 Mobility Measurements

Mobility measurements were done by Malvern Zetasizer 2000.

3.4.7 Titration

For titration of co-monomer microgel dispersions a Titrando 836 system from Metrohm was used. Titration was done by using a 0.025M NaOH solution.

Chapter 4

Control of microgel number density at solid surfaces

One of the important and widely investigated areas of colloidal particles is the controled adsorption of colloids at different interfaces. The aim of these investigations is to produce monolayers of adsorbed colloids with appropriate structures [37–41, 82, 93, 94]. As discussed above, PNIPAM-co-AAc microgels are sensitive to changes of environmental conditions such as pH, temperature and ionic strength [6, 18, 22, 23, 95]. That makes the materials based on PNIPAM interesting for functionalization of surfaces. There are only few works on adsorbed microgel particles, which forms monolayers on different substrates [35, 36, 42]. It was shown that the amount of adsorbed microgels and the structure depends on the deposition method, pH-value of the solvent, and the substrate roughness.

In the present chapter the control of adsorbed microgel particles amount by different preparation conditions is shown. All samples were deposited by spin coating on Si/PEI wafers. For these purposes microgels with 5% BIS and 10% AAc (a3) were used (table 3.1).

To get information about the microgel particle size and mobility in dependence on the pH, ionic strength and temperature, DLS and electrophoretic mobility measurements were done.

4.1 Effect of the rotation speed

Figure 4.1 shows the SFM images of adsorbed microgel particles deposited from microgel dispersions dissolved in 10^{-3}M HCl (a-d) and 10^{-3}M NaOH (e-h). Samples were prepared via spin coating. The concentration of microgel dispersions was 0.5 wt%. For both microgel dispersions, the effect of rotation speed was investigated. For a rotation speed of 500 rpm, both dispersions give a monolayer of closely hexagonally packed particles. With increasing rotation speed, the amount of adsorbed particles decreases. For the samples prepared with rotation speeds from 2000 rpm on (c, d and g, h), the deposition of adsorbed particles for the appropriate pH does not depend on the rotation speed anymore. The steady state is reached.

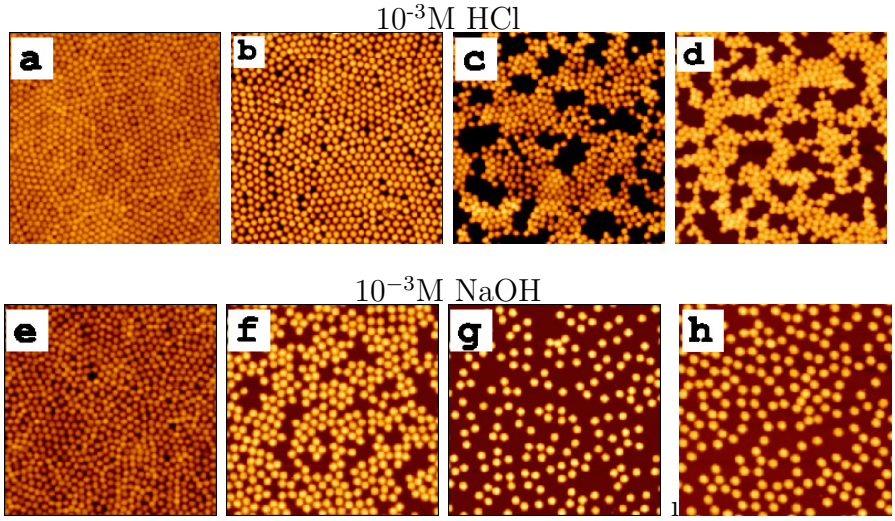

Figure 4.1: *SFM images of dried samples. Effect of rotation speed and pH. All samples prepared from the microgel dispersions with concentration of 0.5 wt%. Substrate: Si/PEI. (a-d) microgels were dissolved in 10^{-3}M HCl, (e-h) in 10^{-3}M NaOH. Rotation speeds: (a, e) - 500 rpm, (b,f) - 1000 rpm, (c,g) - 2000 rpm, (d,h) - 5000 rpm. Scan size: 10x10 μm^2.*

A qualitative explanation is that at the beginning of rotation, an aqueous dispersion film forms and only the microgel particles within this film can adsorb onto the surface. At 500 rpm the dispersion film is quite thick and also particles from the "film bulk" can adsorb at the surface. With increasing rotation speed, the centrifugal force grows and the

thickness of the dispersion film decreases. At 2000 rpm only the particles from a very thin water layer close to the wafer surface can be deposited. The other particles are already expelled together with the solvent. From 2000 rpm on, the time of lateral expulsion of microgel particles in the thin dispersion film is assumed to be longer than the microgel adsorption time. That leads to a constant number of adsorbed particles above 2000 rpm.

4.2 Effect of microgel particle concentration

To change the amount of adsorbed particles, the concentration of the microgel dispersion was reduced from 0.5 wt% to 0.05 wt% (Fig. 4.2). Samples (a-c) were prepared from dispersions at a concentration of 0.05 wt% and samples (d-f) were prepared at 0.5 wt%. For both concentrations the pH of microgel dispersions increases from left to right. The

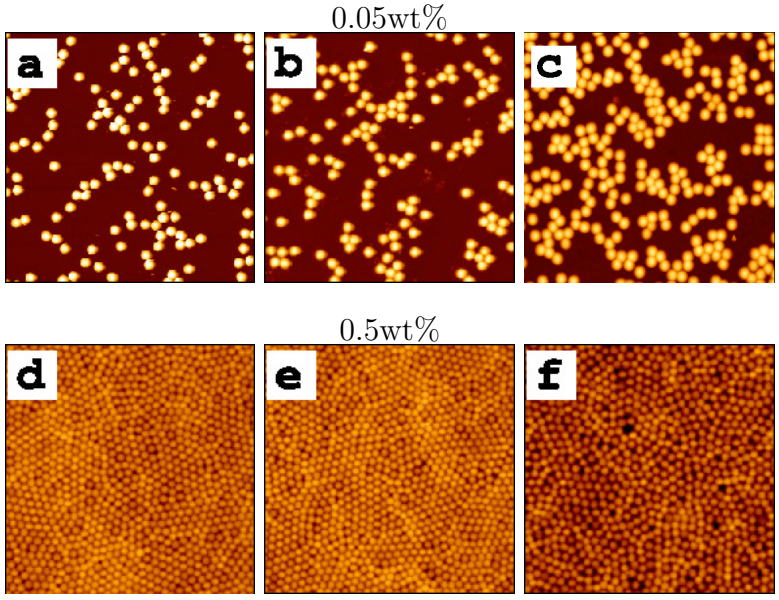

Figure 4.2: *Effect of microgel particle concentration and pH. The rotation speed is 500 rpm for all images. Samples (a-c) were prepared from the microgel dispersion at a concentration of 0.05 wt% on Si/PEI; (d-f) from dispersions at a concentration of 0.5 wt%. For samples (a,d) 10^{-3}M HCl was used as solvent; (b,e) - 10^{-3}M NaCl; (c,f) - 10^{-3}M NaOH. Scan size: 10x10 μm^2.*

rotation speed was fixed at 500 rpm and the ionic strength was kept constant at 10^{-3} M.

The number density of deposited microgel particles increases with increasing particle concentration. At the concentration of 0.5 wt%, the substrate coverage by microgels was mostly homogeneous. Only small domains with a microgel multilayer were found.

For the samples prepared from a dispersion at a concentration of 0.05 wt%, the number density of adsorbed microgels increases with increasing pH. At the higher concentration of 0.5 wt% the adsorbed particles are closely hexagonal packed. The effect of the pH is less pronounced, but with growth in pH, the number of defects *i.e.* holes or empty spaces in the package increases. That means that the pH has an opposite effect on the packing density at both concentrations.

4.3 Effect of pH

pH values of microgel dispersions with concentrations of 0.05 and 0.5 wt% are shown in table 6.1 in chapter 6. Since both the PEI on the substrate and the acrylic acid monomers within the microgel particles are weak electrolytes counteracting effects on the adsorbed amount occurs during pH variation. PEI is positively charged up to a pH about 9-10 [96] and the pK_s of acrylic acid is between 4.5 and 5. That means that between pH 5 and 10, a stronger attraction between particles and substrate than in the acid medium takes place. Due to the increasing particle-substrate attraction with increasing pH, the number of adsorbed particles enhances for samples prepared from microgel dispersions with a concentration of 0.05 wt% (Fig. 4.2 a-c). On the other hand, interparticle repulsion becomes larger between pH 5 and 10 than at acid pH values resulting in the reduction of the number density. At a concentration of 0.5 wt%, the particle density on the substrate decreases with increasing pH (Fig. 4.2 d-f). This indicates a dominating effect of the electrostatic repulsion between particles. That would mean that the effect of the particle-substrate attraction would play a minor role at higher pH.

The fact that the particles also adsorb at low pH, where almost no electrostatic attraction between particles and substrate is present, is explained by hydrogen bonding between

particles (both NIPAM and AAc monomers) and the substrate [97]. Note, that at low pH the silanol group at the silicon wafer are not dissociated and the PEI does not fully cover the substrate. Hence, hydrogen bondings between P(NIPAM-AAc)particles and the silicon substrate silanol groups) can be formed.

4.4 Effect of number of deposition

Another way to control the numerical density of adsorbed particles is the repetition of the spin coating process with the lower concentrated dispersion. Figure 4.3 represents the SFM images of adsorbed microgels deposited from 0.05 wt% microgel dispersion in 10^{-3}M HCl. Due to the small particle concentration the wafer is not covered completely after spin coating (Fig. 4.3a). To increase the surface coverage by particles, the wafer was covered again by microgels via spin coating. The number of adsorbed particles increases (Fig. 4.3b). After the second spin coating the wafer still exhibits a big part of empty surface. After the third spin coating procedure (Fig. 4.3c), the uncovered by microgels surface area decreases. It means that repeated particle deposition is a simple way to increase surface coverage.

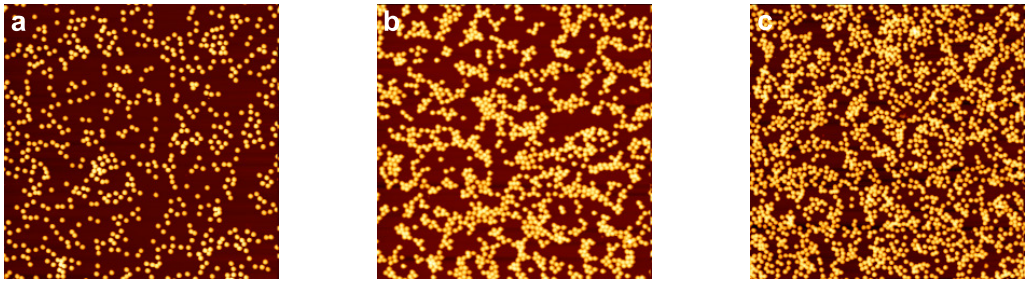

Figure 4.3: *SFM images of microgels deposited on Si/PEI by repeated spin coating with the rotation speed of 1000 rpm. Microgels were deposited from dispersion in 10^{-3}M HCl and a concentration of 0.05wt%. The same wafer was spin coated three times. After every spin coating process the SFM images were taken: (a) after the first spin coating, (b) after the second, and (c) after the third. Scan area is 20x20 μm^2.*

4.5 Summary

pH and temperature sensitive P(NIPAM-co-AAc) particles were deposited on oppositely charged solid substrates. It was shown, that the surface coverage of the microgel particles depends strongly on the pH and on the microgel concentration. The rotation speed during the spin coating process and the number of repeated deposition procedures play an important role. A combination of these parameters can control the amount of adsorbed particles.

With increasing rotation speed, the particle density decreases and is constant from 2000 rpm on, which is explained by a competition between the adsorption time and the time needed for lateral expulsion of the thin dispersion film on top of the silicon substrate. At low particle concentration (0.05 wt%) of the dispersion the particle number density at the solid substrate increases with increasing pH, due to an enhanced attraction between the AAc monomers of the particles and the oppositely charged substrate. At high particle concentration the increasing interparticle repulsion comes into play, which decreases the adsorbed amount with increasing pH.

Chapter 5

Influence of internal microgel parameters

As discussed above, properties of microgels depend strongly on the cross-linker and co-monomer content [9, 17–24]. The current chapter focuses on the influence of the cross-linker content and co-monomer content on the temperature-induced swelling/shrinking behavior of microgel particles.

5.1 Effect of Co-monomer Content

Properties of PNIPAM-based microgels can be tuned by adding co-monomers during synthesis [9, 11, 18–20]. One type of commonly used co-monomers are organic acids like vinylacetic, acrylic, methacrylic, allylacetic acid *etc.* [9, 17–19, 51].

There are some theoretical and experimental works studying charged microgel particles, the influence of the co-monomer types and their concentration on microgel swelling/ deswelling behavior [9, 18, 19, 51, 98]. In case of using weak acids as co-monomer microgels become also pH-sensitive. Due to the deprotonation of carboxylic (-COOH) groups, the interchain electrostatic repulsion increases leading to the increasing particle size [9, 16, 17]. T. Hoare and R. Pelton illustrated that high ionized microgels have a sharp transition and that the LCST is shifted to higher temperatures [18, 19]. Kratz *et.al.* [17] demonstrated

the appearance of a two step volume phase transition for microgels with very high co-monomer concentration. This phenomenon can be attributed to the competition between attractive hydrophobic and repulsive electrostatic forces.

Microgel sensitivity to outer stimuli was also investigated for adsorbed microgel particles. It was shown that the film thickness made of microgels containing co-monomers can be controlled by temperature, ionic strength and as well as pH [16, 36, 42].

Authors [14, 16, 35, 39, 40] investigated the ability of PNIPAM-based microgels to form well organized structures at solid surfaces. Schmidt *et.al.* [35] demonstrated that pure PNIPAM microgels particles and particles containing acrylic acid as co-monomer form well organized structures at solid surfaces. The particle charge was managed by the solvent pH value. The aim of this chapter is a detailed investigation of PNIPAM microgels containing acrylic acid as co-monomer with concentrations of 0%, 5%, 10% and 20%. This chapter focuses mainly on the study of thermoinduced swelling/deswelling behavior of individual adsorbed microgels, microgels in bulk and their adsorption ability, as well.

5.1.1 Microgel characterizations in volume phase

Firstly, the behavior of microgel particles in bulk was investigated. Figure 5.1 demonstrates the dependence of hydrodynamic radius on temperature measured by DLS for four types of microgel particles: (a) pure PNIPAM,(b) with 5%, (c) 10% and (d) 20% of AAc co-monomers. It can be seen that for all types of microgels the thermoinduced swelling and shrinking is completely reversible and a slight shift in the LCST takes place in cooling and heating processes (table 5.1). As it was expected, the hydrodynamic radius increases with increasing AAc content because of the increasing electrostatic repulsion between the polymer chains. Increasing concentration of AAc co-monomers leads to an appearance of the two step phase transition.

Pure PNIPAM microgels demonstrate a sharp transition at the temperature of about 30-31°C, which is in good agreement with the literature [9, 18, 73]. With increasing

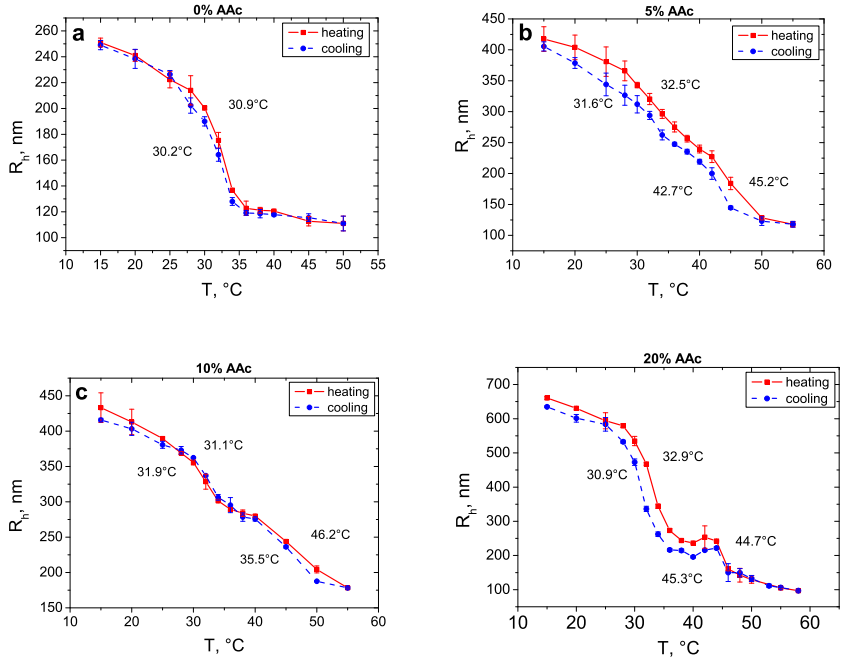

Figure 5.1: *Temperature dependence of the hydrodynamic radii of microgel particles with 0% (a), 5% (b), 10% (c) and 20% (d) AAc contents on temperature measured by DLS in heating (squares) and cooling (circles) processes.*

AAc	R_h, nm		$\|\mu_h\|$, μmcm/Vs	transition temperature, °C			
content, %	20°C	50°C	20°C	heating		cooling	
0	241	111	0.81	30.9		30.2	
5	404	128	1.41	32.5	45.2	31.6	42.7
10	413	204	1.71	31.1	46.2	31.9	45.5
20	631	130	2.24	32.9	44.7	30.9	45.3

Table 5.1: *Characteristics of microgel particles with 0%, 5%, 10% and 20% AAc in bulk: hydrodynamic radius (R_h) at 20°C and at 50°C, mobility (μ) at 20°C and transition temperatures in heating and in cooling cycles.*

AAc content the second transition step becomes more pronounced. It appears due to the charged co-monomers. Microgels with the highest AAc content (20%) exhibit two very well separated and resolved transition steps. The first transition takes place at a temperature of about 32°C, which results from the PNIPAM component caused by hydrophobic attraction. The second transition appears at a temperature of about 45°C and is attributed to the electrostatic repulsion between the charged co-mononers. The transition temperature does not depend on the microgel type.

5.1.2 Swelling behavior of adsorbed microgel particles

In order to investigate the swelling/deswelling behavior of adsorbed PNIPAM microgels SFM measurements were performed in a temperature controlled liquid cell. Figure 5.2 shows the SFM images of all four types of microgel particles deposited on Si/Au wafers at 20°C (swollen state) and at 50°C (collapsed state). It can be observed that the particle size increases with enhancing the amount of co-monomer.

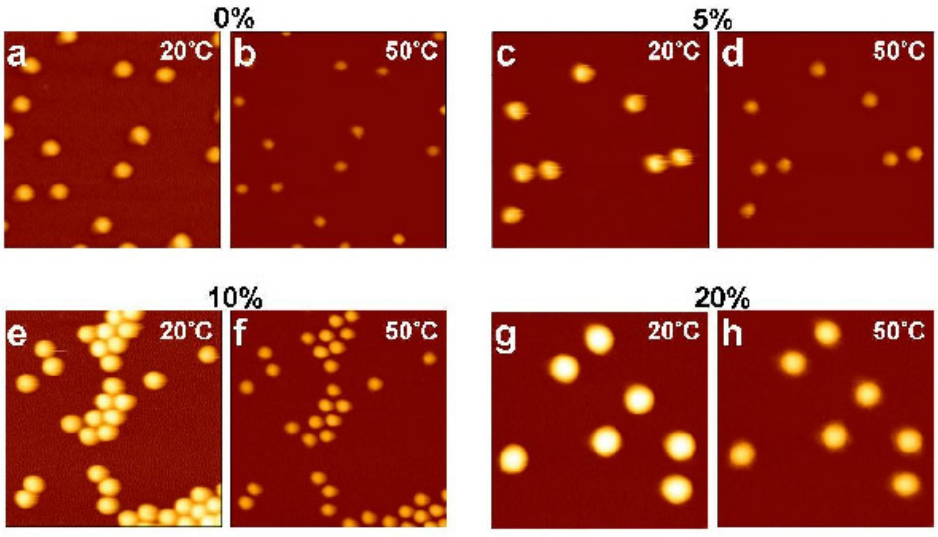

Figure 5.2: *SFM images of microgel particles with 0% (a, b), 5% (c, d), 10% (e, f) and 20% (g, h) AAc content deposited on Si/Au wafers in SFM liquid cell at 20° C (a, c, e, g) and at 50° C (b, d, f, h). Scan area: 5x5 μm^2.*

In order to compare the behavior of deposited microgels, the cross sections of particles with 0%, 5%, 10% and 20% AAc in swollen (20°C) and collapsed states (50°C) in two short cycles are represented in figure 5.3. All adsorbed microgels demonstrate a reversible thermoinduced swelling/shrinking behaviour. The size changes of adsorbed microgels mainly take place in a vertical direction. The particle size increases with increasing co-monomer content due to the increasing intraparticle charge repulsion.

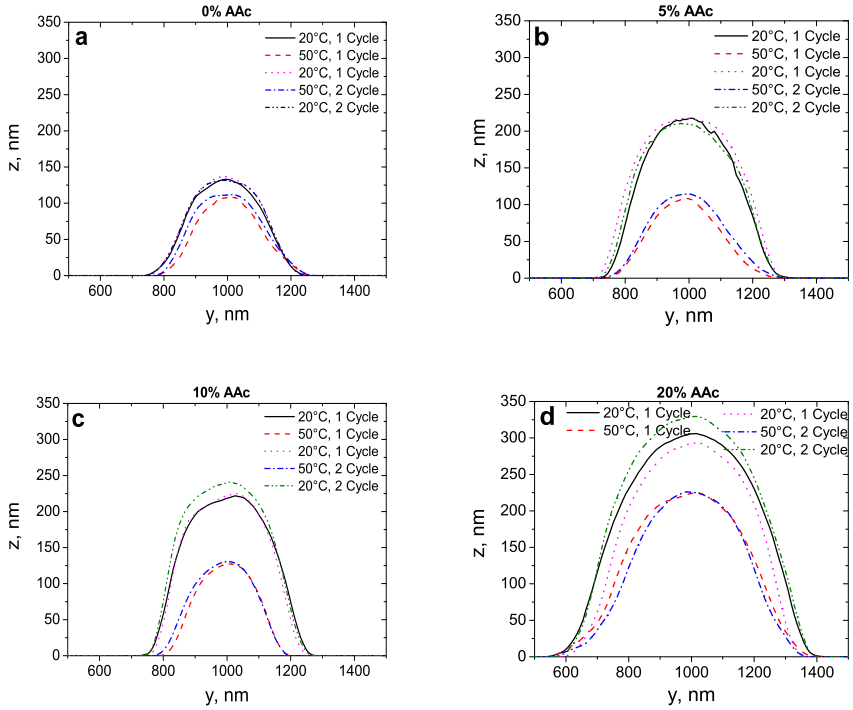

Figure 5.3: *Cross sections of microgel particles with (a) 0%, (b) 5%, (c) 10% and (d) 20% AAc contents adsorbed on Si/Au measured by SFM at two short cycles: 20°C, 50°C, 20°C, 50°C and 20°C.*

For a better understanding in the swelling/deswelling behavior of adsorbed microgels with different AAc contents one long cycle was carried out. Based on cross section data, figure 5.4 demonstrates the volume change of adsorbed microgels as a function of temperature. Adsorbed microgels demonstrate a reversible thermo-induced swelling/shrinking behavior. A slight shift in the LCST takes place in cooling and heating processes (table

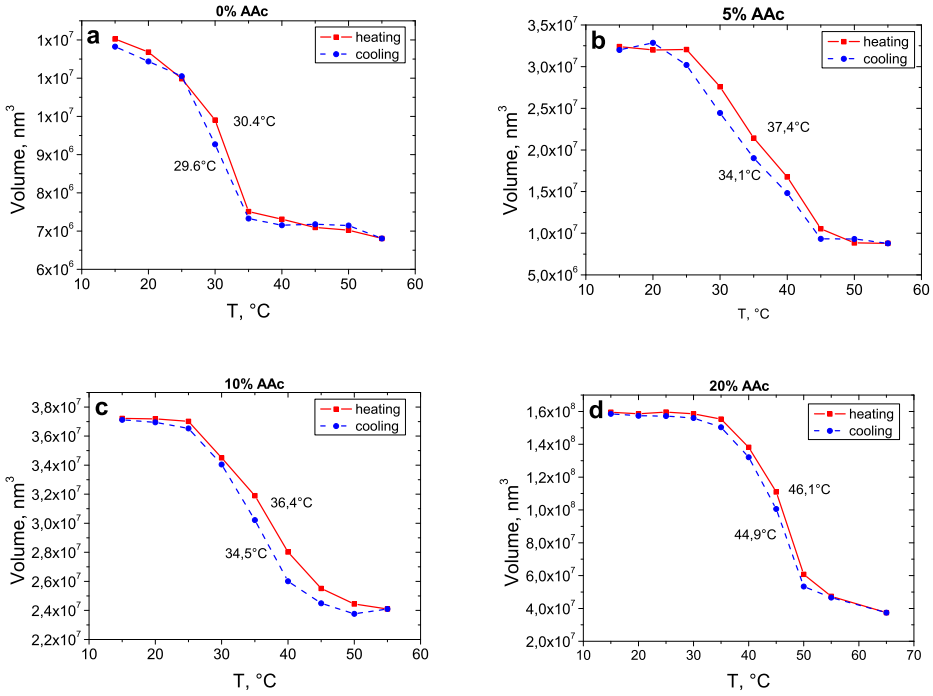

Figure 5.4: *Temperature dependence of volume of microgel particles with 0% (a), 5% (b), 10% (c) and 20% (d) AAc contents deposited on Si/Au measured by SFM.*

5.2). For all four microgel types, adsorbed particles have just one transition temperature.

AAc	LCST, °C		Volume, x10^6 nm^3			$V^T{}_{ads}/V_{dry}$	
content, %	heating	cooling	dried	20°C	50°C	T = 20°C	T = 50°C
0	30.4	29.6	5.34	11.7	7.02	2.2	1.3
5	37.4	34.1	5.76	32.0	8.84	5.6	1.5
10	36.4	34.5	6.95	37.2	24,4	5.4	3.5
20	46.1	44.9	32.9	159	60.8	4.8	1.8

Table 5.2: *Characteristics of adsorbed microgel particles for microgels with 0%, 5%, 10% and 20% AAc contents: LCST in heating and cooling cycles, volume of deposited microgels in dry state and in liquid at 20° C and 50° C, and particle volume in liquid cell ($V^T{}_{ads}$) at temperature T normalized by volume of dried particles (V_{dry}).*

Tendentiously, with increasing co-monomer content the LCST shifts to higher temperatures. The LCST of pure PNIPAM microgels (0% AAc) and extremely high AAc concentration (20%) are sharper compared to those particles with 5% and 10% AAc. Adsorbed pure PNIPAM microgels and microgels in bulk have the LCST at the same temperature of 30°C (tables 5.1 and 5.2). The transition temperature of deposited microgels with 20% AAc is at the temperature of around 45°C. It corresponds to the second transition of microgels in bulk effected by high co-monomer concentration. Particles with an AAc concentrations of 5% and 10% have broad phase transition at temperatures between 34°C and 37°C.

In figure 5.5 the volume of deposited microgels in the swollen and in the collapsed state in long cycle (l.c.) and in two reswelling cycles (r.c.) is represented. Reswelling cycles demonstrate the thermo-induced behavior of adsorbed particles after the complete drying. One can see, microgels still exhibit a sensitivity to temperature changes and show reversible swelling/deswelling behavior. The reswollen microgels exhibit the same volume values as before drying.

Microgels in volume phase and deposited at solid surface demonstrate qualitatively similar behavior (Fig. 5.6). Both systems show a reversible phase transition, where in

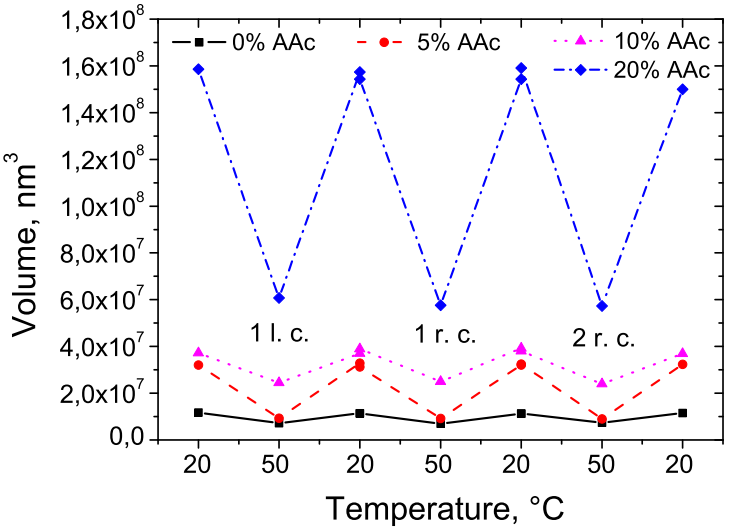

Figure 5.5: *Temperature dependence of volume of microgel particles with 0% (squares), 5% (circles), 10% (triangles) and 20% (rhombs) AAc contents deposited on Si/Au measured by SFM in one long cycle (l.c.) and in two reswelling cycles (r.c.).*

swollen state the particle size increases with increasing AAc concentration.

5.1.3 Influence on number density of adsorbed microgel

In order to investigate adsorption properties of microgel particles with different co-monomer contents at solid interfaces QCM-D and SFM measurements were carried out. 0.05 wt% and 0.5 wt% microgel dispersions solved in 10^{-3}M NaCl were used for QCM and SFM measurements, respectively.

From QCM measurements the mass of adsorbed microgels was calculated according to equation (2.43) (Fig. 5.7). After microgel deposition samples were rinsed with solvent. 27% of pure PNIPAM microgels were desorbed during rinsing process. The amount of adsorbed microgels with 5% AAc is smaller than for pure PNIPAM particles. AAc co-monomers affect the particle charge. With increasing AAc concentration the particle charge increases as well. This fact is proven by the increased value of particle mobility

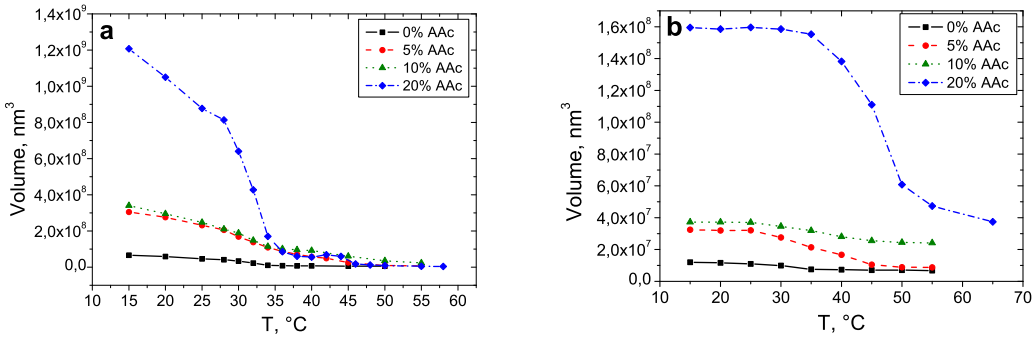

Figure 5.6: *Temperature dependence of microgel particle volume (a) in bulk and (b) deposited on Si/Au with 0% (squares), 5% (circles), 10% (triangles) and 20% (rhombs) AAc contents measured by DLS and SFM, respectivly.*

(Tab. 5.1) and SFM images (Fig. 5.8). Due to the enhanced particle charge, interparticle electrostatic repulsion increases leading to a decrease in the amount of adsorbed particles. On the other hand, the electrostatic substrate-particle attraction becomes stronger resulting in the absence of particle desorption during the rinsing process.

The number density and the amount of adsorbed microgels with 10% AAc is higher than for particles with 0% and 5% AAc (Fig. 5.7 and 5.8). With increasing AAc concentration the particle charge increases resulting in the enhance in the stronger substrate-particle attraction. It seems to be that the substrate-particle attration dominates the interparticle repulsion resulting in an increased number density and mass of adsorbed microgels.

By the further increase in the co-monomer content, the mass of adsorbed particles (20% AAc) decreases and becomes lower than for particles with 10% AAc but it is still higher than for microgels containing 0% and 5% of charged co-monomers. Microgels with 20% AAc are extremely charged and large (Tab. 5.1). Due to the large size, it becomes for such huge particles more difficult to "see" an empty place or an uncovered by microgels substrate surface. The increasing particle charge are resulting in the increasing interparticle repulstion. Both these phenomena lead to the increase in the mass of adsorbed

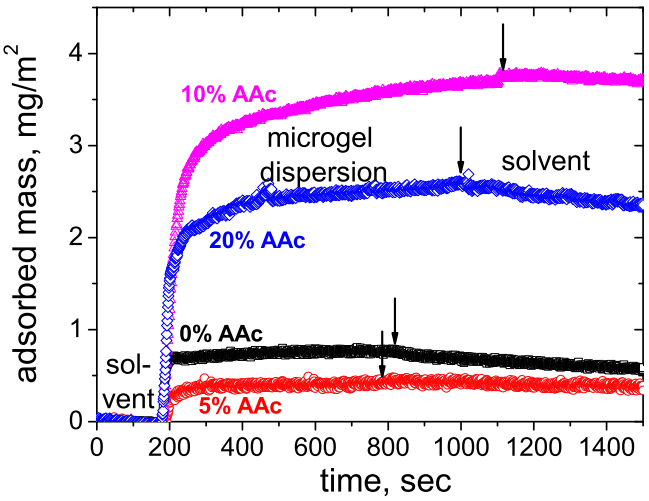

Figure 5.7: *Time dependence of mass changes of microgels with 0% (squares), 5% (circles), 10% (triangles) and 20% (rhombs) AAc contents adsorbed on gold crystals in QCM measurements. In first step the crystal was washed with the solvent (10^{-3}M NaCl). After 180 sec microgels were adsorbed from microgel dispersions with a concentration of 0.05 wt% in 10^{-3}M NaCl. After the equilibrium was achieved (pointer on the graph) crystals were rinsed with the solvent to remove unadsorbed particles.*

particles (Fig. 5.7).

It is also interesting to notice that the adsorption ability of microgel particles at solid interfaces does not depend on the the substrate type. The amount of microgels deposited on gold (Fig. 5.7) and on Si/PEI (Fig. 5.8) as function of co-monomer content exhibits qualitatively the similar behavior in both experiments.

By comparison of volume of adsorbed microgels in dried state and in liquid (table 5.2) one can conclude that the water adsorption ability increases with increasing co-monomer content and microgels at 50°C still contain water. Unfortunately, it was not possible to calculate the absolute amount of water contained in swollen and collapsed microgels particles in the adsorbed state because water amount in dry microgels measured against

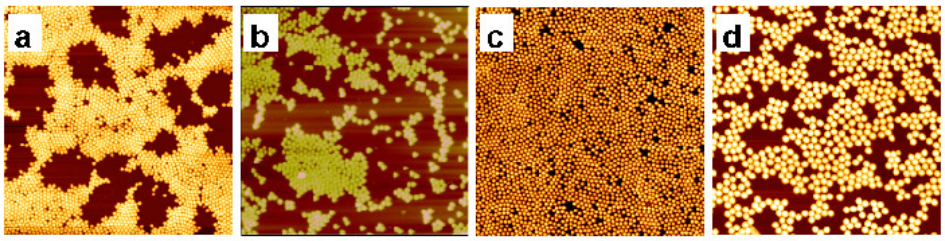

Figure 5.8: *SFM images of microgel particles with (a) 0%, (b) 5%, (c) 10%, and (d) 20% AAc contents deposited from microgel dispersions with concentration of 0.5 wt% on Si/PEI wafers by spin coating with rotation speed of 1000 rpm. Scan area: 20x20 μm^2.*

air is not known and could not be estimated.

5.1.4 Summary

It was shown that the particle size and the transition temperature can be influenced by the co-monomer concentration for both systems: for particles deposited at surface and for particles in bulk. Particle charge plays an important role in the deposition process. Those particles with an AAc concentration below 10%, the particle-surface attractive interactions dominate the interparticle electrostatic repulsion. Consequenctly, the surface coverage increases with increasing AAc content. For particles with 20% AAc interparticle repulsion becomes dominant and the surface coverage decreases. Water absorption abilities of particles increases with increasing co-monomer content. The substrate type does not affect strongly on the adsorption ability of microgels.

5.2 Effect of Cross-linker Content

It was shown that the amount of cross-linker content strongly affects the microgel properties [24, 75]: the particles with more cross-linker content demonstrate a weaker swelling/ shrinking than the microgels with low cross-linker density do. The amount of cross-linker also changes the internal structure of microgels. Microgels with higher cross-linker content

demonstrate the core-shell like structure: a core with high cross-linker density and a shell with lower cross-linker density [24, 75].

For the current investigation microgels containing 5% AAc and different amount of cross-linker BIS were used. The BIS content was 2%, 5% and 10%. The characteristics of these microgel particles are given in table 3.1.

5.2.1 Microgel characteristics in volume phase

Three types of microgel particles with different cross-linker contents (2%, 5%, 10% BIS) were synthesized. All microgels contained 5% AAc. The microgels in volume phase were characterized by DLS. They demonstrate the typical behavior of the value of swelling ratio: particle volume (V) normalized with the volume at 15°C ($V^{15°C}$) increases with increasing cross-linker content at high temperatures (Fig. 5.9). The LCST is determined from the point of inflection (Tab. 5.3).

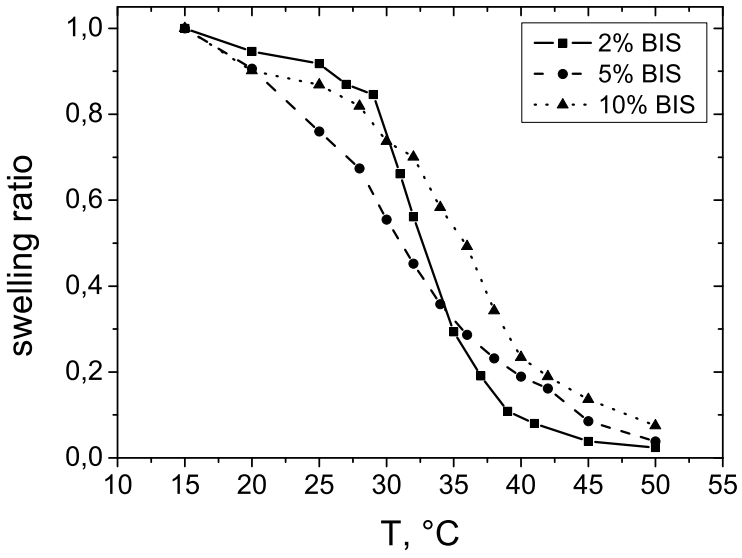

Figure 5.9: *Swelling ratio of microgels in bulk as function of temperature for microgels with 2% (squares), 5% (circles) and 10% (triangels) BIS contents measured by DLS*

	Volume Phase		Adsorbed Microgles					
BIS,	LCST,	α	LCST,	α	height/width		V_{DLS}/ V_{AFM}	
%	°C	50°C	°C	50°C	20°C	50°C	15°C	50°C
2	33	0.024	35	0.19	0.21	0.07	10	1.1
5	30	0.039	37	0.29	0.26	0.1	9.7	1.3
10	35	0.074	33	0.47	0.46	0.48	7.2	1.1

Table 5.3: *Characteristics of microgels in bulk: the LCST and swelling ratio α, and deposited at the surface: LCST, swelling ratio, height/width ratio at 20° C and 50° C; and volume of microgels in bulk normalized with respect to the volume of adsorbed microgels at 15° C and at 50° C. Characteristics for deposited particles were taken from the heating process of the second long cycle.*

The amount of incorporated AAc co-monomers decreases with increasing cross-linker content (table 3.1). It was shown that microgel particles build a core-shell structure [24], where the core has a higher cross-linker density compared to the shell. It was also demonstrated that charged co-monomers are situated preferentially in the outer microgel layer [19]. The increase in the cross-linker content leads to a decrease of the shell thickness. Due to the thin thickness of the shell, the repulsion between charged network units increases leading to the decreasing concentration of incorporated AAc units.

5.2.2 Individual adsorbed microgels

To investigate the thermoresponsive shrinking and swelling behavior of individual microgel particles adsorbed on Si/Au the SFM technique in liquid was used. Figures 5.10 and 5.11 show SFM images and cross sections of microgels with 2% BIS content during the first long cycle: 15°C, 35°C, 55°C, 35°C and 15°C, respectively. The change in microgel size is obvious. In order to get a better insight into the swelling ratio the volume of deposited particles was calculated from cross sections and is shown in figure 5.12. The process does not seem to be completely reversible. Microgels with 2% cross-linker show a strong

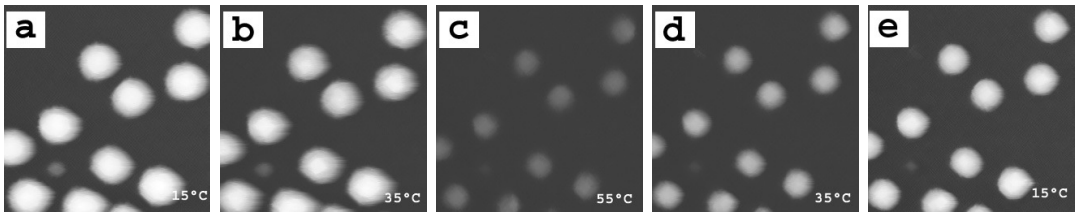

Figure 5.10: *SFM images against water of microgels with 2% BIS adsorbed on Si/Au in the first long cycle: at (a) 15°C, (b) 35°C, (c) 55°C, (d) 35°C, and (e) 15°C. Measurements were carried out in intermittent mode. Scan area: 5*x*5*μm^2.

hysteresis during the first long cycle. The LCST at the cooling process is shifted by 2.2°C to 34.4°C with respect to the heating curve. After the cooling process in the first long cycle the microgel height and footprint becomes smaller than before the heating process; at 15°C particle volume changes from $1.2 \times 10^8 nm^3$ to $7.6 \times 10^7 nm^3$. During the second long cycle the LCST is again shifted by 2.1°C to 32.6°C, and the hysteresis is more or less vanished after the second long cycle. With the increasing cross-linker content the hysteresis decreases. With increasing cross-linker content the slope around the point of inflection increases *i.e.* the transition becomes sharper.

Cheng et. al. [99] showed that PNIPAM homopolymers are able to build intra and inter polymer chain hydrogen bonds during the heating process. Those H-bonds can be broken during a subsequent cooling process to a temperature of about 4°C. In the present experiment the microgels were cooled down to 15°C and the H-bonds were observed not to disappear completely. The remaining H-bonds can be considered as new additional cross linkers. Due to these new cross linkers, the particles can not swell to their initial sizes and the hysteresis takes place. With increasing BIS content the chain length between two cross linkers decreases and the intrachain hydrogen bonds can not be formed during the heating process, resulting in a smaller hysteresis.

In order to compare the effect of cross linker on the swelling/shrinking behavior the swelling ratio of all three gel particles after adsorption at the Si/Au substrate is shown in figure 5.13. The adsorbed particles demonstrate the behavior similar to microgels in the volume phase: with increasing BIS content the swelling ratio of adsorbed microgels

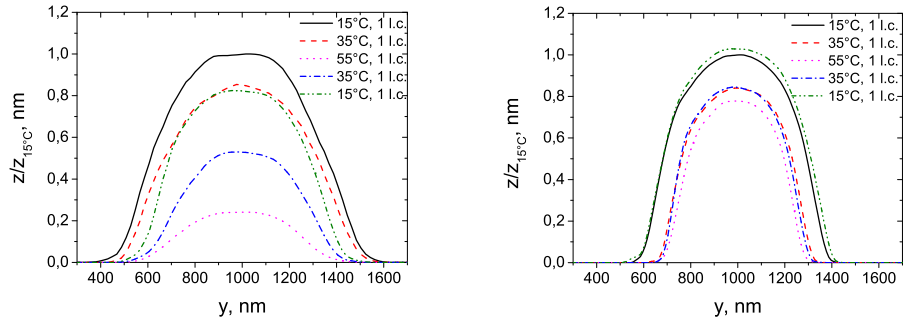

(a) 2% BIS (b) 10% BIS

Figure 5.11: *Cross sections of individual microgel particles with (a) 2% and (b) 5% BIS adsorbed on Si/Au in dependence on temperature. The data from the first long cycle (l. c.). The cross sections at temperatures 15° C, 35° C, 55° C, 35° C,15° C are represented. In order to demonstrate the qualitative differences in the thermo-induced swelling/deswelling behavior of adsorbed particles with lower and higher cross-linker contents, the relative changes in particle height* $z/z_{15°C}$ *are shown.*

decreases.

To be sure that the hysteresis disappears after the first and the second long cycles, two short cycles between 20°C and 50°C with 15°C steps were driven. The volume normalized by the particle volume at 20°C in the first short cycle is shown in figure 5.14. It was observed that all three types of microgels adsorbed on the surface have a reversible thermo-induced behavior. With increasing number of heating processes, the hysteresis decreases. The adsorbed microgels demonstrate the thermoresponsive behavior in reswelling experiments as well. The samples were dried at room temperature over night. For SFM measurements the sample was left in liquid to reswell. After one hour the SFM measurements were performed. No microgel particle desorption could be observed during the reswelling process. It should be noted that the microgels deposited on the solid surface still exhibit the swelling/shrinking behavior even after the complete sample drying.

The characteristics of microgel particles such as the LCST, swelling ratio of microgels in bulk; the LCST in the heating process of the second long cycle, the swelling ratio, the

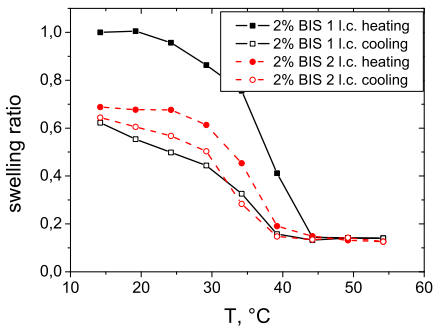

(a) 2% BIS

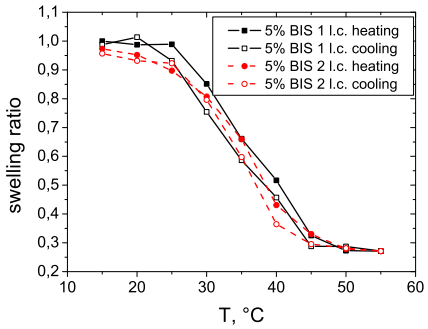

(b) 5% BIS

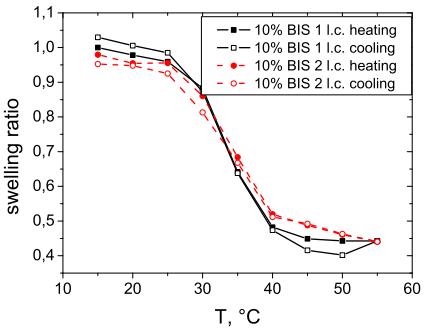

(c) 10% BIS

Figure 5.12: *Swelling ratio of microgels with (a) 2%, (b) 5% and (c) 10% BIS contents adsorbed on Si/Au in the first and in the second long cycle as function of temperature measured by SFM.*

height-to-width ratio at 20°C and at 50°C of adsorbed microgels, and the ratio of particle volume in bulk to the volume of deposited on the Si/Au microgels, are given in table 5.3.

The values of V_{DLS}/V_{SFM} in swollen state (at 15°C) indicate that the internal density of particles deposited at the surface is higher than for the particles in bulk. This ratio decreases with increasing cross-linker content due to decreasing polymer chain length between two cross-linker resulting in an increasing particles stiffness. With increasing temperature up to 50°C the ratio decreases. For this temperature particles exist in the collapsed state and the chain length between two BIS molecules is extremely short, which leads to a decrease of this ratio.

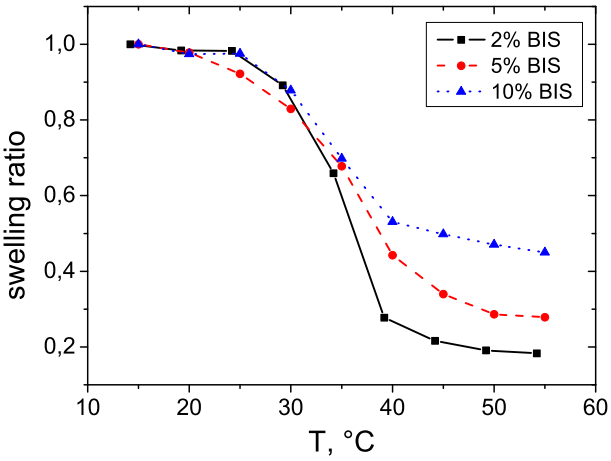

Figure 5.13: *Swelling ratio of microgels with 2% BIS (squares), 5% BIS (circles) and 10% BIS (triangles) adsorbed on Si/Au got by SFM for the heating process in the second long cycle as function of temperature.*

The height/width ratio of adsorbed particles increases with increasing BIS content showing that the particles become stiffer with increasing BIS concentration. Particle stiffness increases due to the decreasing polymer chain length between two cross-linkers in the gel network. The height/width ratio at 50°C is significantly smaller than for the particles at 20°C. This effect is attributed to the collapse mainly in the vertical direction (Fig. 5.11 a). In case of 10% BIS this ratio is almost temperature independent indicating the preservation of particle shape in heating and cooling processes (Fig. 5.11 b). It also indicates much smaller shrinking (0.47) compared to particles with lower BIS contents (0.19 for 2% BIS and 0.29 for 5% BIS). This result shows that microgels with 10% BIS possess a hard particle like behavior. The lower cross-linked microgels collapse mainly in vertical direction and the particles shape changes: becomes flatter. The higher cross-linked microgels collapse in vertical as well as in lateral directions and keep their shape (Fig. 5.11). Due to the higher internal density of adsorbed microgel, the transition of deposited particles becomes sharper (figures 5.9 and 5.13). The LCST of the microgels at surface tends to be higher than in volume phase. The swelling ratio of gel particles in bulk

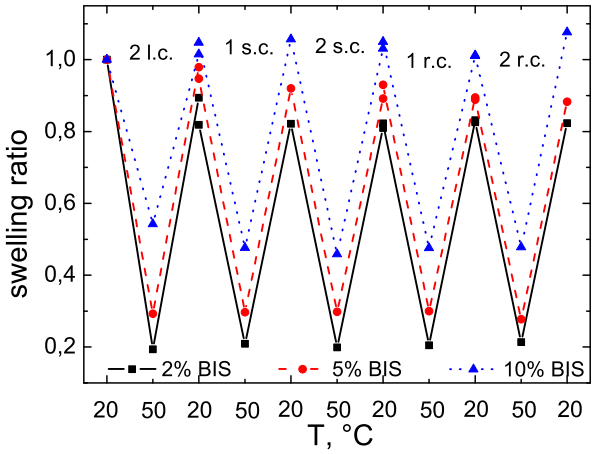

Figure 5.14: *Swelling ratio of adsorbed microgels with 2%BIS (quadrats), 5% BIS (circles) and 10% BIS (triangles) at 20°C and 50°C in different heating/cooling cycles: in the second long cycle (2 l.c.), in the first and in the second short cycle (1 s.c. and 2 s.c.) and in the first and in the second reswelling cycle after drying (1 r.c. and 2 r.c.). Microgels were adsorbed on Si/Au.*

and adsorbed at the surface increases with increasing BIS content indicating a decreasing swelling ability. This phenomenon is explained by decreasing chain length between two cross-linkers in the gel network. With decreasing chain length, the gel network becomes stiffer and looses the network elasticity leading to a decrease in the amount of adsorbed solvent.

5.2.3 Summary

The thermo-induced swelling behavior of microgels with different cross-linker contents was compared between microgels in bulk and after adsorption on the surface. For both the swelling ratio increases with increasing of cross-linker content. Reversible swelling/ shrinking behavior during several cycles was observed and hysteresis decreases with increasing BIS content. Microgels deposited at solid interface have higher internal density

than the microgels in bulk. After adsorption the lower cross-linked microgel particles become flatter in the heating process. The shape of highly cross-linked microgels is invariant in swelling/shrinking processes.

Chapter 6

Influence of outer stimulis

The P(NIPAM-co-AAc) microgels exhibit in bulk responsive behavior upon changing environmental conditions such as pH and temperature (Chapter 3). Due to these unique properties of PNIPAM-based microgels, it is interesting to investigate the response of adsorbed microgels to the changing outer stimuli such as solvent pH value, ionic strength and solvent quality.

The first part of this chapter focuses on the investigating of the thermo-induced swelling/shrinking behavior of microgels adsorbed on Si/PEI in solvents with different pH-values and ionic strengths.

The second part discusses the behavior of adsorbed microgels in alcohol/water mixtures.

6.1 Effect of pH and Ionic Strength

There are few works on the swelling behavior of grafted PNIPAM layers [43, 46, 48, 100]. They demonstrated, that such coatings still show a swelling/deswelling behavior after adsorption. The swelling/deswelling behavior of adsorbed microgel monolayers was investigated by ellipsometry in [36, 42]. This method provides information about the mean value of monolayer thickness but does not inform about the swelling/deswelling behavior of individual adsorbed microgel particles which does not contact with each other, so that

their swelling/deswelling behavior is not influenced by other particles.

For studying the swelling/deswelling behavior of single adsorbed particles in liquid a preparation condition was chosen, where the particles are separated from each other. The microgel particles a3 (10% AAc, 5% BIS) were deposited on Si/PEI by spin coating with a rotation speed of 2000 rpm from a 0.5 wt% microgel dispersion dissolved in 10^{-3} M NaCl. After that the dry samples were fixed in a liquid cell, which was filled with the respective solvent. The effect of pH and the ionic strength on the swelling/deswelling behaviour of adsorbed particles induced by temperature change beyond the LCST was investigated.

6.1.1 Aqueous dispersions of P(NIPAM-co-AAc) microgels

To get information about the microgel particle size and mobility in dependence on the pH, ionic strength and temperature, DLS and electrophoretic mobility measurements were done.

Effect of particle concentration on pH

Table 6.1 shows the pH values of microgel dispersion in dependence on the particle concentration and solvent at 20°C. The ionic strength was kept constant at 10^{-3}M. In the basic medium (10^{-3}M NaOH) the pH value of the microgel dispersion decreases with increasing microgel concentration. This is caused by the increasing amount of dissociated acrylic acid monomers in the system. The free protons partially neutralize the OH^- ions. This effect is less pronounced in the neutral/slightly acid regime (10^{-3}M NaCl) and vanishes in the acid medium (10^{-3}M HCl).

Effect of outer pH

Table 6.2 shows the values of hydrodynamic radii and electrophoretic mobilities of microgels at 20°C in three different solvents HCl, NaCl and NaOH at a constant ionic strength of 10^{-3}M. Since the electrostatic repulsion and osmotic pressure within the microgel par-

solvent:	pH of microgel dispersions		
10^{-3}M	0 wt%	0.05 wt%	0.5 wt%
HCl	3.0	3.2	3.2
NaCl	5.2	5.0	4.1
NaOH	9.7	9.0	5.5

Table 6.1: *pH of microgel dispersions at three concentrations 0 wt% or pure solvent, 0.05 and 0.5wt% at 20° C.*

solvent:	R_h, nm	$\|\mu\|$, mcm/Vs
10^{-3}M	20°C	20°C
HCl	254 ± 3	0.14 ± 0.01
NaCl	416 ± 9	1.56 ± 0.05
NaOH	503 ± 7	2.07 ± 0.05

Table 6.2: *Dependence of hydrodynamical radii R_h and electrophoretic mobility $|\mu|$ on pH.*

NaCl	R_h, nm		$\|\mu\|$, mcm/Vs	
concentration, M	20°C	50°C	20°C	50°C
0	460 ± 8	210 ± 5	2.53 ± 0.04	3.80 ± 0.08
10^{-3}	416 ± 9	256 ± 2	1.56 ± 0.05	3.30 ± 0.06
10^{-2}	359 ± 4	214 ± 5	1.01 ± 0.07	2.35 ± 0.03

Table 6.3: *Dependence of hydrodynamical radii R_h and electrophoretic mobility $|\mu|$ on the temperature and ionic strength.*

ticles increases [72], the particles swell and their hydrodynamic radius increases with increasing pH. An increase in the hydrodynamic radius and particle charge affects oppositely the particles electrophoretic mobility. On one hand, increasing particle size leads to decreasing mobility value. On the other hand, with increasing particle charge, the particle mobility increases. The experimental data (table 6.2) shows that the value of particle mobility increases with increasing pH. It would mean that the particle electrophoretic mobility is defined mainly by the particle charge.

Effect of ionic strength

Table 6.3 shows the values of R_h and the mobility at 20°C and 50°C for dispersions of three different ionic strengths of 0, 10^{-3} and 10^{-2}M. With increasing ionic strength, the mobility decreases due to the enhanced screening. This effect can be observed for both below and above the LCST.

In addition, internal charges are screened, that leads to a decrease in the hydrodynamic radii with increasing ionic strength. Besides, the screening of the internal charge, the osmotic pressure is reduced in the particle network, which also supports the microgel shrinking. This phenomenon is only obvious at 20°C. At 50°C, a non-monotonous behavior is detected with a maximum in size at intermediate ionic strength. This phenomenon is not clarified so far. The similar value for the lowest and highest ionic strength can be explained by the fact that the particles are already in a collapsed state, and that the shrinking due to increasing ionic strength at 50°C is rather minor.

Two counteracting parameters might affect the mobility: electrostatics and particle size. Increasing ionic strength leads to a decrease in particle charge due to counterion screening effect. A decrease of particle charge reduces both the mobility and the hydrodynamic radius. A reduction in hydrodynamic radius, which leads to a more compact internal structure, should decrease the drag forces and might increase the mobility. Since the latter phenomenon was not observed in the presented experiments, the mobility is obviously dominated by electrostatic forces. This is also supported by the fact, that at 50°C the mobility decreases monotonously with increasing ionic strength, while the radius

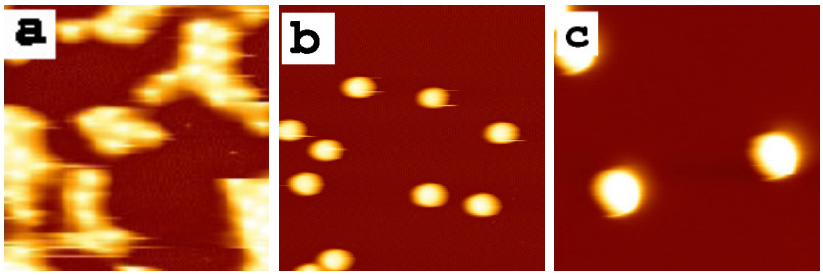

Figure 6.1: *Effect of pH. The particles were deposited on Si/PEI from* 10^{-3} *M NaCl at 2000 rpm and studied in aqueous solutions containing (a)* 10^{-3}*M HCl, (b) in* 10^{-3}*M NaCl and (c) in* 10^{-3}*M NaOH at 20°C. Scan size 5x5* μm^2.

shows a non-monotonous behavior.

6.1.2 Behavior of adsorbed microgels

Effect of pH

Figure 6.1 (a) shows SFM images of adsorbed microgels studied in 10^{-3}M HCl, (b) in 10^{-3}M NaCl and (c) in 10^{-3}M NaOH. Figure 6.2 shows the cross section for the adsorbed microgel particles deposited in 10^{-3}M NaCl and in 10^{-3}M NaOH at 20°C. With increasing pH, the size of particles increases due to enhanced electrostatic repulsion within the particles. This is in good agreement with DLS measurements (table 6.2).

The pH has a strong effect on the strength of adhesion of the particles at the surface. Only in NaCl solution the particles were fixed at the surface below and above the LCST. In NaOH solution the gel particles were fixed at the substrate, but above the LCST material (PNIPAM or PEI is not clear as far) was detached from the substrate to the tip and gave artifact during scanning ("double tip" and "smearing out" effects). At 20°C under both conditions the cross section could be analyzed as shown in Fig. 6.2.

In HCl, the adsorbed particles became already mobile at 20°C. During scanning the particles left the surface or were rolled by the tip, resulting in an image, which is rather smeared out. This is caused by the low particle charge. In addition, the low charge leads to a reduced external repulsion, which causes domains of particles and singles particles

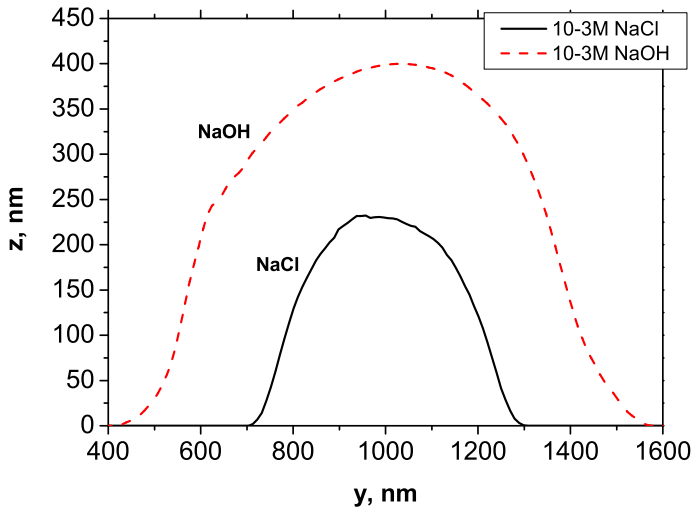

Figure 6.2: *The cross section of particles deposited on Si/PEI in $10^{-3}M$ NaCl and $10^{-3}M$ NaOH at 20°C.*

could not be detected anymore.

Therefore, only measurements in NaCl could be performed for the study of shrinking/swelling behavior of individual microgel particles. This condition was chosen for the studies, described in the following.

Effect of ionic strength

In figure 6.3, SFM images of adsorbed microgel particles, which were deposited in H_2O, 10^{-3}M NaCl and 10^{-2}M NaCl solutions, are shown at two different temperatures: 20°C and 50°C. Figure 6.4 demonstrates cross sections of adsorbed microgel particles in solvents at the ionic strengths of 0, 10^{-3}M and 10^{-2}M.

The adsorbed particles show reversible swelling and deswelling behavior (figure 6.4 and figure 6.5). In order to have a possibility to compare the swelling/deswelling behavior of microgels, the volume of adsorbed particles was calculated (Eq. 2.31). For microgel particles in bulk, the formula for the volume of a sphere was used. Figure 6.5a demonstrates the dependence of adsorbed particle volume as a function of temperature. In figure 6.5b

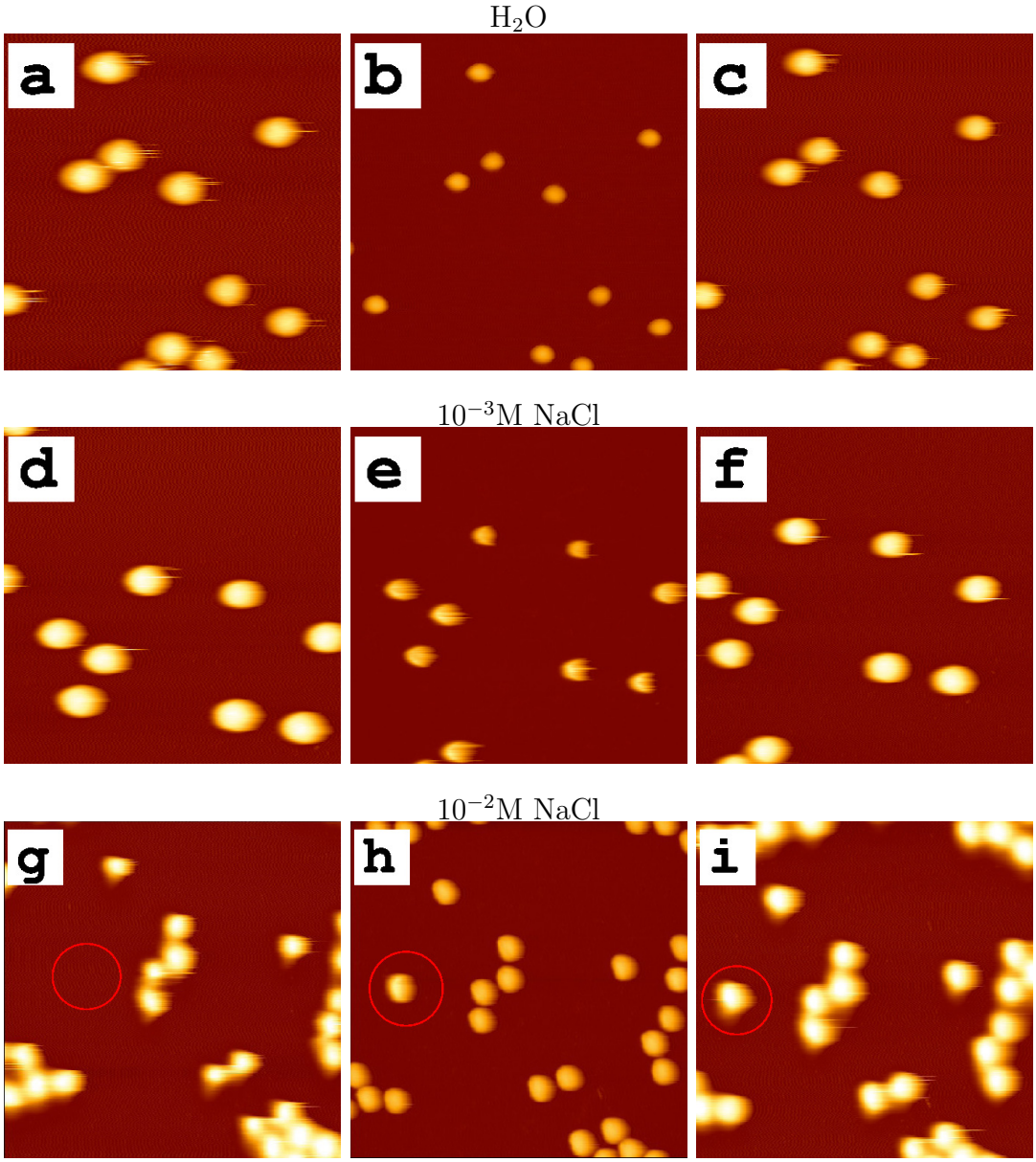

Figure 6.3: *Effect of ionic strength on the swelling behavior of adsorbed microgel particles induced by a temperature change. The particles were deposited from* 10^{-3} *M NaCl at 2000 rpm on Si/PEI and studied in aqueous solutions containing (a-c) 0 M NaCl (pure* H_2O*), (d-f)* 10^{-3}*M NaCl and (g-i)* 10^{-2}*M NaCl. The first heating cycle is represented. The middle images for each solvent are made at 50° C, and the images on the sides were done at 20° C. Left and right columns: 20° C, middle: 50° C. Scan size 5x5* μm^2*. In circle a microgel particle appeared during SFM measurements is shown.*

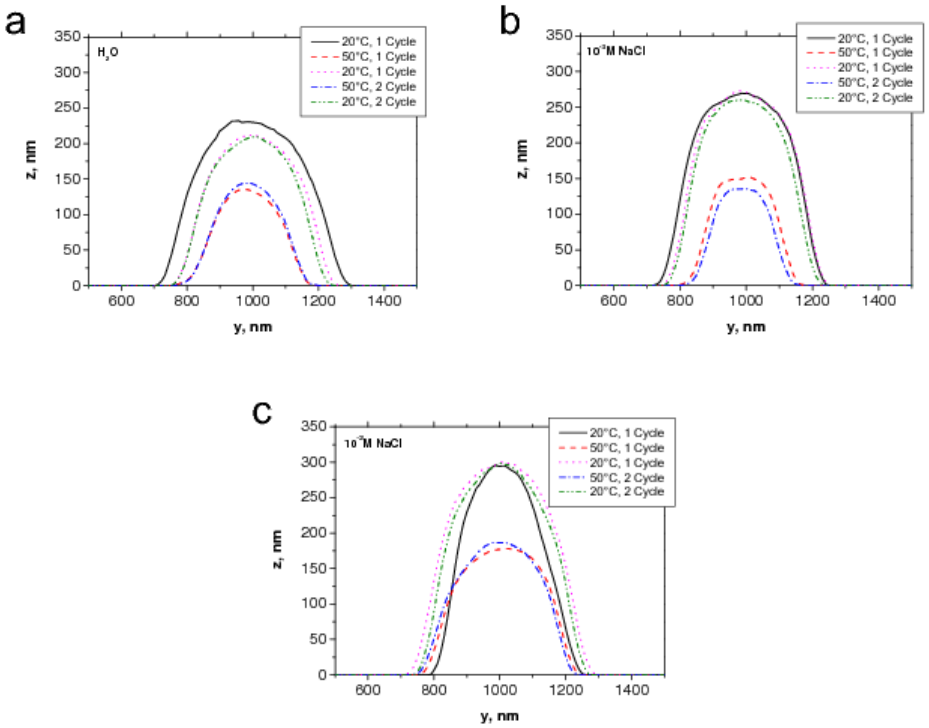

Figure 6.4: *Cross sections of individual particles deposited on Si/PEI in H_2O (a), in $10^{-3}M$ NaCl (b) and in $10^{-2}M$ NaCl (c). On each graph the two first temperature cycles are shown.*

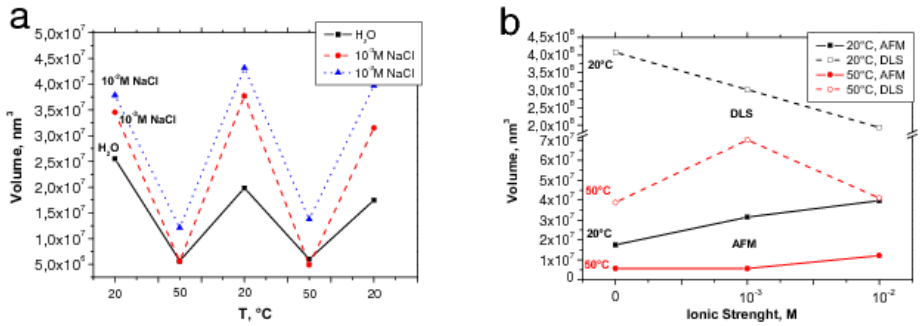

Figure 6.5: *Effect of ionic strength I. (a) Volume of microgel particles adsorbed on Si/PEI in dependence on the temperature. (b) Comparison of the microgel particle volume of adsorbed (filled symbols) and particles in bulk (open symbols) at 20° C (solid lines) and 50° C (dashed lines).*

the volume of adsorbed microgel particles and the particles in bulk are compared.

After the adsorption, the particle volume decreases by more than one order of magnitude. The particle height is significantly smaller than the particle footprint (Fig. 6.4). It means, that the particles are more compressed in vertical direction than in lateral. This can be explained by an attraction between the positively charged Si/PEI surface and the negative charged microgel particles. With increasing ionic strength, the electrostatic attraction is screened, which leads to a swelling of the particles, especially in vertical direction. V. Nerapusri et. al. observed a similar behavior for the microgel monolayer thickness at pH 8 [42]. This is in contrast to the behavior in bulk, where the particles shrink with increasing salt concentration. Due to the more fluffy structure in vertical direction the particles are more thermosensitive in the vertical direction than in lateral direction at the substrate. This is another explanation for the pronounced thermosensitive shrinking/swelling perpendicular to the surface at 10^{-2}M in comparison to the volume changes in lateral direction.

From the cross sections made for all three solvents (figure 6.4), it can be seen that adsorbed particles investigated in solvents at the ionic strengths 0 and 10^{-3}M can swell and deswell in vertical and lateral directions. In contrast to this particles studied in 10^{-2}M NaCl swell and deswell mainly in vertical direction.

An explanation for this difference might be that during swelling and deswelling in lateral direction, the microgels build (swelling) or break (collapse) electrostatic bonds between the microgel and PEI opposite charged groups. With increasing the ionic strength, the amount of counterions screened charges grows. Consequently, PEI and microgel particles form less bonds. It prevents the lateral swelling in the solvents with high ionic strength. From figure 6.4 it is concluded that the particle height has the tendency to enhance with increasing ionic strength.

In figure 6.3(h-i) new adsorbed particles in comparison to (g) is detected. It means that at high ionic strength solution the particles desorb and adsorb again. In NaCl solution at an ionic strength of 1 M, already at 20°C the former adsorbed microgel particles desorb from the surface during scanning.

6.1.3 Summary

The swelling and shrinking of individual adsorbed particles was studied with SFM in the respective liquid at the solid substrate and compared to bulk behavior. The combined results of DLS and electrophoretic mobility measurements support the model [11] that charges are converted to the particle surface during shrinking above the LCST. The results show clearly that electrostatics dominate the electrophoretic mobility, but not the particle diameter.

The particles stay fixed at low ionic strength up to 10^{-3}M and intermediate pH. At higher ionic strength or in the acidic or basic regime, they can be moved by the SFM tip, or they were even desorbed from the surface. The adsorbed microgel particles show a reversible temperature response as in the bulk solution, although their volume is compressed by more than one order of magnitude at the substrate. In contrast to the behavior in bulk the particles swell with increasing ionic strength, which is explained by a screening of the electrostatic attraction between the oppositely charged substrate and the AAc monomers across the particles. This enhances the vertical temperature sensitive swelling/shrinking and suppresses the lateral swelling at high ionic strength (above 10^{-3}M). In all other cases the particles swell laterally and vertically.

6.2 Effect of Cononsolvency

Due to the solubility of PNIPAM in alcohols, PNIPAM-based microgels could be interesting for the storage, transport and control release of alcohol-soluble substances [101, 102].

There are few studies about the behavior of PNIPAM homopolymer chains and hydrogels in binary mixed solvents such as alcohol/water mixture. It was demonstrated that pure water and pure alcohol serve as good solvents for the PNIPAM but their mixture is not. This is so called *cononsolvency* [68, 79, 103–106]. N. Wang *et.al.* showed that the alcohol concentration in confined binary solvents (solvents inside the polymer network) is significantly higher than the alcohol concentration in free binary solvents (outside the polymer network) [68]. It means, that the PNIPAM chains preferentially interact with

alcohol molecules compared to water molecules. The concentration of alcohol in confined binary solvents increases with increasing alcohol hydrophobicity. In the alcohol/water mixture the clathrate structure is formed [107]. Water molecules encapsulate the alcohol molecules in water-rich mixtures. The number of water molecules required to form a clathrate structure around an isopropanol (2-Pr) molecule is higher than for an ethanol (EtOH) molecule [108]. The formation of clathrate structures causes the PNIPAM microgels to collapse. With increasing alcohol concentration above a critical concentration the alcohol molecules could not be encapsulated in the clathrate structures anymore and start to interact with PNIPAM-chains through hydrogen bonding and hydrophobic interactions [106].

The aim of this section is to investigate the thermo-induced swelling/deswelling behavior of individual P(NIPAM-co-AAc) microgels in bulk and deposited on solid substrates in ethanol/water and isopropanol/water mixture and their ability to built well organized structures.

In order to investigate the thermoresponsive behavior of a3 microgels (10% AAc, 5% BIS) in alcohol/water mixtures, the 2-Pr/water mixtures and the EtOH/water mixtures were used. The 0%, 5%, 10%, 20%, 33%, 50%, 66% and 100% alcohol contents in water were chosen. The swelling/deswelling behavior was investigated for particles in bulk and for particles deposited on Si/PAH.

6.2.1 Microgel characteristics in bulk

For the particle characterization in the volume phase DLS and Zeta sizer were used. Unfortunately, the microgels were not soluble in 2-Pr/water mixture still at 5% 2-Pr/H_2O mixture. Hence, the swelling properties of microgels in bulk were investigated only for particle dispersions in EtOH/water mixtures.

Figure 6.6 shows the hydrodynamic radius of microgels in water, 5% and 50% EtOH/ H_2O mixtures and in pure EtOH (100%) as a function of temperature. With increasing EtOH concentration microgels become smaller. In the binary alcohol/water mixtures

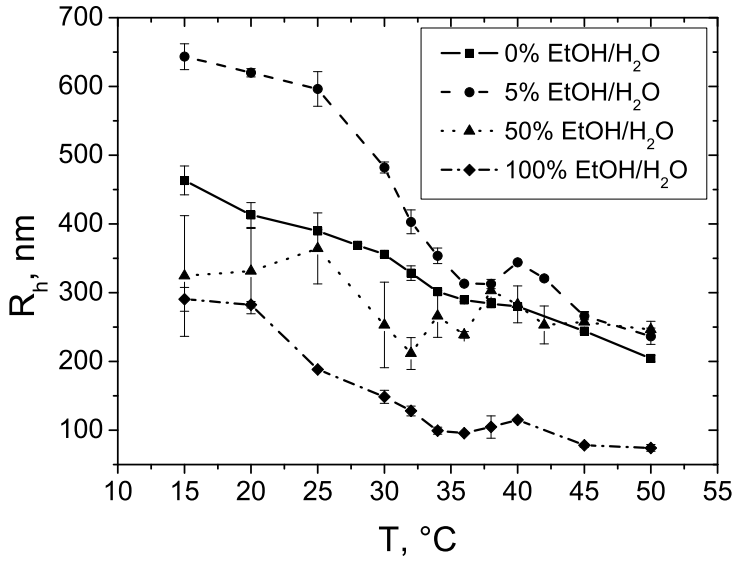

Figure 6.6: *Hydrodynamic radius of microgels in pure water (squares), in EtOH/water mixtures containing 5% EtOH (circles) and 50% EtOH mixture (triangels) and in pure EtOH (rhomb) in dependence on temperature measured by DLS.*

PNIPAM prefers to interact with alcohol [68], but at lower concentrations the water forms the clathrate structures around the alcohol molecules [107]. It leads to an increase in the microgel particle dehydration, resulting in a decrease in particles size.

Microgels, dissolved in 5% EtOH/water mixture, exhibit a large particle size. The second pase transition, which iscommon for P(NIPAM-co-AAc) particles etremly sharp. It could be explained by the decreasing dielectric constant with increasing ethanol content. According to the Coulomb law, the electrostatic repulsion between two negatively charged AAc units increases with decreasing dielectric constant. It leads to an increase in the particle hydrodynamic radius and the appearance of the clear second transition step at a temperature about 40°C. The same behavior is typical for microgels with highly charged co-monomer contents [9, 17].

The pure PNIPAM microgels have an one step phase transition. The LCST is at the temperature about 32°C and is affected by the increasing the hydrophobic interparticle

interactions leading to the particle collapse (Chapter 5). Through out the adding of the charged co-monomer the two step phase transition appears. The first step is at a temperature about 32°C and results from the PNIPAM. At higher temperatures, the second step appears and could be explained by increasing electrostatic repulsion with decreasing distances. With increasing charged co-monomer content, the second step becomes more clearly. The shrinking behavior of microgels in a dispersion of 50% EtOH content can be only slightly affected by temperature. It demonstrates the cononsolvencity. At intermediate concentrations of alcohol PNIPAM loses the ability to thermo-induced swelling and deswelling due to the particle dehydration [78, 106]. In pure alcohol, particles show again a stronger response to temperature changes, due to the increasing concentration of alcohol inside of the microgel particles [68].

EtOH content, %	$\lvert\mu_{20°C}\rvert$, mcm/Vs	$\lvert\mu_{50°C}\rvert$, mcm/Vs	$q^{20°C}_{EtOH/H_2O}/q^{20°C}_{H_2O}$
0	2.98 ± 0.15	4.70 ± 0.01	1
5	1.98 ± 0.06	3.22 ± 0.04	1.19
50	0.64 ± 0.05	1.20 ± 0.04	0.52
100	0.50 ± 0.02	0.77 ± 0.02	0.18

Table 6.4: *The value of electrophoretic mobility of microgels in pure water, in 5%, in 50% EtOH/water mixtures and in pure EtOH at 20° C and 50° C and relative particle charge at 20° C.*

For a better understanding of particle charges, the electrophoretic mobility (μ) was measured (Table 6.4). For all four samples,the mobility value increases with increasing temperature due to the increasing particle charge and decreasing particle size. For both temperatures mobility value decreases with increasing EtOH concentration. According to the definition (Eq. (2.23)), the electrophoretic mobility μ is $\mu = \frac{v}{E}$, where v is the particle velocity in the electric field E. The equation (2.23) could be modified by multiplication and deviation by the particle charge q:

$$\mu = \frac{v}{E} = \frac{qv}{qE} = \frac{qv}{F} \tag{6.1}$$

where $F = qE$ is a force acting on a charged particle in the electric field. According to Stoke's equation $F = 6\pi\eta Rv$, where R is a particle size, η is a solution viscosity. From equation (6.1) follows:

$$\mu = \frac{q}{6\pi\eta R} \propto \frac{q}{\eta R_h} \tag{6.2}$$

Actually, the equation (6.2) could not be used for the exact particle charge calculation because of at least the impossibility of the real size microgel detection. But this equation could be used for the estimation of appropriate relative particle charge: microgel charge in EtOH/water mixture normalized with respect to microgel particle charge in water at 20°C (Table 6.4). Tendentiously, the ratio of charged units decreases with increasing EtOH content. Interestingly, the ratio value reaches a maximum at a concentration of 5% EtOH in water. This fact also conforms the above discussed suggestion about the increased particle charge. This uncommon property can be used in the particle deposition experiments.

6.2.2 Effect of EtOH content on the substrate coverage

Figure 6.7 represent the SFM images of microgel particles deposited by spin coating on Si/PEI from microgel dispersions with (a) 0%, (b) 5%, (c) 50%, and (d) 100% EtOH contents. In the deposition process, capillary forces play an important role. It is known that capillary forces between two wetted colloidal particles are attractive and lead to the formation of two-dimentional crystals [109, 110]. During the spin coating process a thin solvent film is formed, which evaporates [16]. With increasing EtOH content, the evaporation rate of the solvent from the thin solvent film increases, leading to the strong capillary forces. For samples deposited from pure EtOH, there is almost no individual particles. Due to the low particle charge (Tab. 6.4), attractive capillary forces and very fast evaporation, microgels are very closely hexagonal packed.

With decreasing EtOH content the individual particles appears and the distance between particles in areas with tightly packed microgels increases. The high charge of microgels in the dispersion with the EtOH concentration of 5% and lower dielectric constant

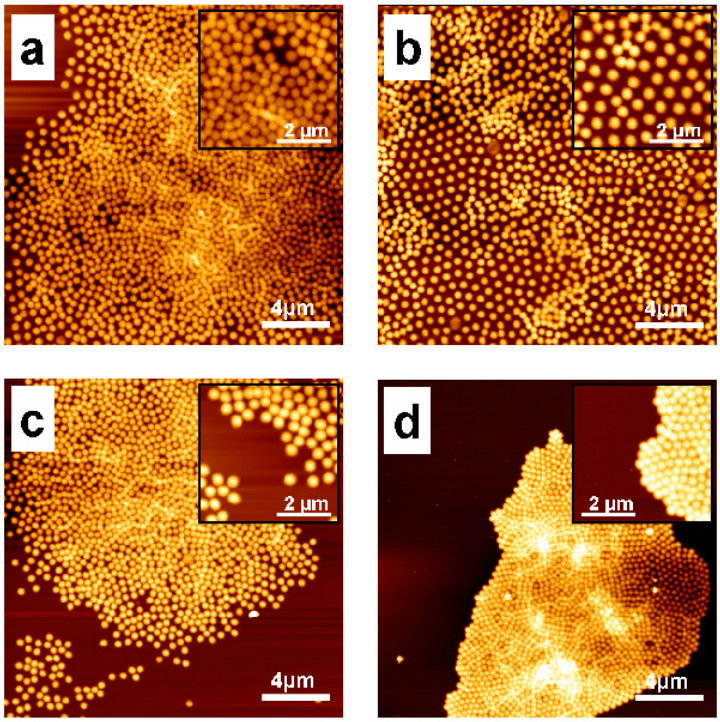

Figure 6.7: *SFM images of particles deposited on Si/PEI by spin coating with rotation speed of 1000 rpm on Si/PEI. Microgels were dispersed in (a) pure water, (b) 5% and (c) 50% EtOH/water mixture and in (d) pure EtOH. The microgel dispersion concentration was 0.05 wt%. Scan area is 20*x*20* μm^2.

allow particles to form areas with ordered structures with high constant interparticles distances (Fig. 6.7b).

6.2.3 Swelling/deswelling behavior of adsorbed microgels

To investigate the swelling/deswelling behavior of adsorbed microgels the SFM technique in liquid was applied. The microgels were deposited from the aqueous dispersion on Si/PAH. In measurements the SFM liquid cell was filled with an appropriate solvent.

Figures 6.8 and 6.9 show the microgels particles deposited in EtOH/water and 2-Pr/water mixtures, respectively. Alcohol/water mixtures contain (a-c) 0%, (d-f) 5%, (g-i) 50%, and (j-l) 100% of alcohol. There are particles at 20°C in (a, d, g, j) the

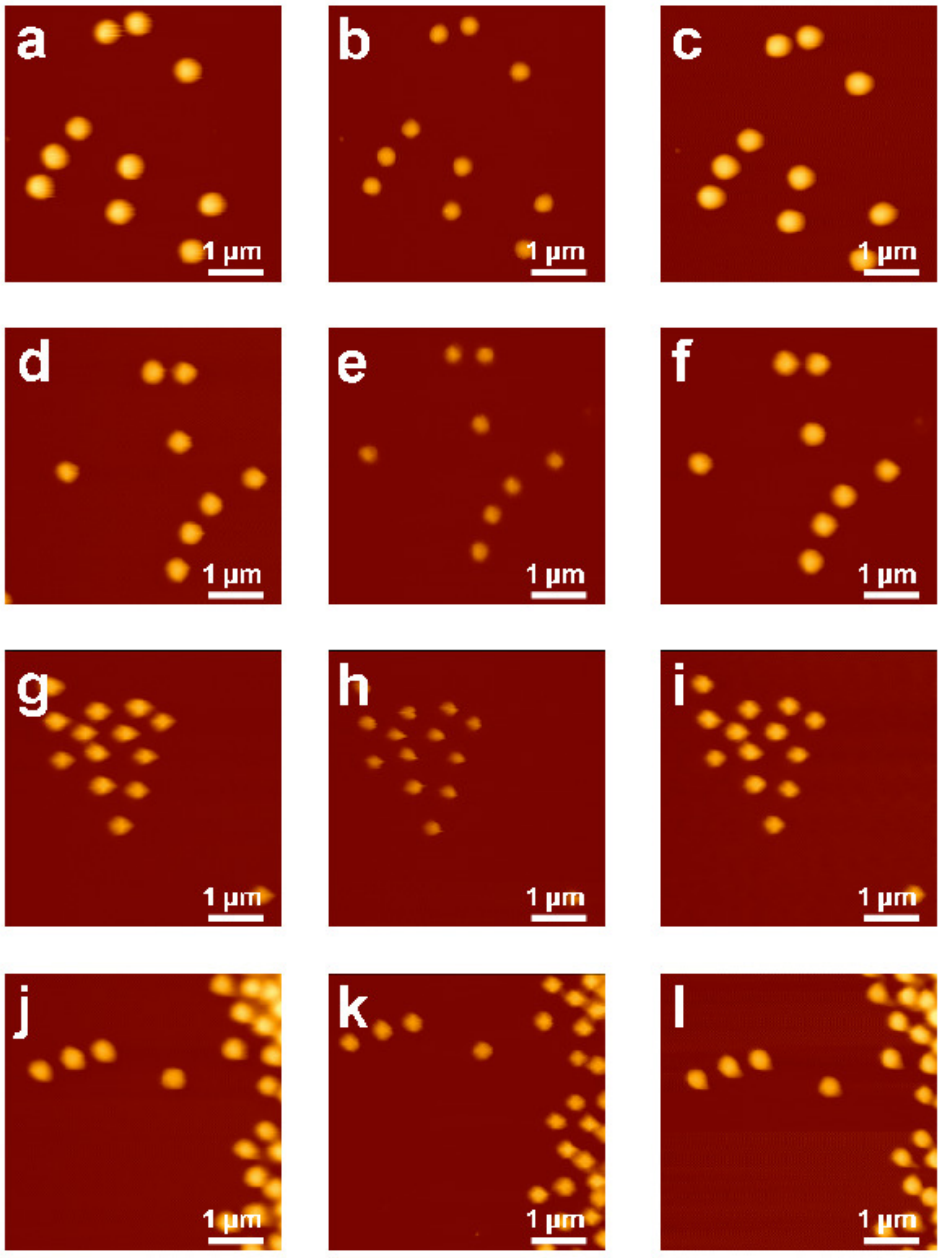

Figure 6.8: *SFM images of microgel particles deposited by spin coating on Si/PAH. The samples immerse in (a-c) pure water, (d-f) in 5% and (g-i) in 50% EtOH/water mixture, and (j-l) in pure EtOH. Images (a, d, g, j) present the microgels in at 20° C, images (b, e, h, k) at 50° C, and (c, f, i, l) at 20° C.*

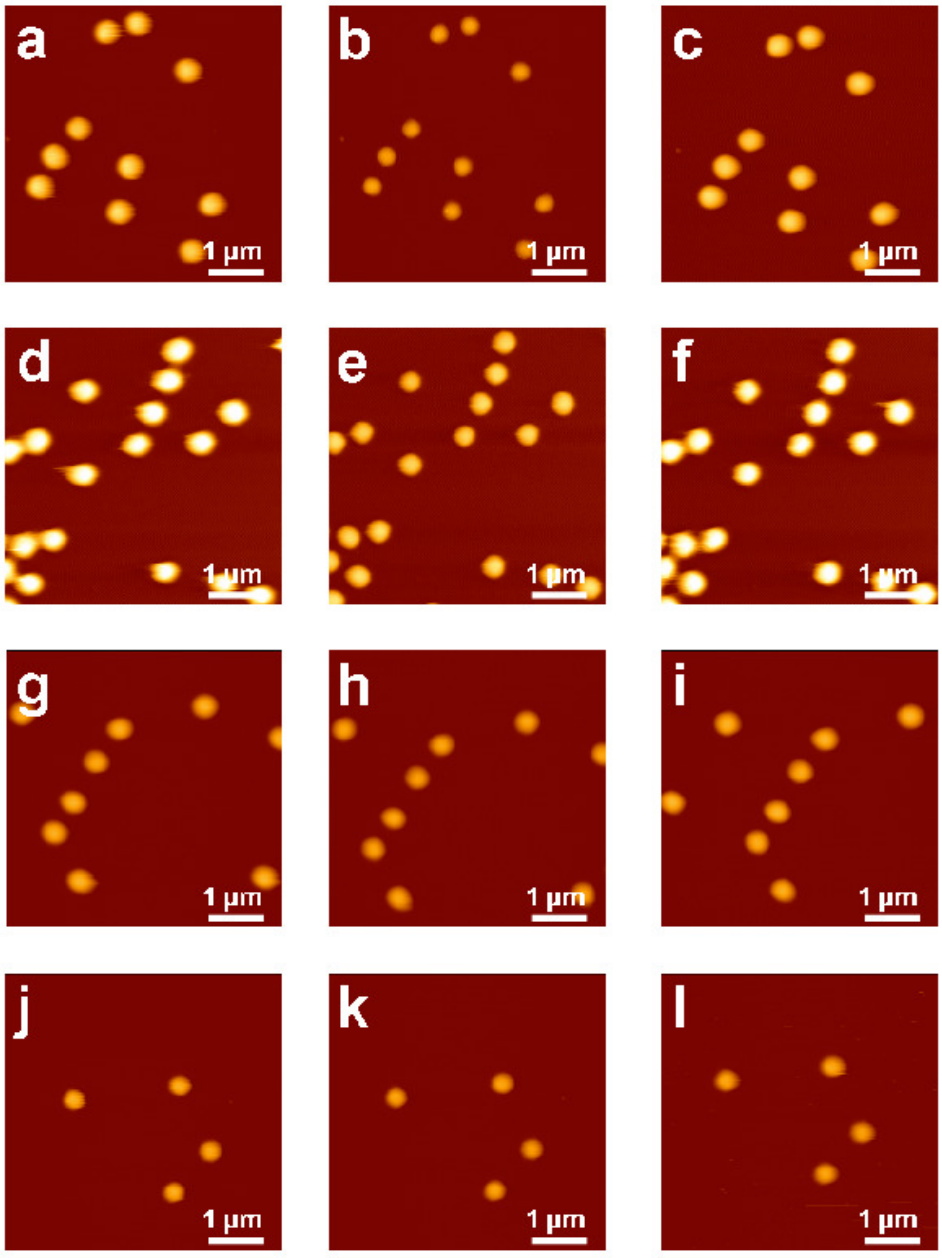

Figure 6.9: *SFM images of microgel particles deposited by spin coating on Si/PAH. The samples immerse in (a-c) pure water, (d-f) in 5% and (g-i) in 50% 2-Pr/water mixture, and (j-l) in pure 2-Pr. Images (a, d, g, j) present the microgels in at 20° C, images (b, e, h, k) at 50° C, and (c, f, i, l) at 20° C.*

first column. In the second column (b, e, h, k) microgels were heated 50°C, and in the third column (c, f, i, l) the same particles are shown at 20°C again. Microgels deposited in EtOH/water and 2-Pr/water mixtures have reversible thermo-induced swelling/deswelling behavior. In order to estimate the thermo-induced behavior of adsorbed microgels, the particle cross sections were evaluated. Figures 6.10 and 6.11 show the cross sections of

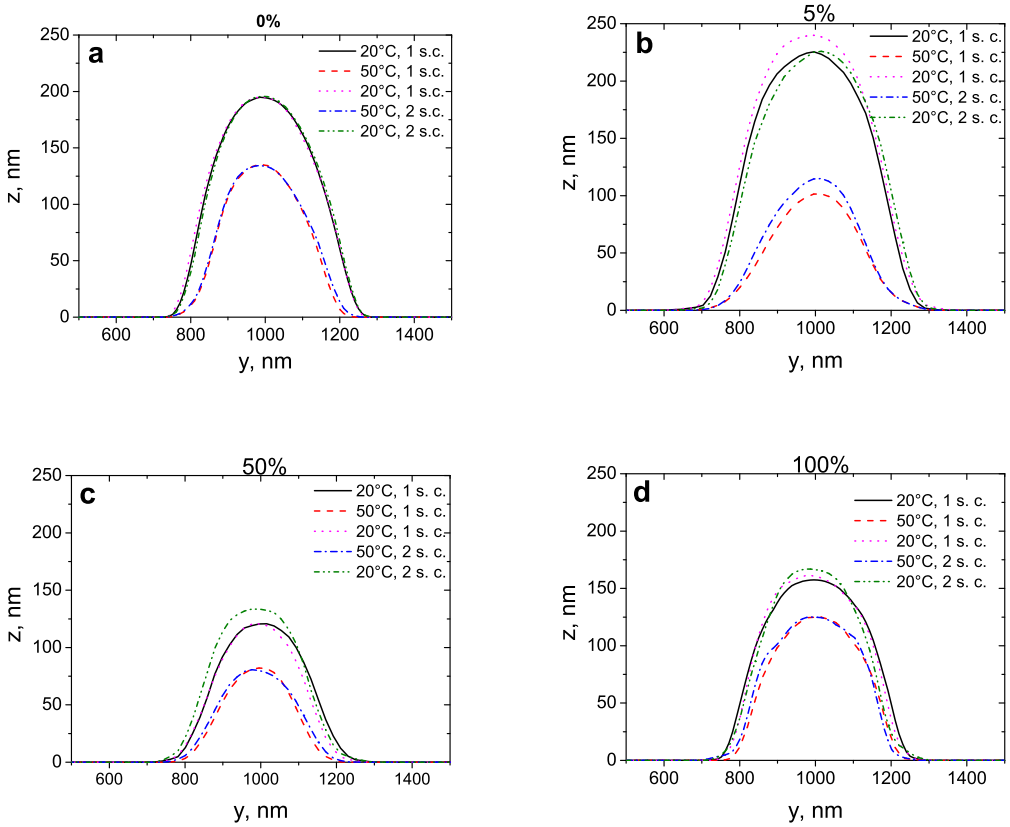

Figure 6.10: *Cross sections of microgels deposited on Si/PAH in EtOH/water mixtures with (a) 0%, (b) 5%, (c) 50% and (d) 100% EtOH content.*

microgels deposited on Si/PAH in (a) 0%, (b) 5%, (c) 50%, and (d) 100% alcohol in alcohol/water mixtures. For both alcohols the thermo-induced swelling/deswelling takes place only in vertical direction. No changes of particle contact area was noticed.

Figure 6.12 demonstrates the dependence of volume of adsorbed particles on the temperature in two short cycles (s. c.) for solutions with 0%, 5%, 50% and 100% alcohol

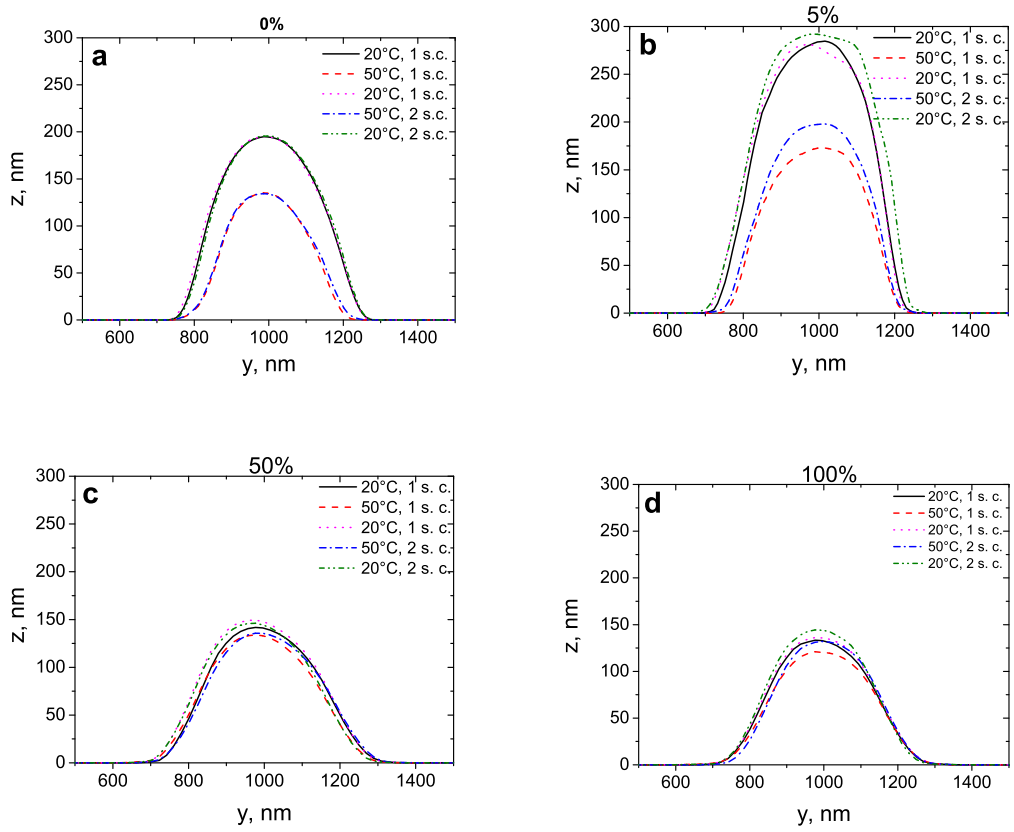

Figure 6.11: *Cross sections of microgels deposited on Si/PAH in 2-Pr/water mixtures with (a) 0%, (b) 5%, (c) 50% and (d) 100% 2-Pr content.*

content in water. (a) represents the volume of particles deposited in EtOH/water mixture, (b) in 2-Pr/water mixture. The volume was calculated from the SFM cross section data according to the formula for the volume calculation of figure of revolution (Eq. (2.31)).In all cases, particles deposited in EtOH/water mixtures exhibit a completely reversible thermo-induced shrinking and swelling behavior. Particles in 2-Pr/water mixtures show the reversible thermo-induced swelling/deswelling in solutions with lower alcohol concentration. With increasing 2-Pr concentration, the particles lose their thermo-sensitivity. The particle size decreases with increasing alcohol concentration. In contrast, particles swell extremely at lower alcohol concentrations, resulting in a large particle size. As discussed above, PNIPAM prefers to interact with alcohol in alcohol-water mixtures [68].

Alcohol molecules are also encapsulated by water molecules, leading to an increasing osmotic pressure insight of particles and their swelling. With increasing alcohol content, the clathrate structure disappears, resulting in a decreasing osmotic pressure and particle dehydration, and consequently, the decreasing particle size.

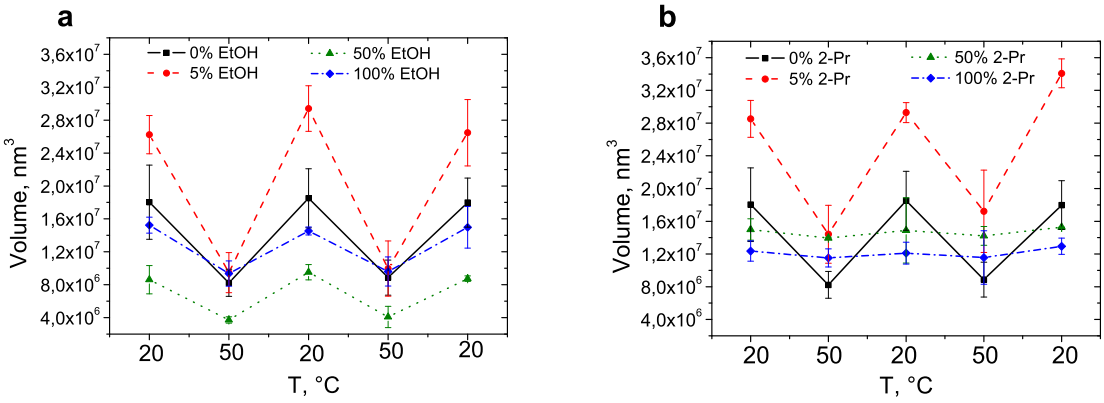

Figure 6.12: *Volume of adsorbed on Si/PAH microgels measured by SFM at 20°C and at 50°C in two cycles for particles in water (squares), in 5% (circles), in 50% (triangels) EtOH/water mixture and in EtOH (rhombs) deposited in (a) EtOH/water and (b) 2-Pr/water mixture.*

In order to compare the swelling ability of individual microgel particles immersed in EtOH/water and 2-Pr/water mixtures, the swelling ratio of microgels was calculated. The swelling ratio is defined as a particle volume at 50°C normalized with respect to the particle volume at 20°C. Figure 6.13 represents the swelling ratio of microgels deposited in EtOH/water (squares) and 2-Pr/water (circles) mixtures as a function of the alcohol content.

For microgel particles, 2-Pr is a 'bad' solvent, which can be attributed to the additional methylene group. This group effects an increase in the hydrophobicity, resulting in a worse swelling ratio compared to the ethanol. In pure isopropanol also no cononsolvency effect for deposited on solid substrate particles was observed.

In order to compare thermo-induced behavior of microgels in EtOH/water mixtures

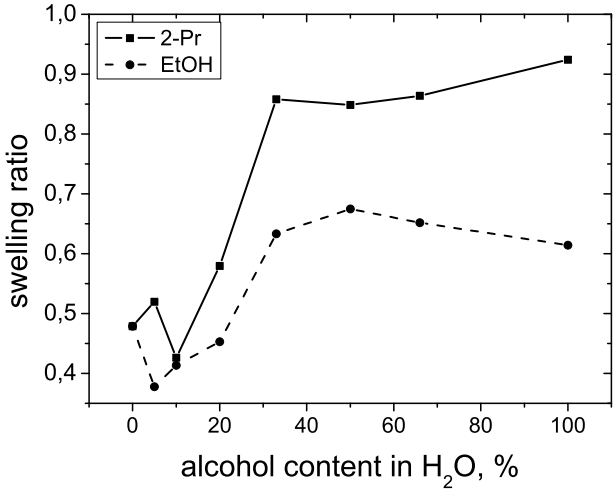

Figure 6.13: *Swelling ratio of deposited on Si/PAH microgels as a function of alcohol content: EtOH (squares) and 2-Pr (circles) measured by SFM.*

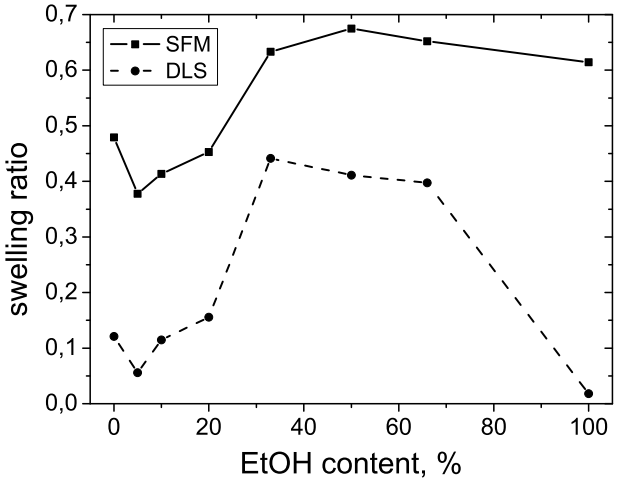

Figure 6.14: *Swelling ratio (squares) of deposited on Si/PAH microgels measured by SFM and microgels in bulk (circles) measured by DLS as a function of EtOH content in EtOH/water mixtures.*

in bulk and adsorbed microgels the swelling ratio of both systems was calculated (Fig. 6.14). The particles in bulk and deposited on the surface demonstrate almost the similar qualitative behavior: at lower alcohol concentrations the particles react very well on the temperature changes, the swelling properties become worse in the intermediate EtOH ratios. It is interesting to notice that both systems exhibit a local minimum in the swelling ratio in the 5% EtOH/water mixture. At this EtOH concentration adsorbed particles and particles in bulk exist in an extremely swollen state (Fig. 6.6 and 6.12), due to the increasing electrostatic repulsion between charged co-monomer units and increased osmotic pressure because of the clathrate structure formation.

The main difference between microgels in bulk and deposited on Si/PAH is their behavior in pure alcohol. In pure EtOH the swelling ratio of particles in bulk is significantly smaller than in the 66% alcohol/water mixture. The clear cononsolvency effect takes place. Oppositely, the swelling ratio of adsorbed microgel decreases slightly in comparison with 66% EtOH in alcohol water mixture. In pure alcohol, particles are still able for the thermo-induced swelling and deswelling behavior. The observed effect was not so pronounced as expected.

6.2.4 Summary

It was shown that P(NIPAM-co-AAc) microgels demonstrate a reversible thermo-induced behavior in alcohol/water mixtures. The concentration of EtOH in microgel dispersions can be used for a controlled surface coverage in deposition process. For microgels in EtOH/water mixtures the cononsolvency was only observed for particles in bulk. In general, no cononsolvency was observed for deposited particles. The swelling ratio of deposited microgel particles increases with increasing alcohol content. In more hydrophobic alcohols microgels loose their swelling abilitiy. At higher 2-Pr concentrations adsorbed microgel particles lose their thermo-sensitivity. At a lower alcohol concentration adsorbed microgels and microgels in bulk exhibit the largest sizes due to the increasing intra-particle osmotic pressure resulting from the increasing electrostatic repulsion between charged co-

monomers.

Chapter 7

Influence of deposition methods and substrates

The substrate and the deposition methods are two important parameters in the microgel adsorption process. It was shown that microgels deposited by different methods has different sizes and form different structures at the solid interfaces [35, 39]. The substrate also influences the number of adsorbed particles [35].

This chapter focuses on the thermo-induced swelling/deswelling behavior of adsorbed microgel particles deposited by three different methods: spin coating, dip coating and direct adsorption. The microgel particles were deposited on different substrates: Si/Au, Si/APMS, Si/PEI, Si/PAH, Si/PEI/PSS/PDADMAC and Si/PEI/$(PSS/PAH)_x$, where $x = 1, 3, 6$ is a number of bilayers. In this chapter the microgel particles a3 with 5% BIS, 10% AAc were used.

7.1 Effect of deposition method

Many groups are investigating the adsorption phenomena of colloidal particles. Few main tendencies of such studies could be determine. On one hand, theoretical researches describe the adsorption process [37, 111]. On the other hand, the experimental works discuss the assembly of particles in well organized structures [16, 35, 38, 83, 93, 109, 112] with their

different swelling properties [16, 36, 42, 50, 77] and application potentials [29, 31, 113]. It was shown that the quality of built colloidal particle films depends on the particles zeta potential, adsorption time, particle softness, particle-surface interactions, deposition method, surface roughness and etc. [35–38, 41, 82, 111]. For example, in [111] authors simulated the particle adsorption process in dependence on the suspension concentration, time of adsorption, Debye thickness, and surface microstructure. It was shown that the ordering of adsorbed particles is mainly controlled by the particle zeta potential. Particles with a larger Debye layer (lower salt concentration) can be ordered more easily.

There are few popular methods to deposit the colloidal particles on the surfaces: spin coating, dip coating, adsorption, Langmuir-Blodgett *etc.* All these techniques are well known and described [35, 39, 83, 93, 114]. In [39] authors compare the microgel films prepared by active (centrifugation) and passive (deposition of substrate in the microgel solution and afterwards rinsing with water) methods. The microgels deposited by active methods are smaller than particles deposited by passive method, because in centrifugation process the high forces are acting during the deposition. It means that microgels deposited by different methods demonstrate different sizes.

This section focuses on the thermo-induced swelling/deswelling behavior of microgels particles deposited by three different techniques: spin coating, dip coating and direct adsorption at two temperatures: at 20°C and at 50°C. The preparation methods differs slightly. In the case of the spin coating and dip coating, the particles were dried during the adsorption process. These particles will be reswell before the SFM measurements. In the direct adsorption, the microgels are continually in liquid. It is interesting to compare the further behavior of microgels deposited from two different states: from swollen state (20°C) and from completely collapsed state (50°C). This section also discusses the question, if the particle deposition technique and sample drying have influence on the further particle behavior?

Firstly, line the thermoresponsive behavior of microgels in bulk was investigated. The microgel particles demonstrate reversible swelling/shrinking behavior in the volume phase (Fig. 7.1). At temperatures below the LCST, particles are swollen and above the LCST

are collapsed because particles become more hydrophobic. Pure PNIPAM microgel particles demonstrates an one step transition at a temperature about 32°C. Particles modified by acrylic acid exhibit two step transition [17]. The first transition is contributed by PNIPAM and is at a temperature of about 32°C. The second transition takes place at a temperature about of 45°C, which is contributed by the co-monomer. With increasing temperature the particle size decreases. Due to the charged co-monomer, the electrostatic repulsion between particles increases preventing the further particle collapse, resulting in the second phase transition. By further enhancing temperature the hydrophobic interactions dominate over the electrostatic repulsion and particles collapse.

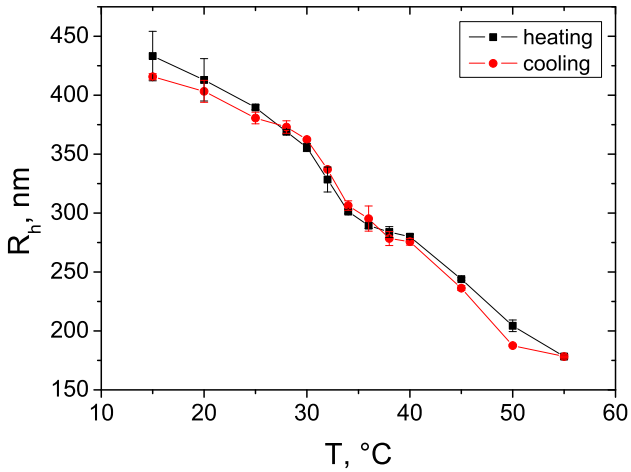

Figure 7.1: *Dependence of hydrodynamic radius of microgels with 5% BIS and 10% AAc on the temperature in heating (squares) and cooling (circles) processes measured by DLS.*

In order to compare the thermo-induced swelling/deswelling behavior two temperatures, at which microgels are swollen (20°C) and collapsed (50°C) were chosen for deposition experiments.

Figure 7.2 demonstrates the SFM images of particles deposited by the three methods from microgel dispersion at a temperature of 50°C. In the first line (a-d) the particles were deposited by spin coating. The second line (e-h) presents microgels deposited by dip

coating. The third line (i-l) exhibit the microgels deposited by direct adsorption. The first column (a, e, i) shows the samples direct after the deposition at 50°C. In the second column (b, f, j) the particle in a swollen state at 20°C are shown. The next column (c, g, k) particles are collapsed at 50°C again. The last column (d, h, l) exhibits swollen microgels at 20°C. In case of direct adsorption technique at 20°C, it was not possible to image the microgels direct after the deposition process. Due to the very swollen state, microgels were rolled by SFM tip during the scanning. The first SFM images were taken at 50°C. At this temperature particles were completely collapsed. For all samples no particle desorption takes place. The particles deposited by three different methods exhibit reversible thermo-induced swelling/shrinking behavior.

The amount of adsorbed microgels was independent on the deposition temperature for particles deposited by spin coating and by direct adsorption. There is a huge difference in a number of adsorbed microgels for samples prepared by dip coating at two different temperatures (Fig. 7.3). The number density of adsorbed microgels increases with increasing deposition temperature. It could be explained by two phenomena. On one hand, the diffusion coefficient of microgel particles increases with increasing temperature resulting in a faster particle movement. Due to the fast diffusion more particles can be adsorbed at the surface. On the other hand, with increasing temperature particles become more hydrophobic and prefer to be situated at the air-water interface. R. M. Richardson *et.al.* showed that at the temperature above the LCST, the thickness of layer formed by PNIPAM chains is ten time higher than below the LCST [115]. J. Zhang and R. Pelton demonstrated that microgel particles are able to form well organized structures at the air-water interface [116]. In the dip coating procedure the wafer is slowly pulled out from the microgel solution. Therefore the particles situated in the interface layer are carried along by the substrate. Both of these phenomena lead to the enhance of the number density of adsorbed particles with increasing temperatures.

In figure 7.4 the cross sections of microgels deposited by all three methods at 20°C and 50°C are shown. The microgels deposited by different methods demonstrate reversible swelling/ shrinking behavior. Only particles deposited by dip coating swell and shrink in

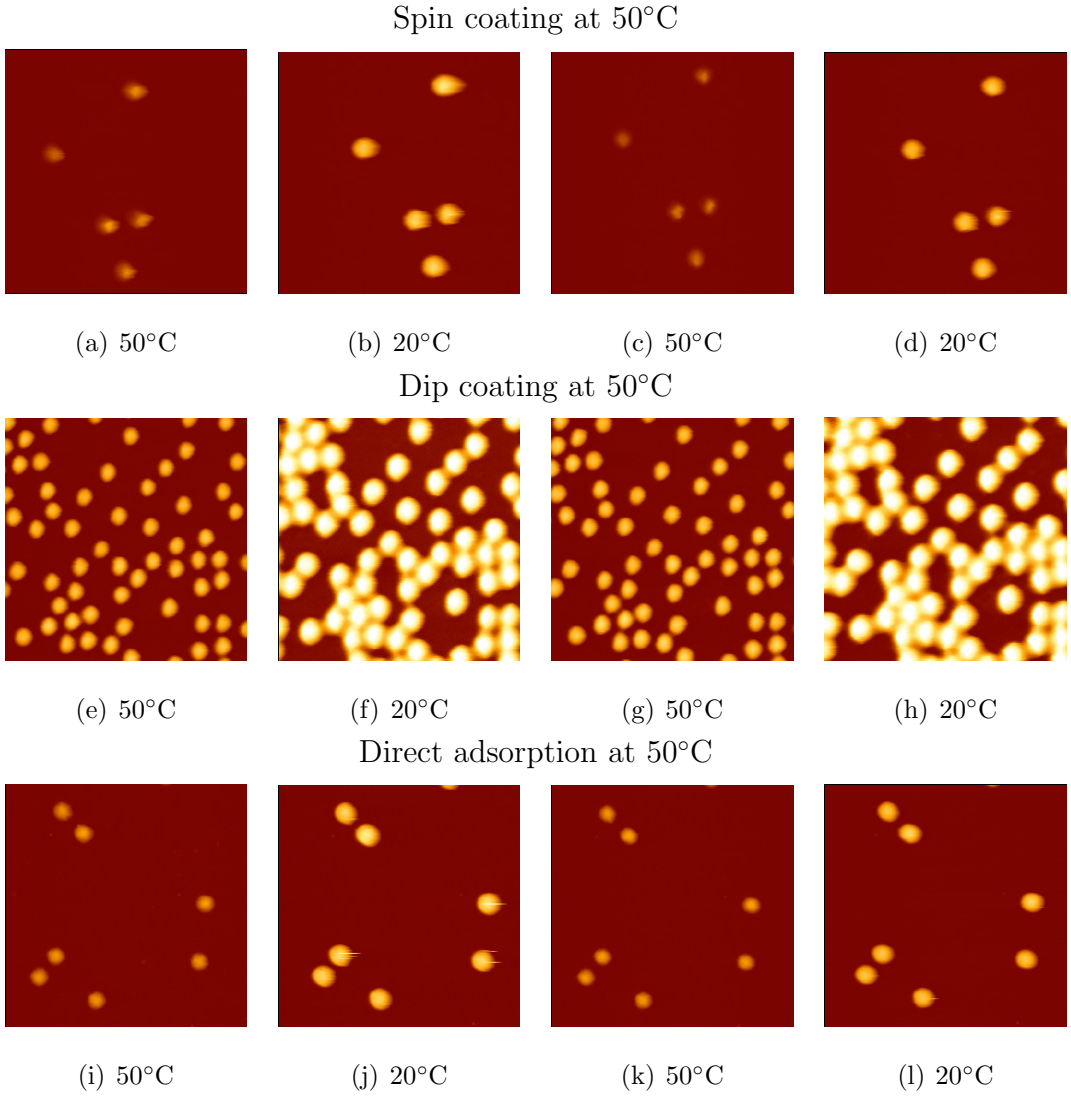

Figure 7.2: *SFM images of microgels deposited on Si/PAH at 50° C by spin coating at 2000 rpm (a-d), by dip coating (e-h), and by direct adsorption (i-l). Scan area is* 5x5 μ m^2.

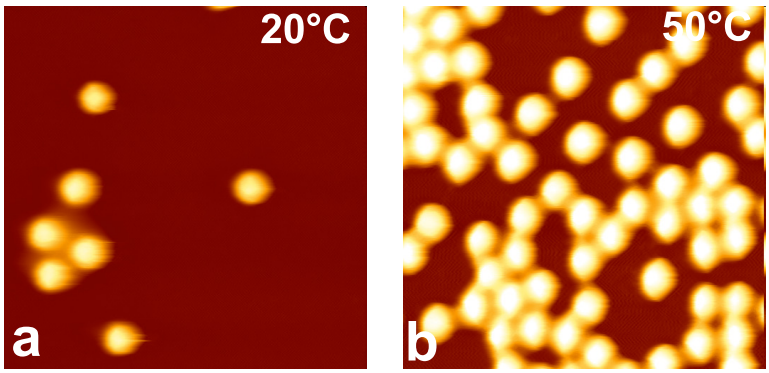

Figure 7.3: *SFM images of swollen microgel particles deposited by dip coating at (a) 20° C and (b) at 50° C on Si/PAH. Scan area is 5x5 μm^2.*

vertical as well as lateral directions. Particles deposited by one of the other techniques swell/shrink mainly in vertical direction.

In order to compare the swelling/deswelling behavior of particles deposited by different methods, the particle volume was calculated [16] (Fig. 7.5). The thermo-induced shrinking and reswelling is reversible over three cycles.

The particles deposited by spin coating are insensitive to the deposition temperature(Fig. 7.4 and Fig. 7.5). Oppositely, the particles deposited by dip coating and direct adsorption are susceptible to the deposition temperature. During the spin coating microgels are affected by large forces [39] and it seems, that the initial (swollen or collapsed) state of microgel does not play a significant role. In two other techniques the particles are not exposed to any forces acting during the deposition. So, the initial particle conformation determines the particle size in the further heating and cooling cycles in the dip coating and direct adsorption techniques.

The microgels deposited by direct adsorption and dip coating at 20°C are larger than the particles deposited by spin coating at 20°C (Fig. 7.5). The similar results were observed in [39]. They showed that the dried microgels deposited by active technique such as centrifugation were smaller than deposited by passive techniques due to the high

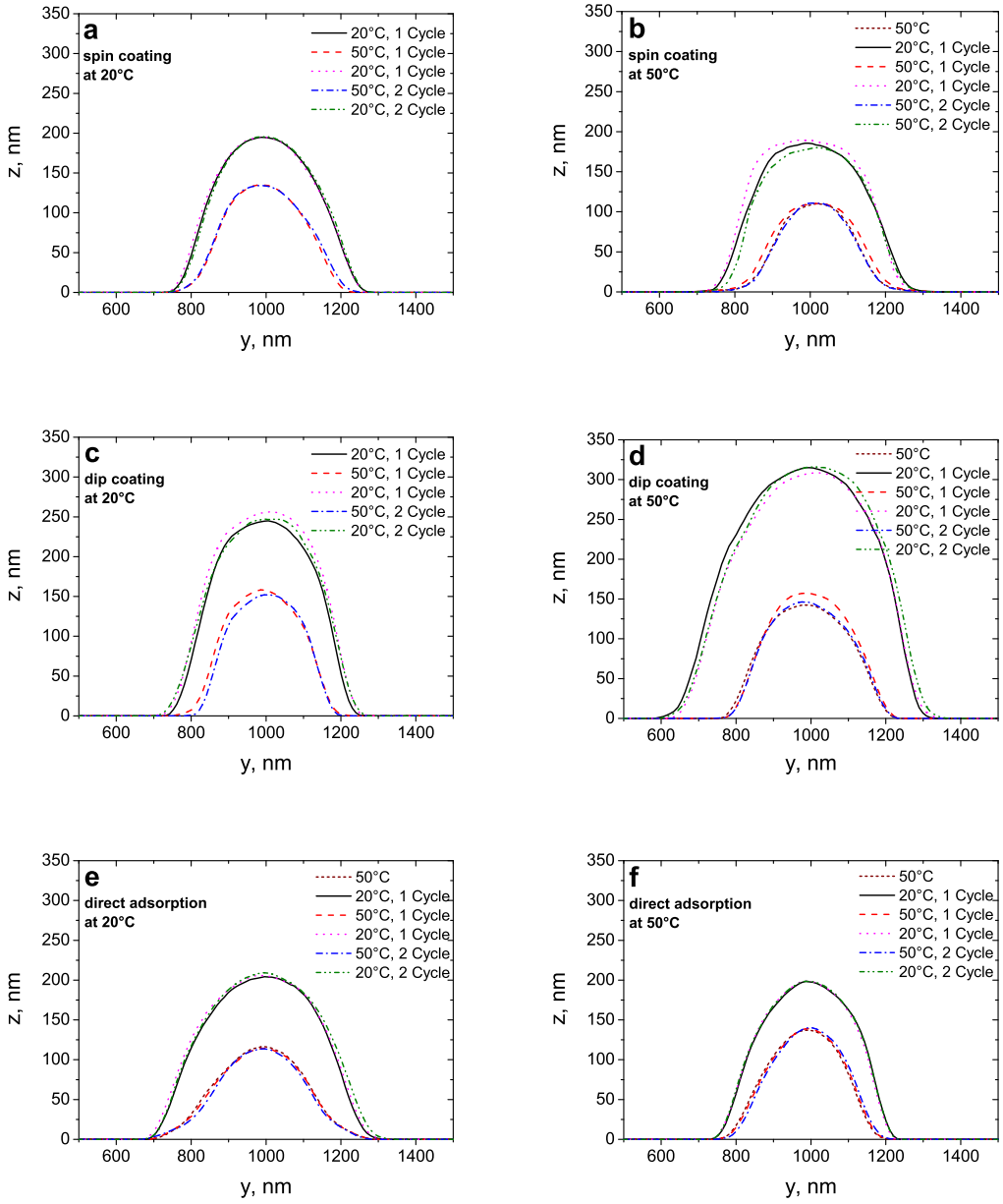

Figure 7.4: *Cross sections of microgel particles deposited on Si/PAH by (a) spin coating at 20° C, (b) spin coating at 50° C, (c) dip coating 20° C, (d) dip coating at 50° C, (e) direct adsorption at 20° C and (f) direct adsorption at 50° C measured by SFM.*

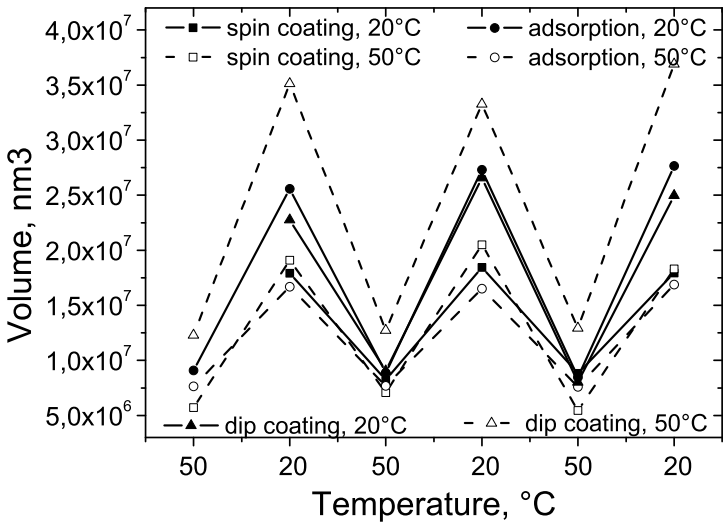

Figure 7.5: *Volume of microgel particles deposited o Si/PAH by spin coating (squares), direct adsorption (circles) and dip coating (triangles) at 20° C (full symbols) and 50° C (empty symbols) in two cycles.*

force effected during the deposition process, as discussed above.

The particles deposited by adsorption technique at diverse temperatures indicate differences in their thermo-induced swelling/ deswelling behavior (Fig. 7.5). In collapsed state particles offer more compact internal density than in swollen state. In adsorption process, connection between the substrate and the microgel particle are formed. Due to the higher internal density, collapsed particles should be able to form more connections than swollen particles. It leads to a decrease of the particle size for microgels deposited at higher temperatures in comparison with microgels adsorbed in swollen state (lower temperature).

By dip coating deposited microgels demonstrate the opposite behavior. The particles deposited at 50°C are much larger than the particles deposited at 20°C (Fig. 7.5). In this technique wafer were slowly pulled out from the microgel dispersion. Probably, in pulling out process the microgels sticked to the surface were dried in lateral direction and

the contact area of microgel particles with the substrate decreased. At the same time the evaporation process takes place (Fig. 7.6). In case of dip coating at 50°C the evaporation process is much faster than in case of 20°C. Due to the fast evaporation the particles grows in verticle direction. This effect is even more pronounced at higher temperatures.

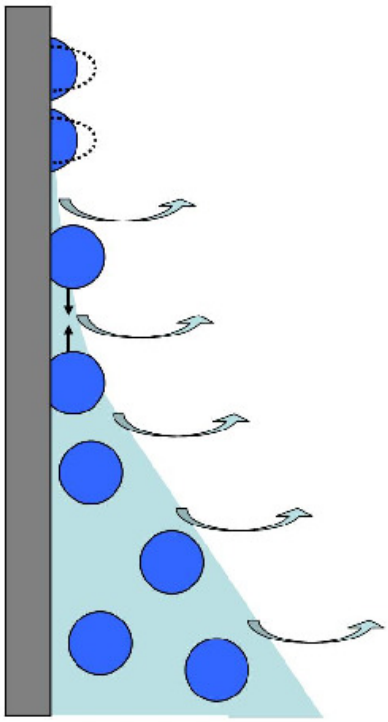

Figure 7.6: *Demonstration of evaporation process during the wafer pulling out from the microgel dispersion process in dip coating technique.*

7.1.1 Summary

The particles deposited on Si/PAH by different techniques demonstrate a reversible thermoresponsive behavior. The deposition method influences the size of deposited particles. Particles deposited by spin coating are insensitive to the deposition temperature. Oppositely, the deposition temperature in dip coating and direct adsorption affects strongly the microgel size. At 50°C the number density of deposited microgels is extremely high

also after very short deposition time. The huge number of adsorbed particles is explained by the increasing particle diffusion coefficient and the higher microgel concentration at the air-water interface.

7.2 Effect of substrate

For study of the thermo-induced behavior of the negatively charged P(NIPAM-co-AAc) adsorbed microgel particles, a positively charged substrate should be used.

The most easy way to get the positively charge substrate is the modification of the silicon wafers by polyelectrolytes layers assembled by layer-by-layer technique [117–119].

PEI is a "classical" polycation used as the first layer adsorbed on the solid substrates [16, 35, 36, 120–124]. Due to its branched structure it forms a suitable smoothed first layer. Unfortunately, during the swelling/deswelling experiments, PEI was also desorbed from the substrate and adsorbed on the SFM tip. It results in the formation of the "double tip" and impossibility to take the real SFM images. Therefore another substrates were used.

S. Schmidt *et.al.* investigated the adsorption ability of microgels on silicon wafers modified by polyelectrolyte layers [35] and showed that substrate plays important role in the microgel deposition process. It was shown that the surface roughness effects the number of adsorbed microgel particles. With increasing substrate roughness the number of adsorbed microgel increases.

In this section the effect of the substrate on the thermo-induced swelling/deswelling behavior of individual adsorbed microgels (a3-batch: 10% AAc and 5% BIS) was studied. Microgels were deposited on a so called simple substrates or silicon wafer precoated by gold (Au), surfactant (Si/APMS), polycations (Si/PEI and Si/PAH) and on the polyelectrolyte multilayers: Si/PEI/$(PSS/PAH)_x$, where $x = 1, 3, 6$ is a number of multilayers, and Si/PEI/PSS/PDADMAC.

7.2.1 Substrate characterization

At first, substrates were characterized by ellipsometry, contact angle measurements, streaming potential and SFM. The layer thickness, roughness, hydrophobicity (contact angle) and zeta potential were measured (Tab. 7.1 and 7.2).

substrate	h, nm	roughness, nm		
	air	air	liquid	
			20°	50°
Si/Au	≈ 100	1.32 ± 0.06	1.4 ± 0.1	1.6 ± 0.1
Si/APMS	1.2 ± 0.6	0.12 ± 0.03	0.42 ± 0.01	0.48 ± 0.01
Si/PEI	1.6 ± 0.2	0.20 ± 0.07	0.31 ± 0.03	0.30 ± 0.04
Si/PAH	1.1 ± 0.2	0.36 ± 0.07	0.46 ± 0.02	0.6 ± 0.1
Si/PEI/$(PSS/PAH)_1$	4.8 ± 0.2	1.2 ± 0.2	2.3 ± 0.3	1.6 ± 0.4
Si/PEI/$(PSS/PAH)_3$	9.5 ± 0.4	2.6 ± 0.4	2.4 ± 0.3	2.4 ± 0.3
Si/PEI/$(PSS/PAH)_6$	12.4 ± 0.5	2.1 ± 0.4	2.5 ± 0.2	2.5 ± 0.1

Table 7.1: *Substrate characteristics: the layer thickness h measured by ellipsometry excepting Si/Au, roughness measured for dry samples (air) and in liquid at temperatures 20°C and 50°C. Substrate roughness was measured by SFM.*

The thickness of PAH layer deposited on Si is significant lower than for PEI in Si/PEI. Probably it is connected with the worse coverage of Si by PAH compared to branched PEI. The thickness of multilayers $(PSS/PAH)_x$ increases with increasing number of multilayers x, resulting a rougher surface 7.1). The film roughness increases during the swelling process in the liquid SFM cell. The substrate roughness is almost independent on the temperature increase.

The substrate wettability was investigated by the contact angle measurements. The values of the contact angle of the water drops are reflected in table 7.2. The contact angle of the polyelectrolyte monolayer Si/PEI and Si/PAH is almost the same, for polyelectrolyte multilayers $(PSS/PAH)_x$ it is independent on the film thickness. The multilayers

substrate	contact angle, °			microgel width, nm	
	θ_0	$\theta_{MG}^{20°C}$	$\theta_{MG}^{50°C}$	20°C	50°C
Si/Au	30 ± 3	58 ± 3	14 ± 4	577	439
Si/APMS	49 ± 1	54 ± 10	47 ± 16	586	479
Si/PEI	21 ± 1	67 ± 3	43 ± 15	625	459
Si/PAH	19 ± 1	42± 9	13 ± 4	567	518
Si/PEI/$(PSS/PAH)_1$	38 ± 1	41 ± 12	31 ± 6	791	635
Si/PEI/$(PSS/PAH)_3$	40 ± 2	40 ± 9	18 ± 2	576	557
Si/PEI/$(PSS/PAH)_6$	38 ± 1	25 ± 8	12 ± 2	639	644

Table 7.2: *Contact angle of H_2O drops θ_0 and the contact angle of individual adsorbed microgel particles at temperatures 20°C $\theta_{MG}^{20°C}$ and at 50°C $\theta_{MG}^{50°C}$ and width of adsorbed microgels at 20° and 50° in the first short cycle given from SFM cross section profiles.*

are more hydrophobic than monolayers. There are two reasons. On one hand, the Si wafers are not completely covered by the polyelectrolyte monolayer and the hydrophilic silicon affects strongly on the water drop contact angle. On the other hand, (PSS/PAH) multilayers form homogeneous layer and cover completely the Si. These two facts leads to a decrease in the wettability of the $(PSS/PAH)_x$ layers.

7.2.2 Thermo-induced swelling/deswelling behavior of adsorbed microgels

Microgel particles were deposited on the substrates by spin coating with a rotation speed of 2000 rpm. Figures 7.7 and 7.8 demonstrate the deposited microgels in a swollen (20°C) and in a collapsed state (50°C).

In order to estimate the differences in microgel thermo-induced swelling/deswelling behavior cross sections of particles adsorbed on different substrates were evaluated (Fig. 7.9). From the cross section data, the volume of adsorbed particles was calculated (eq. 2.31). The volume dependence on temperature in two short cycles is shown in figure

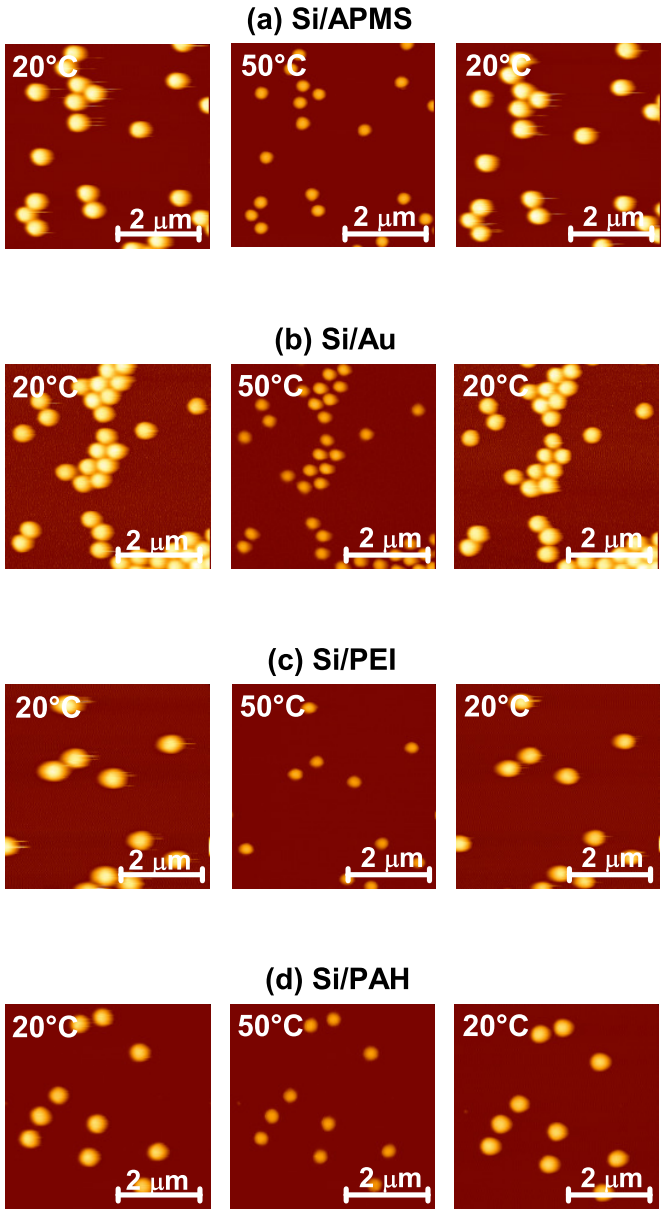

Figure 7.7: *SFM images of microgels deposited on (a) Si/APMS, (b) Si/Au, (c) Si/PEI, and (d) Si/PAH by spin coating at 2000 rpm. After imaging of microgels at 20° C (left images), samples were heated up to 50° C (middle images) and cooled down to 20° C again (right images).*

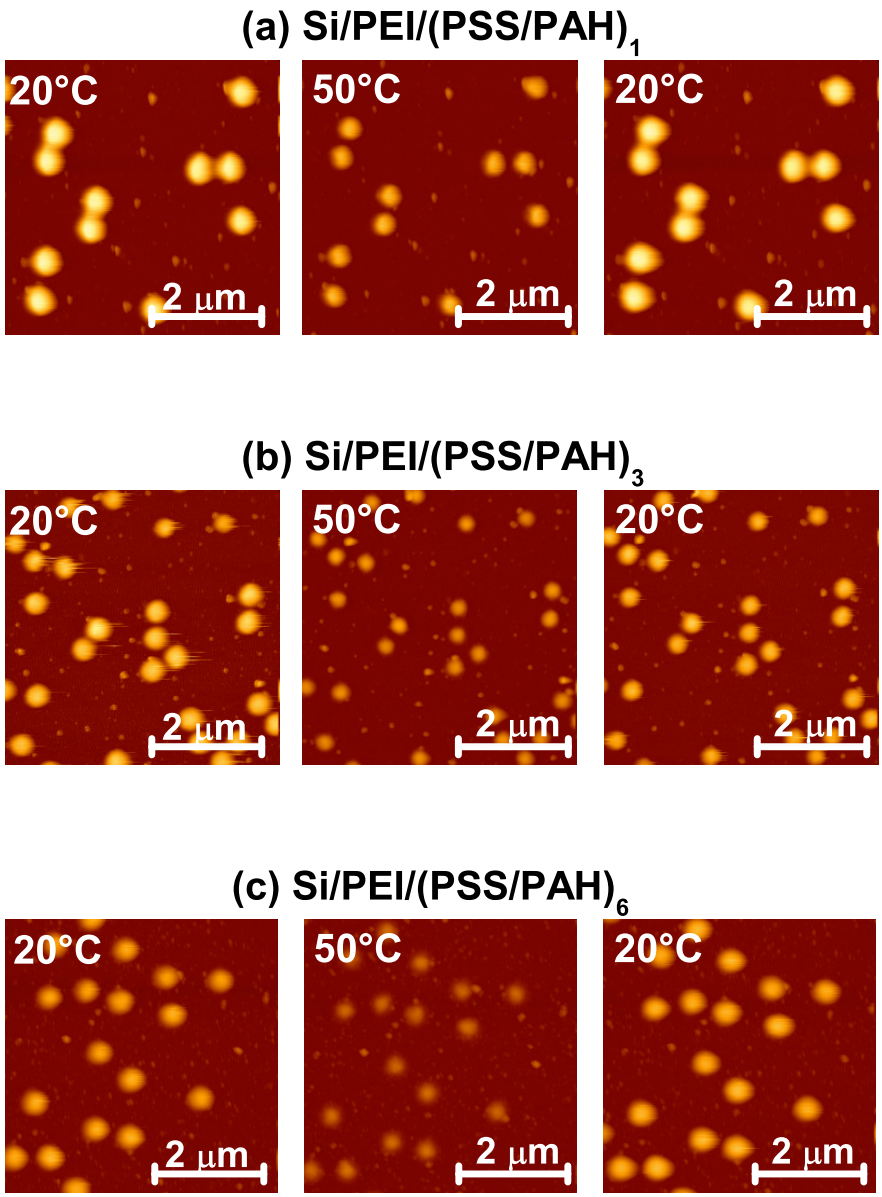

Figure 7.8: *SFM images of microgels deposited on (a) Si/PEI/(PSS/PAH)$_1$, (b) Si/PEI/(PSS/PAH)$_3$, and (c) Si/PEI/(PSS/PAH)$_6$ by spin coating at 2000 rpm. After imaging of microgels at 20°C (left images), samples were heated up to 50°C (middle images) and cooled down to 20°C again (right images). Small white spots are PAH coils.*

7.10. Tendentiously, the volume of particles deposited on "simple" substrates (Fig. 7.7) increases with increasing the water contact angle (θ_0) of the substrate. Microgels deposited on the Si/APMS have the largest volume. Probably, the huge water amount in the inner particle structure plays an important role. Due to that the particles are hydrophilic and don not connect to the hydrophobic substrate. Particles are pulled out from the substrate. The Si/PEI and Si/PAH exhibit almost the same values of the particle volume and the water contact angle (θ_0) excepting the first 20°C for Si/PEI. It seems to be, that PEI penetrates a little bit inside of 'porous-like' microgel particles. Due to the smaller length of polymer chains, microgels built more connections with the PEI branches insight of particle. Therefore the particle volume in swollen state slightly decreases in comparison with its initial value (Fig. 7.9 and 7.10a).

Microgels deposited on $(PSS/PAH)_x$ multilayers becomes smaller with increasing number of multilayers. Probably, for $x = 1$ the surface is still not completely homogeneously covered by the (PSS/PAH) layer. Due to the high branched structure of PEI, it still could affect on microgels. Therefore the contact area of particles with the substrate increases enormously. With increasing number of double (PSS/PAH) layers the thickness of the substrate increases as well and the influence of PEI on the P(NIPAM-co-AAc) microgels disappears. Particles become smaller and do not swell in lateral direction (Fig. 7.9). This phenomena is discussed below.

Microgels were also deposited on the Si/PEI/PSS/PDADMAC. Figure 7.11 demonstrates (a) the SFM image of adsorbed microgel particles on the Si/PEI/PSS/PDADMAC and (b) the cross section of an adsorbed microgel particle at 20°C. The glass transition temperature of PSS/PDADMAC system is about 35 - 40 °C [125]. Due to such lower value of the transition temperature, at higher temperatures the 'double' tip was formed and the data was not suitable for the numeric evaluation.

Due to the high water amount insight of microgel particles, the contact angle formed by an individual adsorbed microgel particle and the substrate was calculated from the SFM images (Fig. 7.9) and compared with the values of θ_0 (Tab. 7.2). It is interesting to notice that the contact angle of microgels in swollen state in the first short cycle or direct

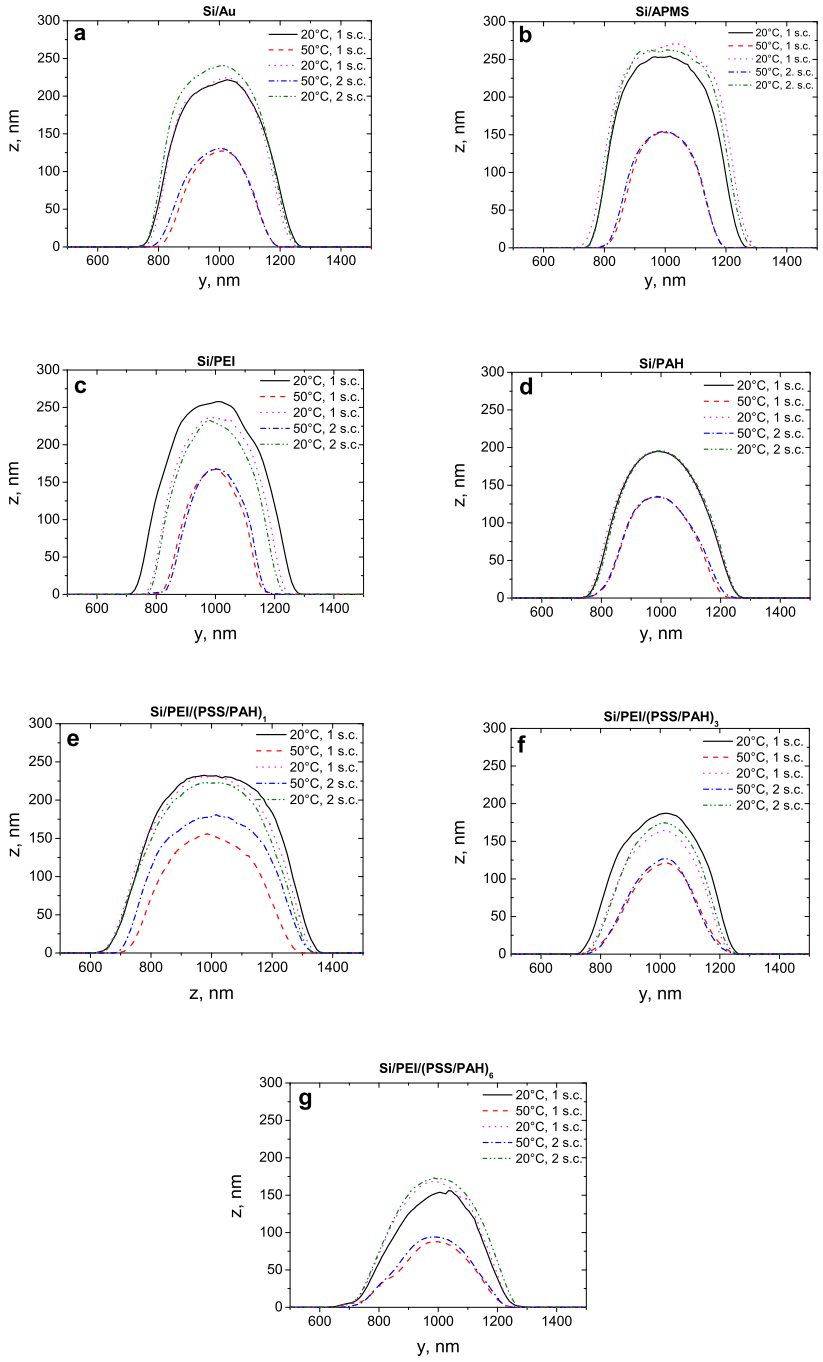

Figure 7.9: *Cross sections of microgel particles deposited on (a) Si/Au, (b) Si/APMS, (c) Si/PEI, (d) Si/PAH, (e) Si/PEI/(PSS/PAH)$_1$, (f) Si/PEI/(PSS/PAH)$_3$ and (g) Si/PEI/(PSS/PAH)$_6$.*

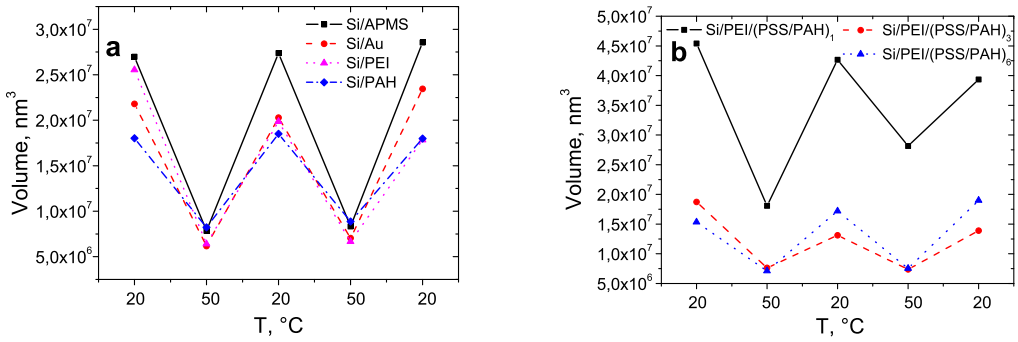

Figure 7.10: *Volume of microgel particles (a) deposited on "simple" substrate: Si/APMS (squares), Si/Au (circles), Si/PEI (triangles), and Si/PAH (rhombus); (b) deposited on Si/PEI/(PSS/PAH)$_x$, where $x = 1$ (squares), $x = 3$ (circles), and $x = 6$ (triangles). The particle volume was calculated for particles in swollen (20° C) and in collapsed (50° C) state in two short cycles.*

after adsorption depends on the outer polyelectrolyte layer and not on the film thickness. Microgels deposited on the PAH have smaller contact angle than microgels deposited on another substrates due to the glassy like state of PSS/PAH multilayers [123].

Tendentiously, the contact angle of microgels decreases with increasing temperature. It is connected with that fact that microgel particles becomes flatter in collapsed process.

Figure 7.12 shows the relative changes in the particle width. The microgel width was normalized with respect to the particle width at first 20°C or direct after deposition. The outer layer effects strongly on the particle width. Microgels deposited on the monolayers (Si/Au, Si/APMS, Si/PEI, Si/PAH) the amplitude of changes in the microgel width increases with decreasing the substrate wettability. Due to the high water content, particles deposited on a more hydrophobic surface loose the ability to swell/collapse in lateral direction. Polyelectrolyte as outer substrate layer effects on the reversibility of the width changes. Microgels deposited on Si/Au and Si/APMS demonstrate reversible behavior in the microgel width changes. Microgels deposited on polyelectrolytes have often a hysteresis in particle width. Probably, polyelectrolyte layers are able to restructure in heating

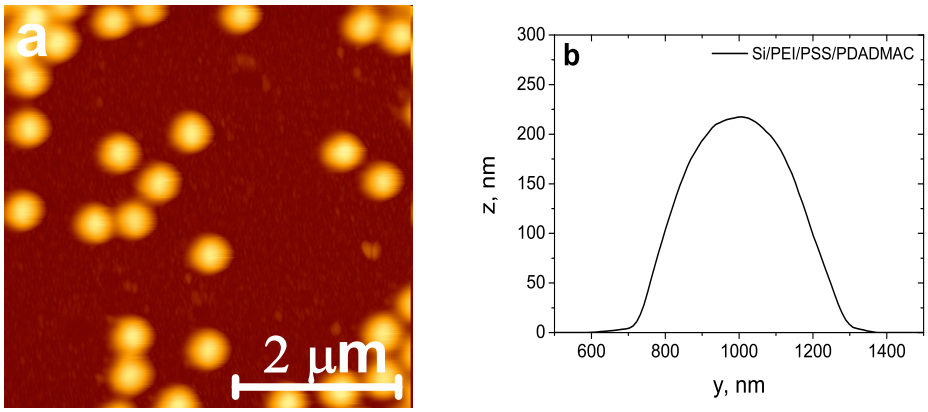

Figure 7.11: *(a) SFM image of microgel particles adsorbed on Si/PEI/PSS/PDADMAC via spin coating at 2000 rpm at 20° C and (b) it cross section.*

and cooling process and thereby effect on the contact area of microgels and substrates.

Microgels deposited on the Si/PEI/$(PSS/PAH)_x$ exhibit irreversible swelling/shrinking in lateral direction. The amplitude of the relative microgel width decreases with increasing x (Fig. 7.12). In case of $x = 0$ (Si/PEI), PEI layer is more movable than (PSS/PAH) multilayers due to the branched PEI structure. The PEI branches could penetrate inside of the soft microgel particle. It makes it easier for the particles to collapse and swell in lateral direction.

With increasing number of (PSS/PAH) bilayers particles lose their ability to swell and collapse in lateral direction. For $x = 1$ particles are still able to react on the temperature laterally but the relative particle width decreases with increasing number of temperature cycles. For $x > 1$ the particle width is almost insensitive to the changes in the temperature. This phenomena could be explained by increasing "glass-like" polyelectrolyte multilayer film thickness with increasing x. It leads to the decreasing polyelectrolyte layer "mobility" and impossibility to follow the thermo-induced particle lateral swelling and shrinking. Due to the "unmovable" polyelectrolyte multilayer, microgel width becomes almost constant at lower and higher temperatures.

Briefly, it should be noticed that the percentage of 'good' SFM images of particles

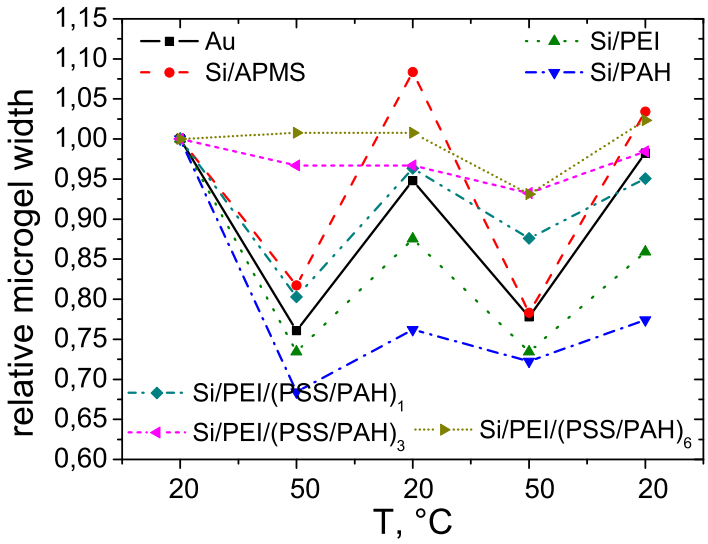

Figure 7.12: *Relative changes of width of adsorbed microgels at different substrates in swollen (20° C) and collapsed (50° C) states. The particle width was normalized with respect to the particle width at first 20° C.*

deposited on the Si/PEI, which was suitable for the numerous evaluation, is very small. Due to the very high adsorption properties of PEI, it was adsorbed on the SFM tip during the measurements and 'double' tip was built. For other substrates such effect was not observed.

7.2.3 Summary

It was shown that the substrate plays important role in thermo-induced swelling/deswelling behavior of adsorbed microgels. The substrate wettability effects the particle sizes in case of simple substrates such as Si/APMS, Si/PAH, Si/Au and Si/PEI. With increasing water contact angle, the microgel size increases as well. For microgels deposited on the Si/PEI/$(PSS/PAH)_x$, the ability to react on the temperature in the lateral direction disappears with increasing x. "Soft" substrates such as PEI or PDADMAC are not suitable

for the SFM measurements in liquid cell due to the polyelectrolyte desorption from the substrate and its adsorption on the SFM tip.

Chapter 8

Conclusions

The main aim of this work was to investigate the thermo-induced behavior of adsorbed PNIPAM-based microgel particles and to control the number density of particles adsorbed at solid substrates.

Six types of microgels were synthesized via emulsion polymerization with a different cross-linker (BIS) and anionic co-monomer (AAc) content. The cross-linker density is responsible for the particle stiffness. With increasing BIS content the elasticity of polymer network decreases resulting in the decreasing amount of adsorbed solvent. Co-monomer content affects strongly the particle charge. With increasing particle charge, the intra-particle repulsion increases leading to an enhance in the particle size.

The amount of incorporated co-monomers during the synthesis depends strongly on the cross-linker content. With increasing cross-linker content, amount of incorporated AAc co-monomers decreases. During the synthesis a core-shell structure is formed. Internal area of particles is core and have higher cross-linker density than "soft" shell exhibiting very lower BIS concentration. AAc is situated preferably in the particle periphery with a lower cross-linker density. With increasing BIS content the shell becomes thiner resulting in a decrease in an amount of incorporated AAc units.

P(NIPAM-co-AAc) microgels are temperature sensitive. Pure PNIPAM colloids exhibit an one-step transition at a temperature about 32°C caused by increased hydrophobic interactions leading to the particle collapse. Microgels containing charged co-monomers

exhibit a two-step transition. The first transition occurs at a temperature of about 32°C and is contributed from PNIPAM component. The second transition is affected by the increasing intra-particle electrostatic repulsion. It takes place at a temperature of about 45°C.

Due to the using thermo-responsive properties of PNIPAM-based microgels, they are high potential materials in coating industry. Therefore, microgels adsorption properties and their stimuli-responsive behavior war investigated in details. It is interesting to note that microgels with different BIS contents exhibit qualitatively the same behavior in bulk and in adsorbed state. The swelling ability of microgel particles decreases with increasing cross-linker content due to the decreasing elasticity of a gel network. Generally, microgels in an adsorbed state have significantly higher internal density than in a volume phase.

Microgels with lower BIS concentration becomes flatter during the heating process. Particles with the high cross-linker density exhibit a hard particle like behavior and preserve its shape at different temperatures.

The adsorbed microgel containing charged co-monomers exhibit only one transition temperature. It shifts to the higher temperatures with increasing co-monomer content.

For all six types of microgels the reswelling experiment were carried out. It was shown that adsorbed microgels could reswell to their prevent state after complete drying and their further immerse into the liquid. Reswollen microgels exhibit reversible thermo-induced swelling/deswelling behavior.

For one type of microgels (a3: 5% BIS and 10% AAc), the influence of outer stimulis, substrate, deposition procedure was investigated.

In present work it was shown that "soft" substrates such as PEI or PDADMAC are not appropriate for the SFM measurements in liquid due to the desorption of polycations from the substrate and their further adsorption on the SFM tip. Si/Au, Si/APMS, Si/PAH are more suitable for such kind of experiments.

Deposition technique and temperature are also affect the behavior of adsorbed microgels in heating/cooling cycles. Three different deposition techniques were chosen: spin coating, dip coating and direct adsorption. The deposition temperature was 20°C and

50°C. Particles deposited by spin coating and dip coating were dried during the deposition and were reswelled in the liquid SFM cell. Microgels deposited by direct adsorption were constantly in liquid. Due to the very swollen state the first images of microgels deposited by direct adsorption at 20°C were taken at 50°C, where particles were completely collapsed. Particles deposited by spin coating are insensitive to the deposition temperature. Oppositely, the deposition temperature in dip coating and direct adsorption affects strongly the microgel size. At 50°C the number density of deposited microgels is extremely high also after very short deposition time. The huge number of adsorbed particles is explained by the increasing particle diffusion coefficient and the higher microgel concentration at the air-water interface.

In order to investigate the response of microgel particles on outer stimulis, the effect of pH, ionic strength, and cononsolvency was studied. The effect of pH and ionic strength on the thermo-induced swelling/shrinking behavior of adsorbed microgels was investigated on particles deposited at Si/PEI surfaces. It was shown that only microgels deposited on Si/PEI into the solvents with neutral pH values stayed fix during the heating/cooling procedures. At lower pH microgels exhibit small charge, but the substrate is charged. During the scanning, microgels were still unstable at 20°C and could be easily moved by the SFM tip. Oppositely, at high pH values, microgels are charged but PEI is uncharged. At a high temperature (50°C) microgels were desorbed. At intermediate pH, both the microgels and the substrate are charged, resulting in the stability of adsorbed particles in swollen and in collapsed state.

For the same particle-substrate system, the effect of ionic strength was proven. Adsorbed microgels were stable below the salt concentration of 1 M and demonstrated a reversible thermo-induced swelling/deswelling behavior.

The effect of cononsolvency was proven on a3 microgel particles in bulk and in an adsorbed state on Si/PAH. EtOH and 2-Pr were used as organic co-solvents. The microgels were not dissolved in 2-Pr/water mixtures due to the enhanced hydrophobicity of solvent. For microgels in EtOH/water mixtures the cononsolvency was only observed for particles in bulk. In general, no cononsolvency was observed for deposited particles. The swelling

ratio of deposited microgel particles increases with increasing alcohol content. For more hydrophobic 2-Pr, the swelling ratio of adsorbed microgel is higher than for EtOH. At higher 2-Pr concentrations adsorbed microgel particles loose their thermo-sensitivity. At a lower alcohol concentration adsorbed microgels and microgels in bulk exhibit the largest sizes due to the increasing intra-particle osmotic pressure resulting from the increasing electrostatic repulsion between charged co-monomers.

To answer the second question about the control over the number density of adsorbed particles, a3 microgels with 5% BIS and 10% AAc were deposited via spin coating on the Si/PEI. It was shown that the number density of microgels deposited on a positively charged substrate could be controlled by the microgel dispersion concentration, pH value of the microgel solution, the rotation speed, co-monomer content, and the solvent quality. The number density of adsorbed microgels increases with increasing microgel concentration and pH, due to the increasing electrostatic attraction between negatively charged particles and the positively charged substrate. But this effect disappears, if samples were prepared from very concentrated particle dispersions. At high concentrations the closed hexagonal packed microgel films were formed. The number density decreases with increasing rotation speed. The "limit" rotation speed was determined: for speeds higher than "limit" speed no speed effect was observed. By a suitable combination of the pH value of the microgel dispersion and the rotation speed microgels form a pattern with a large distance between two single particles adsorbed at the solid substrate.

Ethanol as a solvent component plays an important role in the formation of microgel layer. Due to the fast evaporation, microgels deposited from pure EtOH generate very close hexagonal package. With increasing water content in the microgel dispersion, the distance between adsorbed microgels increases due to decreasing solvent evaporation rate in the deposition process and changing dielectric constant leading to the changing electrostatic and capillary forces.

Chapter 9

Outlooks

Microgel particles are an interesting material for different application goals especially in coverage industry. Therefore the behavior of adsorbed microgels should be investigated in more details. The swelling/deswelling of pure PNIPAM microgel particles with different cross-linker content should be studied for adsorbed microgels.

In [35] was shown that the microgel number increases with increasing substrate with higher roughness. The effect of the substrate on the amount of adsorbed microgels could be qualitatively investigated by QCM measurements. The effect of the substrate drying on the amount of adsorbed particles could be also proved by QCM.

In order to get more detailed information about the contact angle of adsorbed microgel particles, the side microgel area should be taken with higher resolution by SFM. It is also interesting to prove, if the correlation between a microgel contact angle and a water contact angle at different temperatures takes place.

In order to prevent the influence of particle charge, it should be proven, if the conon-solvency could be observed for pure PNIPAM microgels in bulk and in an adsorbed state. The adsorption ability of microgels deposited from alcohol/water mixtures should be also estimated. The behavior of microgels with different charged co-monomer contents in alcohol/water mixtures with lower alcohol contents should be compared. It also should be proved, if the distance between adsorbed particles could be controlled by tuning the particle charge and the solvent dielectric constant. The behavior of microgels in alcohol/water

mixtures could be interesting in some application areas. For instance, in the controlled release of alcohol soluble substances.

Due to the thermo-induced swelling/shrinking behavior of adsorbed microgel particles, the experiments of controlled release of substances containing in microgels could be carried out. On one hand, the microgels, containing for instance a dye, could be adsorbed on the suitable substrate. After the sample deposition in a suitable solvent, the content of released amount of substance should be detected. The effect of the temperature, deposition technique, solvent parameters such as pH, ionic strength, quality, *etc.* should be proved. On the other hand, it is important to prove, if the microgels deposited by techniques, where the samples are dry after the preparation, are still containing the substance and if it could be released from the microgel after the sample reswelling.

Abbreviations

α	swelling ratio
χ	polymer/solvent interaction parameter
δ	phase
Δ	phase difference
ϵ	dielectric constant
ϵ_0	dielectric permittivity of vacuum
φ	volume fraction
γ	surface tension
Γ	relaxation rate
η	viscosity
λ	wave length
μ	electrophoretic mobility
ν	chain density
π	osmotic pressure
θ	angle
ρ	density
τ	relaxation time
ω	frequency
ζ	zeta potential
2-Pr	isopropanol
AAc	acrylic acid

APMS	3-Aminopropyltrimethoxysilane
b	friction coefficient
B	magnetic field
BIS	N,N'-methylenebisacrylamide
D	diffusion coefficient
D	dissipation in QCM measurements
DLS	dynamic light scattering
E	electric field
et.al	et altera
etc.	et cetera
EtOH	ethanol
f	number of counterions per chain
f	frequency in QCM and
F_0	force amplitude
F	free energy
F_{ts}	tip-surface interaction
$g_1(t)$	time autocorrelation function
$g_2(t)$	intensity time autocorrelation funcrion
$G_2(t)$	time autocorrelation function
h	layer thickness
H	particle heigth
I	initiator in synthesis
I	light intensity
I	ionic strength
$I.r.$	incorporation ratio
$\vec{k}$	wave vector
k	Boltzmann constant
k	srping constant
KPS	potassium persulfate

l.c.	long cycle
LCST	lower critical solution temperature
m	mass
M	monomer
n	refractive index
N_A	Avogadro's number
NIPAM	N-isopropylacrylamide
P	polarization
PAH	poly(allylamine hydrochloride)
PDADMAC	poly(diallyl-dimethyl-ammonium chloride)
PDI	polydispersity index
PAH	poly(ethelenimine)
PNIPAM	poly(N-isopropylacrylamine)
PSS	poly(styrene sulphonate)
$\vec{q}$	scattering vector
QCM	quartz crystal microbalance
R_h	hydrodynamic radius
R_q	root mean squared roughness
r.c.	reswelling cycle
rpm	rounds per minute
S	stopper
s.c.	short cycle
SEM	scanning electron microscopy
SFM	scanning force microscopy
Si	silicon
T	temperature
T	transfered molecule in synthesis
UCST	upper critical solution temperature
v	solvent volume

$\vec{v}$	velosity
V	volume
x	coordinate or fast scan axis in SFM
y	coordinate or slow scan axis in SFM
z	coordinate or deflection in SFM

List of publications

- A. Burmistrova, R. v. Klitzing, Control of number density and swelling/shrinking behavior of P(NIPAM-AAc) particles at solid surfaces, Journal of Materials Chemistry, 2010, Volume 20, Issue 17, 3502-3507
- A. Burmistrova, R. Steitz, R. v. Klitzing, Temperature response of PNIPAM derivatives at planar surfaces: Comparison between polyelectrolyte multilayers and adsorbed microgels, ChemPhysChem, Volume 11, Issue 17, 3751-3579
- A. Burmistrova, M. Richter, C. Üzüm, R. v. Klitzing, Effect of cross-linker density of P(NIPAM-co-AAc) microgels at solid surfaces on the swelling/shrinking behavior and Young's Modulus, Colloid and Polymer Science, in press

Bibliography

[1] Hideya Kawasaki, Shigeo Sasaki, and Hiroshi Maeda. *J. Phys. Chem. B.*, 101(26):5089–5093, 1997.

[2] L. H. Gan, Y. Y. Gan, and G. Roshan Deen. *Macromolecules*, 33:7893–7897, 2000.

[3] Akira Mamada, Toyoichi Tanaka, and Dawan Kungwatchakun and. *Macromolecules*, 23:1517–1519, 1990.

[4] Mitsuhiro Shibayama, Shin ya Mizutani, and Shunji Nomura. *Macromolecules*, 29:2019–2024, 1996.

[5] Robert Pelton. *Advances in Colloid and Interface Science*, 85:1–33, 2000.

[6] Karl Kratz and Wolfgang Eimer. *Ber. Bunsenges. Phys. Chem.*, 102(6):848–854, 1998.

[7] Takasi Sawai, Shinsuke Yamazaki, Yoshihito Ikariyama, and Masuo Aizawa. *Macromolecules*, 24:2117–2118, 1991.

[8] Toyoichi Tanaka. *Physica*, 140A:261–268, 1986.

[9] Matthias Karg, Isabel Pastoriza-Santos, Benito Rodriguez-Gonzalez, Regine von Klitzing, Stefan Wellert, and T. Hellweg. *Langmuir*, 24(12):6300–6306, 2008. PMID: 18489184.

[10] Helene Dalmont, Orawan Pinprayoon, and Brian R. Saunders. *Langmuir*, 24:2834–2840, 2008.

[11] Shuiqin Zhou and Benjamin Chu. *J. Phys. Chem. B*, 102:1364–1371, 1998.

[12] Sergey Kazakov, Marian Kaholek, Irina Gazaryan, Boris Krasnikov, Korki Miller, and Kalle Levon. *The Journal of Physical Chemistry B*, 110(31):15107–15116, 2006.

[13] Christine M. Nolan, Catherine D. Reyes, Justin D. Debord, Andres J. Garcia, and L. Andrew Lyon. *Biomacromolecules*, 6(4):2032–2039, 2005.

[14] T. Hellweg, C. D. Dewhurst, E. Brueckner, K. Kratz, and W. Eimer. *Colloid Polym Sci*, 278:972–978, 2000.

[15] Hidenobu Shimizu, Risei Wada, and Masaru Okabe. *Polymer Journal*, 41(9):771–777, 2009.

[16] Anna Burmistrova and Regine von Klitzing. *Journal of Materials Chemistry*, 20(17):3502–3507, 2010.

[17] Karl Kratz, Thomas Hellweg, and Wolfgang Eimer. *Colloids and Surfaces A: Physicochemical and Engineering Aspects*, 170:137–149, 2000.

[18] Todd Hoare and Robert Pelton. *Macromolecules*, 37:2544–2550, 2004.

[19] Todd Hoare and Robert Pelton. *Langmuir*, 20:2123–2133, 2004.

[20] Nodar Al-Manasir, Kaizheng Zhu, Anna-Lena Kjoniksen, Kenneth D. Knudsen, Goeran Karlsson, and Bo Nystroem. *J. Phys. Chem. B*, 113:11115–11123, 2009.

[21] Kwang Suk Oh, Jeong Seok Oh, Hyun Seok Choi, and Young Chan Bae. *Macromolecules*, 31:7328–7335, 1998.

[22] Thomas Hellweg. *Nanoscale Materials*. Kluwer Academic Publishers, 2003.

[23] Alexander F. Routh and Brian Vincent. *Langmuir*, 18:5366–5369, 2002.

[24] Imre Varga, Tibor Gilnyi, Robert Meszaros, Genoveva Filipcsei, and Miklos Zrinyi. *The Journal of Physical Chemistry B*, 105(38):9071–9076, 2001.

[25] Emma Daly and Brian R. Saunders. *Phys. Chem. Chem. Phys.*, 2:3187–3193, 2000.

[26] Emma Daly and Brian R. Saunders. *Langmuir*, 16:5546–5552, 2000.

[27] Madeline Torres-Lugo and Nikolaos A. Peppas. *Macromolecules*, 32:6646–6651, 1999.

[28] Bastian Brugger, Brian A. Rosen, and Walter Richtering. *Langmuir*, 24(21):12202–12208, 2008. PMID: 18839977.

[29] W. Wang, E. Metwalli, J. Perlich, C. M. Papadakis, R. Cubitt, and P. Mueller-Buschbaum. *Macromolecules*, 42(22):9041–9051, 2009.

[30] L. Andrew Lyon, Zhiyong Meng, Neetu Singh, Courtney D. Sorrell, and Ashlee St. John. *Chemical Society Reviews*, 38:865–874, 2009.

[31] Feng Zhang and Chang-Chun Wang. *Langmuir*, 25(14):8255–8262, 2009.

[32] Christine M. Nolan, Michael J. Serpe, and L. Andrew Lyon. *Biomacromolecules*, 5:1940–1946, 2004.

[33] Jongseong Kim, Michael J. Serpe, and L. Andrew Lyon. *J. Am. Chem. Soc.*, 126:9512–9513, 2004.

[34] To Ngai, Sven Holger Behrens, and Helmut Auweter. *Chem. Commun.*, pages 331–333, 2005.

[35] Stephan Schmidt, Thomas Hellweg, and Regine von Klitzing. *Langmuir*, 24(21):12595–12602, 2008. PMID: 18847289.

[36] Stephan Schmidt, Hubert Motschmann, Thomas Hellweg, and Regine von Klitzing. *Polymer*, 49 (3):749–756, 2008.

[37] P. E. Dyshlovenko. *Physical Review Letters*, 95(3):119801, 2005.

[38] Antony S. Dimitrov and Kuniaki Nagayama. *Langmuir*, 12:1303–1311, 1996.

[39] Antoinette B. South, Rachel E. Whitmire, Andres J. Garcia, and L. Andrew Lyon. *Applied materials and interfaces*, 1(12):2747–2754, 2009.

[40] L. Andrew Lyon, Justin D. Debord, Saet Byul Debord, Clinton D. Jones, Jonathan G. McGrath, and Michael J. Serpe. *The Journal of Physical Chemistry B*, 108(50):19099–19108, 2004.

[41] Saet Byul Debord and L. Andrew Lyon. *J. Phys. Chem. B.*, 107:2927–2932, 2003.

[42] Verawan Nerapusri, Joseph L. Keddie, Brian Vincent, and Ibraheem A. Bushnak. *Langmuir*, 22:5036–5041, 2006.

[43] Ana L. Cordeiro, Ralf Zimmermann, Stefan Gramm, Mirko Nitschke, Andreas Janke, Nicole schaefer, karina Grundke, and Carsten Werner. *Soft Matter*, 5:1367–1377, 2009.

[44] Kyle N. Plunkett, Xi Zhu, Jeffrey S. Moore, and Deborah E. Leckband. *Langmuir*, 22:4259–4266, 2006.

[45] Dirk Schmaljohann, Detlev Beyerlein, Mirko Nitschke, and Carsten Werner. *Langmuir*, 20:10107–10114, 2004.

[46] Paul A. FitzGerald, Javier I. Amalvy, Steven P. Armes, and Erica J. Wanless. *Langmuir*, 24 (18):10228–10234, 2008.

[47] Shaun C. Howard, V. S. J. Craig, Paul A. FitzGerald, and Erica J. Wanless. *Langmuir*, 26(18):14615–14623, 2010.

[48] Naoyuki Ishida and Simon Biggs. *Macromolecules*, 40:9045–9052, 2007.

[49] Kun Wu, Bing Wu, Ping Wang, Yi Hou, Guangzhao Zhang, and Da-Ming Zhu. *J. Phys. Chem. B*, 111:8723–8727, 2007.

[50] Michael J. Serpe and L. Andrew Lyon. *chem. Mater.*, 16:4373–4380, 2004.

[51] Sarah Hoefl, Lothar Zitzler, Thomas Hellweg, Stephan Herminghaus, and Frieder Mugele. *Polymer*, 48:245–254, 2007.

[52] Oya Tagit, Nikodem Tomczak, and G. Julius Vancso. *Small*, 4(1):119–126, 2008.

[53] Justyna Wiedemair, Michael J. Serpe, Jongseong Kim, Jean-Francois Masson, L. Andrew Lyon, Boris Mizaikoff, and Christine Kranz. *Langmuir*, 23:130–137, 2007.

[54] Dietrich Braun, Harald Cherdon, Matthias Rehahn, Helmut Ritter, and Brigitte Voit. *Polymer Synthesis: Theory and Practice. Fundamentals, Methods, Experiments*. Springer, 2005.

[55] Olga E. Philippova, Dominique Hourdet, Roland Audebert, and Alexei R. Khokhlov. *Macromolecules*, 30:8278–8285, 1997.

[56] Hideya Kawasaki, Shigeo Sasaki, and Hiroshi Maeda. *J. Phys. Chem. B*, 101:4184–4187, 1997.

[57] Andy C. W. Lau and Chi Wu. *Macromolecules*, 32:581–584, 1999.

[58] Larisa M. Mikheeva, Natalia V. Grinberg, Alexander Ya. Mashkevich, Valerij Ya. Grinberg, Le Thi Minh Thanh, Elena E. Makhaeva, and Alexei R. Khokhlov. *Macromolecules*, 30:2693–2699, 1997.

[59] Y. Okazaki, K. Ishizuki, S. Kawauchi, M. Satoh, and J. Komiyama. *Macromolecules*, 29:8391–8397, 1996.

[60] Jin-Oh You and Debra R. Auguste. *Langmuir*, 26(7):4607–4612, 2010.

[61] M. Jesus Molina, M. Rosa Gomez-Anton, and Ines F. Pierola. 111:12066–12074, 2007.

[62] A. Yu. Grosberg and A. R. Khokhlov. *Staticheskaya fizika makromolekul*. Moskva Nauka, 1989.

[63] Toyoichi Tanaka, David Fillmore, Shao-Tang Sun, Izumi Nishio, Gerald Swislow, and Arati Shah. *Physical Review Letters*, 45(20):1636–1639, 1980.

[64] Etsuo Kokufuta, Benlian Wang, Ryo Yoshida, Alexei R. Khokhlov, and Mitsuo Hirata. *Macromolecules*, 31:6878–6884, 1998.

[65] Mitsuhiro Ebara, Takao Aoyagi, Kiyotaka Sakai, and Teruo Okano. *Macromolecules*, 33:8312–8316, 2000.

[66] Alexander J. Marshall, Jeff Blyth, Colin A. B. Davidson, and Christopher R. Lows. *Anal. Chem.*, 75:4423–4431, 2003.

[67] Tiantin Gan, Yongjiun Zhang, and Ying Guan. *Biomacromolecules*, 10(6):1410–1415, 2009.

[68] Nian Wang, Geying Ru, Liying Wang, and Jiwen Feng. *Langmuir*, 25(10):5898–5902, 2009.

[69] Jongseong Kim, Satish Nayak, and L. Andrew Lyon. *J. Am. Chem. Soc.*, 127:9588–9592, 2005.

[70] Michael J. Serpe, Kristen A. Yarmey, Christine M. Nolan, and L. Andrew Lyon. *Biomacromolecules*, 6:408–413, 2005.

[71] Todd Hoare and Robert Pelton. *The Journal of Physical Chemistry B*, 111(41):11895–11906, 2007. PMID: 17894483.

[72] B. Sierra-Martin, M. S. Romero-Cano, A. Fernndez-Nieves, and A. Fernndez-Barbero. *Langmuir*, 22 (8):3586–3590, 2006.

[73] Anders Larsson, Dirk Kuckling, and Monika Schoenhoff. *Colloid and Surfaces A: Physicochemical and Engineering Aspects*, 190:185–192, 2001.

[74] S. Seelenmeyer, I. Deike, N. Dingenouts, Ch. Norhausen, M. Ballauff, and T. Narayanan. *Journal of Applied Crystallography*, 33:574–576, 2000.

[75] B. Sierra-Martin, Y. Choi, M. S. Romero-Cano, T. Cosgrove, B. Vincent, and A. Fernandez-Barbero. *Macromolecules*, 38:10782–10787, 2005.

[76] Karl Kratz, Alain Lapp, Wolfgang Eimer, and Thomas Hellweg. *Colloids and Surfaces A: Physicochemical and Engineering Aspects*, 197:55–67, 2002.

[77] Anna Burmistrova, Marcel Richter, Cagri Uezuem, and Regine von Klitzing. *in preparation*, 2010.

[78] Katsuya Mukae, Masao Sakurai, Seiji Sawamura, Kimiko Makino, Sung Wan Kim, Iassak Ueda, and Keishiro Shirahama. *J. Phys. Chem.*, 97:737–741, 1993.

[79] Guangzhao Zhang and Chi Wu. *J. Am. Chem. Soc.*, 123:1376–1380, 2001.

[80] Howard G. Schild, . Muthukumar, and David A. Tirrell. *Macromolecules*, 24:948–952, 1991.

[81] Makoto Asano, Francoise M. Winnik, Takashi Yamashita, and Kazuyuki Horie. *Macromolecules*, 28:5861–5866, 1995.

[82] Courtney D. Sorrell and L. Andrew Lyon. *Langmuir*, 24:7216–7222, 2008.

[83] Zhiyong Meng, Jae Kyu Cho, Stella Debord, Victor Breedveid, and L. Andrew Lyon. *The Journal of Chemical Physics B*, 111:6992–6997, 2007.

[84] Courtney D. Sorrell and L. Andrew Lyon. *J. Phys. Chem. B*, 111:4060–4066, 2007.

[85] Anna Burmistrova, Roland Steitz, and Regine von Klitzing. *ChemPhysChem*, 11:3571–3579, 2010.

[86] Bruce J. Berne and Robert Pecora. *Dynamic Light Scattering With Applications to Chemistry, Biology, and Physics*. Dover Publications, Inc. Mineola, New York, 2000.

[87] J. Lyklema. Academic Press, 2001.

[88] Holger Schoenherr and G. Julius Vancso. *Scanning Force Microscopy of Polymers*. Springer, 2010.

[89] Alvaro San Paulo and Ricardo Garcia. *Physical Review B*, 66:041406–1–4, 2002.

[90] JPK Instruments AG. *The NanoWizardR AFM*, 08 2007.

[91] Optrel GBR, Strasse der Jugnd 27-29, 14532 Kleinmachnow. *The Multiscope*.

[92] R. H. Pelton and P. Chibante. *Colloid Surf.*, 20:247–256, 1986.

[93] Hans Joachim Schoepe. *J. Phys.: Condens. Matter*, 15:L533–L540, 2003.

[94] H. J. Schoepe, A. Barreira, H. Koenig, J. Marques Hueso, and R. Biehl. *Langmuir*, 22:1828–1838, 2006.

[95] Todd Hoare and Robert Pelton. *Langmuir*, 22:7342–7350, 2006.

[96] Zbigniew Adamczyk, Aneta Michna, Magdalena Szaraniec, Anna Bratek, and Jakub Barbasz. *Journal of Colloid and Interface Science*, 313(1):86 – 96, 2007.

[97] Joseph Iruthayaraj, Evgeni Poptoshev, Ausvydas Vareikis, Ricardas Makuska, Albert van der Wal, and Per M. Claesson. *Macromolecules*, 38(14):6152–6160, 2005.

[98] A. Fernandez-Nieves, A. Fernandez-Barbero, B. Vincent, and F. J. de las Nieves. *Macromolecules*, 33(6):2114–2118, 2000.

[99] He Cheng, Lei Shen, and Chi Wu. *Macromolecules*, 39:2325–2329, 2006.

[100] Franck Montagne, Jerome Polesel-Maris, Raphael Pugin, and Harry Heinzelmann. *Langmuir*, 25(2):983–991, 09.

[101] Shuo Bai, Changzhu Wu, Kornelia Gawlitza, Regine von Klitzing, Marion B. Ansorge-Schumacher, and Dayang Wang. *Langmuir*, 26(15):12980–12987, 2010.

[102] Zhishen Ge, Dang Xie, Daoyong Chen, Xiaoze Jiang, Yanfeng Zhang, Hewen Liu, and Shiyong Liu. *Macromolecules*, 40(10):3538–3546, 2007.

[103] Hirohisa Miki, Shin Yagihara, Sada atsu Mukai, and Masyuki Tokita. *Progr Colloid Polym Sci*, 136:101–106, 2009.

[104] Fumihiko Tanaka, Tsuyoshi Koga, and Francoise M. Winnik. *Progr Colloid Polym Sci*, 136:1–8, 2009.

[105] T. Iwatsubo, K. Ogasawara, A. Yamasaki, T. Masuoka, and K. Mizoguchi. *Macromolecules*, 28:6579–6585, 1995.

[106] H.M. Crowther and B. Vincent. *Colloid & Polymer Science*, 276(1):46–51, 1998.

[107] F. Franks. In *Water a Compreshinsive Treatise*, 1973.

[108] G. Onori. *Chem. Phys. Lett.*, 154:212, 1989.

[109] N. Denkov, O. Velev, P. Kralchevski, I. Ivanov, H. Yoshimura, and K. Nagayama. *Langmuir*, 8(12):3183–3190, 1992.

[110] Brian G. Prevo and Orlin D. Velev. *Langmuir*, 20(6):2099–2107, 2004.

[111] Jeffrey J. Gray and Roger T. Bonnecaze. *Journal of Chemical Physics*, 114(3):1366–1381, 2001.

[112] Marcel Boehmer. *Langmuir*, 12(24):5744–5750, 1996.

[113] Zhengzhi Yin, Jingjing Zhang, Li-Ping Jiang, and Jun-Jie Zhu. *J. Phys. Chem. C*, 113:16104–16109, 2009.

[114] Michael J. Serpe, Clinton D. Jones, and L. Andrew Lyon. *Langmuir*, 19:8759–8764, 2003.

[115] Robert M. Richardson, Robert Pelton, Terence Cosgrove, and Ju Zhang. *Macromolecules*, 33:6269–6274, 2000.

[116] Ju Zhang and Robert Pelton. *Langmuir*, 12:2611–2612, 1996.

[117] John E. Wong, Heidemarie Zastrow, Werner Jaeger, and Regine von Klitzing. *Langmuir*, 25(24):14061–14070, 2009. PMID: 19705859.

[118] Dongsik Yoo, Seimei S. Shiratori, and Michael F. Rubner. *Macromolecules*, 31(13):4309–4318, 1998.

[119] Donald T. Haynie, Ling Zhang, Jai S. Rudra, Wanhua Zhao, Yang Zhong, and Naveen Palath. *Biomacromolecules*, 6(6):2895–2913, 2005.

[120] Ulrike Voigt, Werner Jaeger, Gerhard H. Findenegg, and Regine von Klitzing. *J. Phys. Chem. B*, 107:5273–5280, 2005.

[121] Katarzyna Haenni-Ciunel, Gerhard H. Findenegg, and Regine von Klitzing. *Soft Materials*, 5:61–73, 2007.

[122] A. Pfau, W. Schrepp, and D. Horn. *Langmuir*, 15:3219–3225, 1999.

[123] P. Nazaran, V. Bosio, W. Jaeger, D. F. Anghel, and R. v. Klitzing. *The Journal of Physical Chemistry B*, 111(29):8572–8581, 2007. PMID: 17461569.

[124] Bruno Jean, Frederic Dubreuil, Laurent Heux, and Fabrice Cousin. *Langmuir*, 24(7):3452–3458, 2008. PMID: 18324845.

[125] Karen Koehler, Helmuth Moehwald, and Gleb B. Sukhorukov. *The Journal of Physical Chemistry B*, 110(47):24002–24010, 2006. PMID: 17125370.

Eidesstattliche Erklärung

Die selbstständige und eigenhändige Anfertigung
versichere ich an Eides statt.

Datum/Unterschrift